

**Semi-Empirical Analytical Determination of the Transient Thermal Evolution
within a Substrate during Low-Pressure Cold Spraying**

by

Amirhossein Mahdavi

A thesis submitted in partial fulfillment of the requirements for the degree of

Doctor of Philosophy

Department of Mechanical Engineering
University of Alberta

© Amirhossein Mahdavi, 2018

Abstract

Hard-faced coatings are used to protect surfaces against wear, corrosion, and thermal degradation. Cold-gas dynamic spraying is a coating fabrication process in which a supersonic gas flow is produced to propel un-molten metal or alloy powder particles to deposit, with high impact forces, upon a substrate to form a highly adherent coating. Due to the high velocity of the under-expanding gas jet upon the substrate, and the high temperature of the impinging jet, a significant amount of thermal energy is expected to be transferred from the gas jet to the substrate. The quality of the final coating, as well as the deposition efficiency of the particles, can be significantly affected by the substrate surface or particle-substrate interface heating during the cold spraying process. With knowledge of the significant role that substrate temperature plays on the quality of cold-sprayed coatings, it becomes important to study the gas-substrate heat exchange. In this regard, the first phase of this PhD research project focused on developing a semi-empirical analytical model to determine the heat transfer coefficient of an impinging air jet generated by a cold spraying nozzle. A method involving Green's functions was employed to solve a transient two-dimensional heat conduction problem to obtain an expression for the temperature distribution within the substrate. By coupling the analytical results of temperature distribution and experimental surface temperature data, the spatially-varying heat transfer coefficient of the impinging air jet upon the substrate, in the form of the non-dimensional Nusselt number, was estimated. The results showed that the maximum values of the heat transfer coefficient were close to the stagnation point of the air jet. It was found that the heat transfer coefficient was independent of the time that the cold spray nozzle remained stationary over the substrate surface. It was found further that by increasing the stand-off distance of the nozzle, the radial variations of the heat transfer coefficient became negligible, compared to those for small

stand-off distances. In the second phase of the PhD research project, the effect of the air temperature and pressure, as process parameters, and surface roughness and thickness, as substrate parameters, on the heat transfer coefficient of the impinging air jet was investigated. It was found that increasing the total pressure would increase the Nusselt number of the impinging air jet, while the total temperature of the air jet had negligible effect on the Nusselt number. It was also found that increasing the roughness of the substrate enhanced the heat exchange between the impinging air jet and the substrate. As a result, higher surface temperatures on the rough substrate were measured. The study of the effect of the substrate thickness on the heat transfer coefficient showed that the Nusselt number that was predicted by the model was independent of the thickness of the substrate. The surface temperature profile, however, decreased with increasing radial distances from the stagnation point of the impinging jet as the thickness of the substrate increased. The final phase of this PhD research project focused on developing a mathematical model to predict the surface temperature profile of a substrate that was exposed to the impingement of a moving cold spray heat source. In this regard, a three-dimensional heat conduction model that was coupled with the travelling wave solution technique was developed. The analytically-predicted surface temperature profile was in good agreement with experimentally-measured data. Analytical modeling was further utilized to investigate the effect of the non-dimensional characteristic velocity of the travelling heat source on the surface temperature profile of the substrate. It was found that both the maximum surface temperature and the spatial variation of the surface temperature profile of the substrate decreased as the non-dimensional characteristic velocity increased.

Preface

Some of the sections presented in this thesis document have been or will be published in peer-reviewed journal or conference proceedings. The research studies were conducted under the guidance of Dr. André McDonald in his role as my research supervisor.

- Some sections of the work presented in Chapters 1 and 5 of this thesis document have been or will be published in peer-reviewed journals or conference proceedings of Paper No. 1 - Paper No. 7 as indicated below.
- Some sections of the work presented in Chapter 2 of this thesis document have been published in peer-reviewed journal Paper No. 2 and conference proceedings Paper No. 7.
- Some sections of the work presented in Chapter 3 of this thesis document have been published in peer-reviewed journal Paper No. 3 and conference proceedings Paper No. 6.
- Some sections of the work presented in Chapter 4 of this thesis document have been or will be published in peer-reviewed journal Paper No. 1 and conference proceedings Papers No. 3. and No. 4.

Paper No. 1: Amirhossein Mahdavi, André G. McDonald, “Semi-empirical Analytical Determination of Transient Temperature Distribution within a Flat Substrate during a Cold Spray Deposition Process”, *Surf. Coat. Technol.*, under review (Manuscript number: SURFCOAT-D-18-00724).

- Paper No. 2: Amirhossein Mahdavi, André G. McDonald, “Analytical Study of the Heat Transfer Coefficient of the Impinging Air Jet during Cold Spraying”, *Int. J. Therm. Sci.*, 2018, 130, 289-297.
- Paper No. 3: Amirhossein Mahdavi, André G. McDonald, “Effect of Substrate and Process Parameters on the Gas-Substrate Convective Heat Transfer Coefficient during Cold Spraying”, *J. Therm. Spray Technol.*, 2018, 27, 433-445.
- Paper No. 4: Amirhossein Mahdavi, André G. McDonald, “Heat Transfer Coefficient of an Under-expanding Cold Spray Air Jet on a Flat Substrate”, in: 5th International Conference on Fluid Flow, Heat and Mass Transfer (FHMT’18), June 7-9, 2018 (Niagara Falls, Canada), (2018), # 170, 7 pages on compact disk.
- Paper No. 5: Amirhossein Mahdavi, André G. McDonald, “Determination of the Temperature Distribution of a Substrate Exposed to a Moving Cold or Thermal Spray Heat Source”, in: International Thermal Spray Conference (ITSC 2018), May 7-10, 2018 (Orlando, FL, USA), ASM International, (2018), # 44653, 6 pages on compact disk.
- Paper No. 6: Amirhossein Mahdavi, André G. McDonald, “The Effect of Substrate Roughness on the Heat Transfer Coefficient of an Impinging Cold Spray Air Jet”, in: International Thermal Spray Conference (ITSC 2017), June 7-9, 2017 (Düsseldorf, Germany), ASM International, (2017), # 5171, 6 pages on compact disk.

Paper No. 7: Amirhossein Mahdavi, André G. McDonald, “Analytical Evaluation of Temperature Distribution within a Substrate under an Impinging Cold Spray Hot Air Jet”, in: International Thermal Spray Conference (ITSC 2016), May 10-12, 2016 (Shanghai, People’s Republic of China), ASM International, (2016), # 4706, 5 pages on compact disk.

Acknowledgments

Foremost, I would like to express my sincere gratitude to my supervisor, Prof. André G. McDonald for his patience, guidance, motivation, and the continuous support during my doctoral program in the University of Alberta. Completion of this research program would have been impossible without his hard work and encouragement. I could not have imagined having a better supervisor and mentor for my Ph.D. program.

I would like to thank the members of my doctoral supervisory committee, Prof. Zengtao Chen and Dr. Morris R. Flynn for their valuable and informative suggestions during my program. I am also thankful to the members of the examining committee, Prof. Timothy Eden and Dr. Arman Hemmati and the examining committee chair, Dr. Alexandra Komrakova.

I would like to thank Prof. David S. Nobes for providing the infrared camera for temperature measurement. I would also like to acknowledge the support from Natural Sciences and Engineering Research Council of Canada (NSERC).

Last, but not least, I dedicate this dissertation to my mother for her endless love and support throughout my life. Everything that I have today is because of her dedication and self-devotion and I am and will be always grateful for that. I would like to thank my father for his encouragement and valuable life lessons. I am thankful to my beloved sister, Elnaz, for her continuous love and support. I am also thankful to my dear brothers, Soheil and Saman, and my lovely nephew and niece, Arvin and Paryas, for supporting me. Finally, I would like to thank my friends for helping me and I wish everyone to be as lucky with their opportunities in life as I have been.

Table of Contents

Abstract.....	ii
Preface.....	iv
Acknowledgment.....	vii
List of Tables	xi
List of Figures.....	xii
Chapter 1: Introduction	1
1.1 Overview of Thermal Spraying Process.....	1
1.2 Cold Spraying Process	3
1.3 Heat Transfer in Cold Spraying	6
1.4 Heat Transfer Coefficient of the Under-expanding Air jet	8
1.5 Effect of Substrate Parameters on Heat Transfer Coefficient	14
1.6 Transient Temperature Distribution during Cold Spraying Process	15
1.7 Summary	17
1.8 Objectives.....	19
1.9 Thesis Organization.....	19
Chapter 2: Analytical Study of the Heat Transfer Coefficient of the Impinging Air Jet during Cold Spraying	21
Chapter 2 Nomenclature	22
2.1 Experimental Procedure	23
2.1.1 Low-Pressure Cold Spray System	23
2.1.2 Substrate Preparation	23
2.1.3 Temperature Measurements.....	24

2.2 Mathematical Model and Uncertainty Analysis.....	25
2.2.1 Mathematical Model	25
2.2.2 Propagation of Uncertainty in the Estimation of Heat transfer Coefficient	31
2.3 Results and Discussion.....	34
2.3.1 Determination of the Adiabatic Wall Temperature	34
2.3.2 Determination of the Heat Transfer Coefficient	40
2.3.3 Effect of the Nozzle Stand-off Distance on the Heat Transfer Coefficient	44
2.3.4 Verification of the Semi-empirical Analytical Model	46
Chapter 3: Effect of Substrate and Process Parameters on the Gas-Substrate Heat Transfer Coefficient during Cold Spraying.....	49
Chapter 3 Nomenclature	50
3.1 Experimental Procedure	51
3.1.1 Low-Pressure Cold Spray System	51
3.1.2 Substrate Preparation	52
3.1.3 Temperature Measurements.....	52
3.2 Mathematical Model	54
3.3 Results and Discussion.....	55
3.3.1 Effect of Process Parameters on the Heat Transfer Coefficient	55
3.3.2 Effect of Substrate Parameters on the Heat Transfer Coefficient	60
Chapter 4: Semi-empirical Analytical Determination of Transient Temperature Distribution within a Flat Substrate during a Cold Spray Deposition Process	71
Chapter 3 Nomenclature	72
4.1 Experimental Procedure	73
4.2 Mathematical Model	74

4.3 Results and Discussion.....	80
4.3.1 Effect of the Presence of the Particles on the Heat Transfer Coefficient	80
4.3.2 Surface Temperature Profile of the Substrate Exposed to a Moving Heat Source ...	87
4.3.3 Effect of Velocity of the Heat Source on Maximum Surface Temperature	90
Chapter 5: Conclusions	94
Chapter 6: Future Work and Extended Studies	99
References.....	102
Appendix A	115
Appendix B	121

List of Tables

Table 2-1	The coefficients and regression values of the fitted adiabatic wall temperature for different stand-off distances	40
Table 3-1	Low-pressure cold spray system parameters	51
Table 3-2	Average roughness, skewness, and kurtosis of the smooth and the rough (grit-blasted) aluminium 6061-T6 substrates	62

List of Figures

Figure 1-1	Schematic of deposition and coating formation by direct current plasma spraying process [1]	2
Figure 1-2	Velocity of the cold-sprayed Cu particles as a function of the gas pressure for various gas temperatures [41]	5
Figure 1-3	Morphologies of deposited particles for (a) gas pressure: 0.4 MPa, gas temperature: 250°C, (b) 0.5 MPa, 250°C, (c) 0.6 MPa, 250°C, (d) 0.4 MPa, 650°C, (e) 0.5 MPa, 650°C, and (f) 0.6 MPa, 650°C [41].....	6
Figure 1-4	Normalized heat transfer coefficient of an under-expanding air jet as a function of non-dimensional distance from the stagnation point at different normalized stand-off distances [55].....	10
Figure 1-5	Values of the average Nusselt number for different Mach numbers of the impinging air jet at different non-dimensional stand-off distances [57].....	11
Figure 1-6	Variation of Nusselt number with non-dimensional radial distance from the stagnation point of the jet [67]	12
Figure 1-7	Non-dimensional maximum surface temperatures of steel 1020 substrates with the natural logarithm of the Peclét number [68]	13
Figure 2-1	Image and schematic of the experimental assembly.....	24
Figure 2-2	Schematic of the geometry for the mathematical model	26
Figure 2-3	Curves of non-dimensional adiabatic wall temperature versus non-dimensional radius of the spreading air jet upon the substrate	36
Figure 2-4	The flow pattern of the impinging air jet at small stand-off distances [54].....	38
Figure 2-5	Curves of the Nusselt number of the impinging air jet as a function of non-dimensional radial distance from the stagnation point for different Fourier numbers	42

Figure 2-6	Curves of the heat flux between the air film and the substrate as a function of non-dimensional radial distance from the stagnation point for different Fourier numbers	42
Figure 2-7	Curves of the Nusselt number of the impinging air jet as a function of non-dimensional radial distance from the stagnation point for different non-dimensional stand-off distances	45
Figure 2-8	Schematic of the axial velocity distribution of the air jet [23]	46
Figure 2-9	Non-dimensional surface temperature variation of the substrate at a) $\psi = 2.38$, b) $\psi = 3.96$, c) $\psi = 7.93$, and d) $\psi = 15.87$	48
Figure 3-1	Morphology of the garnet sand particles	53
Figure 3-2	Schematic of the experimental assembly for measuring the emissivity of rough aluminium substrate	54
Figure 3-3	Radial variation of the Nusselt number of the under-expanding air jet over the substrate for different total pressures of the air jet	56
Figure 3-4	Nusselt number of the under-expanding air jet over the substrate versus non-dimensional radius for different total temperatures of air	59
Figure 3-5	Heat transfer coefficient of the under-expanding air jet over the substrate versus the non-dimensional radius for different total temperatures of air	60
Figure 3-6	(a) 3-D representation of the surface topology and (b) cross-sectional profile of the front surface of the smooth (top) and rough (grit-blasted) (bottom) aluminium 6061-T6 substrates	62
Figure 3-7	Emissivity of the grit-blasted Al 6061-T6 substrate at different surface temperatures	65
Figure 3-8	Comparison of the radial variation of the non-dimensional steady-state surface temperature of the rough and smooth substrates under cold spray air jet impingement	66

Figure 3-9	Comparison of predicted and experimentally-measured non-dimensional surface temperature variation of the substrate at different substrate thicknesses.....	70
Figure 4-1	Schematic of the experimental assembly and nozzle movement direction	74
Figure 4-2	Schematic of the geometry for the mathematical model	75
Figure 4-3	Results of the numerical simulation of the particle dispersion pattern over a range Stokes numbers, extracted from Tang, <i>et al.</i> [101]. The vertical and horizontal coordinates were non-dimensionalized with respect to the width of the bluff body.....	82
Figure 4-4	Comparison of the experimental and analytical non-dimensional temperature profile at different Fourier numbers for (a) – (c) average and (d) spatially-varying heat transfer coefficient	86
Figure 4-5	Comparison of the temporal variation of the predicted and experimentally-measured non-dimensional temperature at the center of the front surface of the flat substrate exposed to a heat source travelling with velocity of (a) 2.5 mm/s, (b) 5 mm/s, and (c) 10 mm/s at different Fourier numbers	89
Figure 4-6	Comparison of the predicted and experimentally-measured non-dimensional maximum temperature of the substrate as a function of the non-dimensional characteristic velocity of the moving heat source for different non-dimensional stand-off distance of (a) 2.38, (b) 3.96, and (c) 7.93	92
Figure 5-1	Flow chart of the sequential steps in semi-empirical analytical modelling of the current PhD research project	95

CHAPTER 1

Introduction

1.1. Overview of the Thermal Spraying Process

Thermal spraying is defined as a set of coating processes which utilize high energy gas flow in order to accelerate, heat, or direct molten, semi-molten, or un-molten metallic and ceramic materials toward the target substrate in order to form a dense and adherent coating [1, 2]. The feedstock material for the coating may be in the form of powder, rod, or wire. The energetic gas flow is typically generated by a thermal spray torch or a cold spray nozzle. The main motivation for using thermal spraying processes is due to the need for enhancing the performance of the components and parts in high-temperature environments, increasing the durability and life-span of the components that are exposed to abrasive, erosive, and corrosive environments, extending the functionality and sustainability of sub-components by repairing and rebuilding the damaged parts instead of replacing the entire component, and reducing the manufacturing cost by improving the quality of low-cost material with costly coating materials [1]. Thermal spray processes can be classified into three main groups. These categories are mainly defined based on the working temperature of the process and the method by which the high-energy gas flow is generated [1 - 5]. These main classes are, namely, compressed gas expansion (low- and high-pressure cold gas dynamic spraying), combustion spraying (flame spraying, high-velocity oxy-fuel spraying (HVOF), and detonation gun spraying), and electrical discharge plasma spraying (direct current plasma spraying, radio frequency plasma spraying, and wire arc spraying) [1]. Figure 1-1 shows a schematic that is representative of the thermal

spraying and deposition processes as well as coating formation by use of direct current plasma spraying [1].

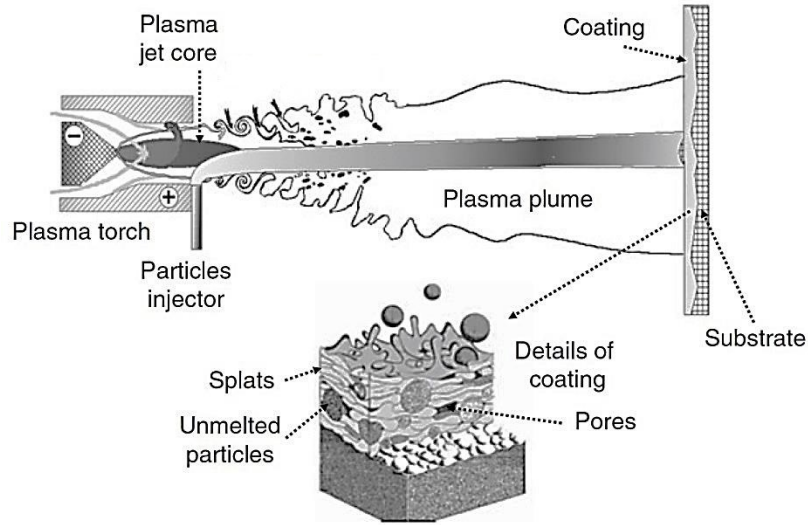


Figure 1-1: Schematic of deposition and coating formation by a direct current plasma spraying process [1].

During the impingement and deposition process, the thermal energy of the thermal spray flame, plasma, or gas is transferred to the in-flight particles and the target substrate [6]. The dominant mode of heat exchange between the carrier gas, the particles, and the substrate during thermal spraying process is convective heat transfer [7]. On the other hand, the kinetic energy of the in-flight solid or molten particles is expended to overcome the surface tension energy of the impacting particles on the substrate to deform the particles, and is converted to heat during flattening of the particles to create a splat [8 - 10]. The continuation of the deposition process results in the formation of a lamellar structure of the splats and eventually builds a coating layer on the substrate, as shown in Fig. 1-1. In order to characterize thermal and dynamic behavior of

the in-flight particles and the coating during the thermal spraying processes, conservation of mass, momentum, and energy can be used [11 - 13]. In most of the thermal spraying processes such as flame, HVOF, and plasma spraying, it is essential to work with high temperature gas flow (order of 2,500°C to 10,000°C) in order to partially or fully melt the particles to form an adherent coating on the substrate [4, 6, 12]. However, the high-temperature operation of the aforementioned thermal spray processes is a challenging issue when it comes to spraying onto temperature-sensitive substrates or substrates containing material such as nanostructured and amorphous materials, carbide composites, and several polymers [15 - 18]. To that end, cold-gas dynamic spraying, which is a relatively new coating deposition process with working temperature that is significantly below the melting point of most deposited coating feedstock material (order of 100°C to 1,000°C), can be utilized to alleviate the problem of spraying on temperature-sensitive material [19].

1.2. Cold Spraying Process

Cold-gas dynamic spraying (cold spraying) is a coating process in which a supersonic gas flow is generated by a converging-diverging de Laval nozzle to accelerate small un-molten metal or alloy powder particles (~ 5 to $40 \mu\text{m}$) to achieve high velocities (~ 300 to $1,200 \text{ m/s}$) in order to cause high impact force of the particles on the substrate [20]. As a result, the un-molten particles undergo plastic deformation during the impact on a substrate, which promotes mechanical and metallurgical bonding of the deformed particles with the substrate. In other words, the high speed of particles results in the creation of significant impingement forces, which leads to shear instabilities around the particles, which, in turn, causes plastic deformation of the

colliding particles [21, 22]. As a result, a dense and adherent coating or freestanding structure forms on the substrate. Nevertheless, the adhesion of the particles on the substrate occurs only on condition that the impact velocity of the particles exceeds a so-called critical velocity, whose value is highly dependent on the temperature and the material of the in-flight particle [23, 24]. The working gas and the particles are usually heated; however, as mentioned earlier, the temperature of the gas jet from the cold spray nozzle remains sufficiently lower than the melting point of most materials that are deposited. Therefore, the process temperature of the cold spraying process is much lower than that of conventional thermal spraying processes (less than 1,000°C) [25]. This feature of cold spraying permits deposition of the metallic and non-metallic powder on temperature-sensitive substrate materials. In addition, several studies have been done on the advantages of cold spray fabrication of coatings such as (i) no oxidation of the in-flight powder particles [18], (ii) high density, low porosity, and high bond strength of the final coatings [19, 26, 27], and (iii) compressive residual stresses in the final coating [28, 29]. In light of the advantages of cold spraying, attempts have been made to study the influential parameters on the quality of the final cold-sprayed coatings [30 - 35].

As speed of the powder particles increases, the propensity for plastic deformation increases. As a result, the quality of the final coating improves [15, 36 - 39]. To this end, it has been shown that higher gas pressure causes an increase in gas density, resulting in increased acceleration of the particles [25, 40, 41]. Consequently, the deposition efficiency of the deposited coating increases. In this regard, the cold spraying process can be categorized into two different groups, namely high-pressure and low-pressure cold spraying. The working gas pressure in high-pressure cold spraying is greater than 2 MPa [36, 42, 43]; While low-pressure cold spraying typically employs a working gas pressure below 1 MPa [44, 45]. Figure 1-2 shows the effect of

the cold spray gas pressure on the velocity of in-flight Cu particles with diameter of 5 μm [41]. The data was experimentally collected using Particle Imaging Velocimetry (PIV) measurement equipment.

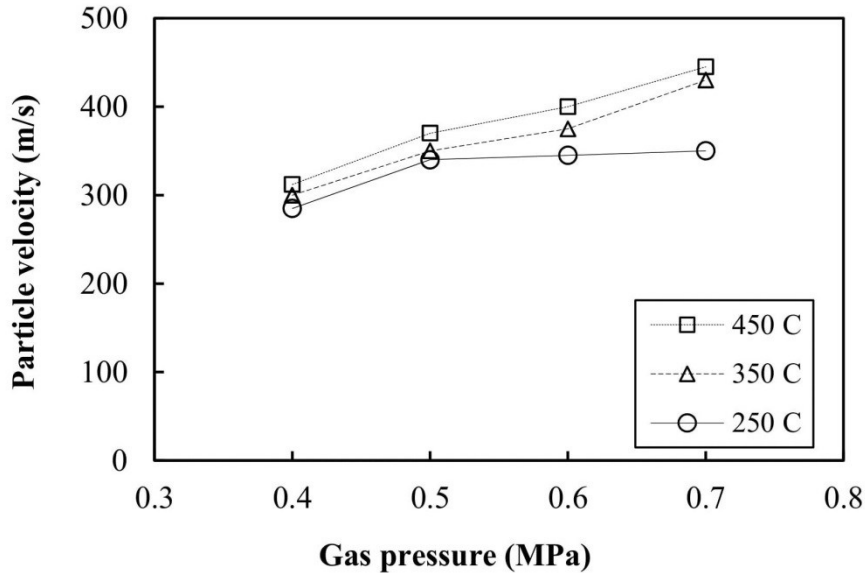


Figure 1-2: Velocity of the cold-sprayed Cu particles as a function of the gas pressure for various gas temperatures [41].

An alternative to increasing speed of the gas and the particles, as well as the deposition efficiency of cold-sprayed coatings is to pre-heat the propellant gas [24, 25, 41], especially when it is difficult or expensive to operate the cold spray system at high pressures. Increasing the gas temperature will increase the velocities of the gas and powder particles that exit the nozzle [25]. Schmidt, *et al.* [24] showed that increasing the propellant gas temperature from 300 to 900°C at a pressure of 3 MPa increased the speed of 25 μm copper particles from 490 to 620 m/s. In a parallel study, Fukumoto, *et al.* [41] observed that the particle deposition efficiency significantly improved with the increase in propellant gas temperature, which corresponded to heating of the

particles while in flight. Figure 1-3 shows the results of Scanning Electron Microscopy (SEM) imaged morphologies of the deposited particles to investigate the effect of gas temperature and gas pressure on the deposition behavior of Cu powder particles, with average particle diameter of $\sim 5 \mu\text{m}$, on AISI 304 substrate [41]. It can be observed that the deposition efficiency of the cold-sprayed coatings increased, as temperature and pressure of the working gas (air) increased.

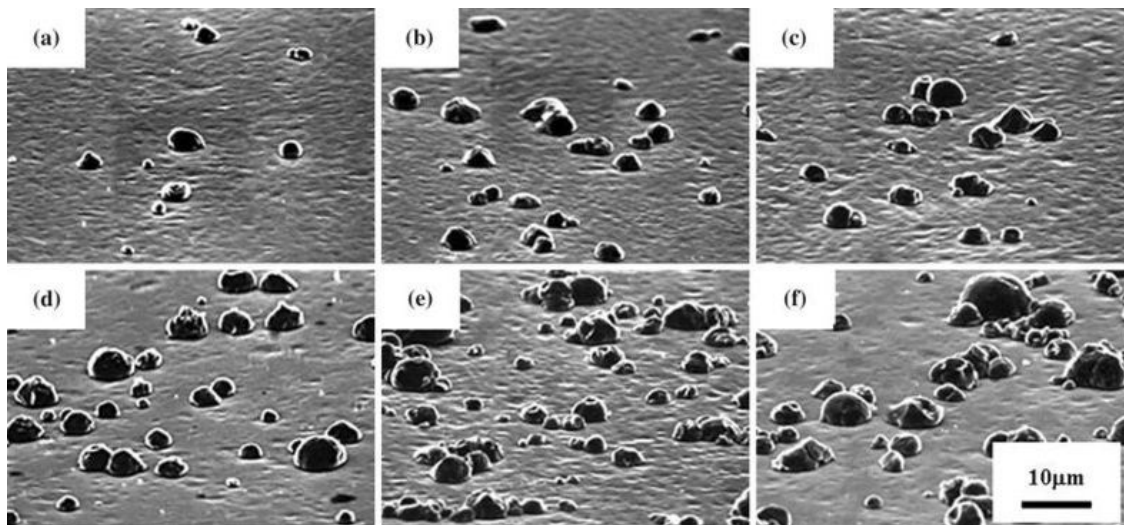


Figure 1-3. Morphologies of deposited particles for (a) gas pressure: 0.4 MPa, gas temperature: 250°C, (b) 0.5 MPa, 250°C, (c) 0.6 MPa, 250°C, (d) 0.4 MPa, 650°C, (e) 0.5 MPa, 650°C, and (f) 0.6 MPa, 650°C [41].

1.3. Heat Transfer in Cold Spraying

In light of the desired high temperature and speed of the propellant gas, a notable amount of thermal energy is expected to be transferred from the impinging working gas jet to the particles and the base substrate during operation of the cold spray system [46]. Several

investigations have been conducted through experimental work and analytical and numerical modelling such as Computational Fluid Dynamics (CFD) and Finite Element Analysis (FEA), to study the thermal energy exchange between the cold spray hot gas jet, the in-flight particles, and the target substrate [21, 47 - 50]. Generally, the thermal energy of the heated cold spray gas jet is used to heat the in-flight particles and exchange heat with the target substrate, while a portion of the thermal energy may be lost due to the entrainment of cold ambient air into the gas jet. The spatial variation of temperature within the particles in cold spraying is typically assumed to be negligible [10, 51 – 53]. Values of the Biot (Bi) number, which is the non-dimensional ratio of the conductive and convective thermal resistances to heat transfer, can be used to support the assumption. The Biot number is defined as [7]

$$\text{Bi} = \frac{hd_p}{k_p}, \quad (1-1)$$

where h , d_p , and k_p are heat transfer coefficient, particle diameter, and thermal conductivity of the particle material, respectively. When $\text{Bi} \ll 1$, spatial variation of temperature in the medium is negligible and temperature is uniform. The aforementioned assumption is valid for cold spray powder particles [52]. The interfacial heating of the particles during the cold spraying process have been studied extensively, and suitable heat transfer models to predict the heat exchange between the air jet and the in-flight particles have been established previously [10, 54]. On the other hand, due to the complex physical nature of the gas jet impingement on the substrate, the determination of the heat transfer rate and temperature distribution within the substrate becomes challenging.

According to recent studies, the quality of the final coating, as well as the deposition efficiency of the particles, can be significantly affected by the substrate surface heating during the cold spraying process [41, 46, 55 - 57]. As discussed earlier, Fukumoto, *et al.* [41] showed that substrate heating is an effective method for improving the deposition efficiency of the cold-sprayed coatings, especially during the formation of the first layer of the coating. Legoux, *et al.* [46] suggested that the optimum deposition efficiency can be expressed as a function of the ratio of the substrate impact temperature to the melting temperature of the powder particles. They experimentally determined that the optimum temperature ratio, which was defined as the ratio of the particle temperature prior to impact to the melting temperature of the particle material, was in the range of 0.6 to 0.7. Moreover, Watanabe, *et al.* [55] investigated the effect of surface temperature on the adhesion strength of cold-sprayed coatings. It was shown that higher substrate temperatures increased the adhesion strength of Cu coatings on A5083, Fe and Cu substrates. Moreover, it was reported that the adhesion strength of Al coatings on aluminium alloy (A5083) substrates at 200°C was approximately 2.5 and 5.5 times higher than that with temperatures of 100°C and 25°C, respectively. With knowledge of the significant role that substrate temperature plays on the quality of cold-sprayed coatings, it becomes important to study heat exchange between the gas and substrate during the cold spray process.

1.4. Heat Transfer Coefficient of the Under-expanding Air Jet

The dominant mode of energy exchange between the compressed gas working fluid and the substrate during cold spraying is expected to be convective heat transfer, due to the high-velocity gas jet impingement on the substrate [7]. Therefore, estimation of the heat transfer

coefficient between the under-expanded gas jet and the base substrate is necessary to determine the heat transfer rate and temperature distribution within the substrate. In this regard, several numerical and experimental investigations have been conducted to quantify the heat transfer coefficient of impinging air jets in a wide variety of applications and geometries [58 - 66]. In an earlier work, Donaldson and Snedeker [58] studied the behavior of free jets and the effect of the jet flow pattern on the heat transfer coefficient during impingement on a flat substrate. The measurements were obtained over a wide range of Reynolds numbers (1×10^4 to 2×10^5) and nozzle-to-substrate distances (1.96 to 58.7 nozzle diameter). It was observed that for small nozzle-to-substrate distances, due to the pressure difference within an assumed ring surrounding the stagnation point of the impinging jet, an inward radial flow occurred toward the stagnation point. Rahimi, *et al.* [59] employed the results of the aforementioned study to estimate the heat transfer coefficient of an impinging air jet at different nozzle pressure ratios and nozzle-to-substrate distances. It was suggested that the Nusselt number of an under-expanded air jet should be presented as a function of Mach number, the pressure ratio, as well as the Reynolds number and nozzle-to-substrate distance. Figure 1-4 shows the spatially-varying normalized heat transfer coefficient between the impinging air jet and a flat substrate at different non-dimensional stand-off distances (distance between the nozzle and the target substrate). The distance from the stagnation point of the impinging jet and the nozzle stand-off distance were non-dimensionalized with respect to the nozzle diameter. The estimated Reynolds number at the nozzle exit was 8.9×10^5 .

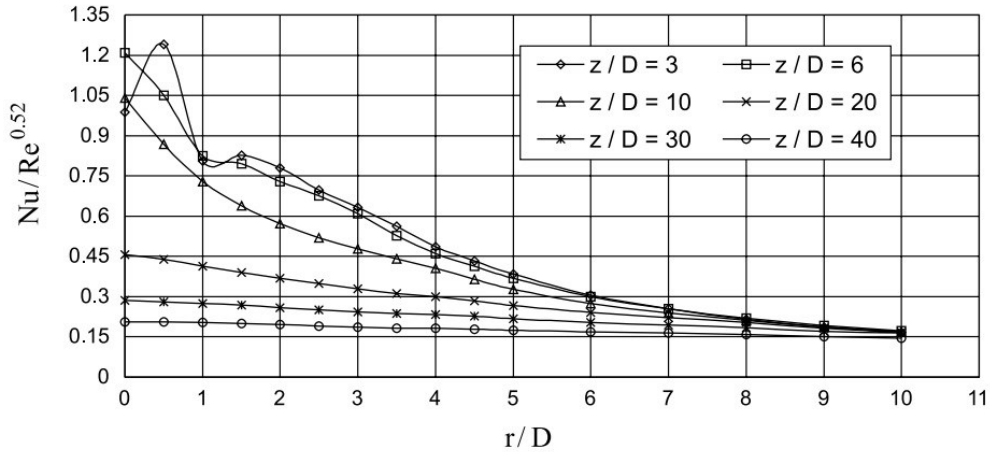


Figure 1-4: Normalized heat transfer coefficient of an under-expanding air jet as a function of non-dimensional distance from the stagnation point at different normalized stand-off distances [59].

On the other hand, Ramanujachari, *et al.* [60] used a simplified lumped heat transfer model, coupled with a set of experiments, to obtain the approximate heat flux over the substrate. It was observed that Nusselt number of the impinging jet was influenced by the mixing of air jet at higher nozzle-to-substrate distances. In a parallel study, Limaye, *et al.* [61] employed the so-called experimental thin metal foil technique to estimate the heat transfer coefficient of an impinging air jet on a heated substrate. It was found that by increasing the Mach number of the jet, which was measured at the nozzle exit, the average Nusselt number between the air jet and the substrate increased for all nozzle-to-substrate distances. Figure 1-5 shows the values of average Nusselt number of the impinging air jet at different non-dimensionalized stand-off distances. The average Nusselt numbers were estimated over a range of gas jet velocity at nozzle exit.

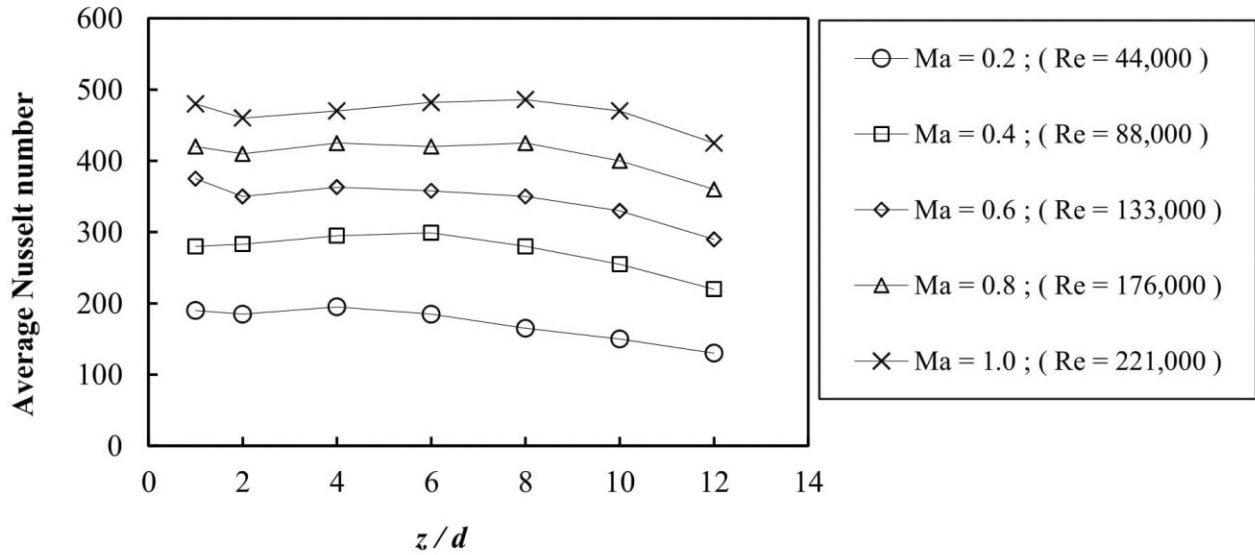


Figure 1-5: Values of the average Nusselt number for different Mach numbers of the impinging air jet at different non-dimensional stand-off distances [61].

Sagot, *et al.* [67], Afroz and Sharif [68], and Singh, *et al.* [69] combined the results of experiments with numerical computational fluid dynamics (CFD) modelling and commercial codes to study the heat transfer from the impinging air in various applications and geometries. In a recent numerical investigation, Zhou, *et al.* [70] adopted a modified turbulent flow model to analyze the impingement heat transfer rate at high temperature differences. It was suggested that the Nusselt number was independent of the temperature differences between the substrate surface and the air jet, and it could be calculated from the correlation equation that was developed for small temperature differences between the air jet and the substrate.

Along with these numerical and experimental investigations on the heat transfer of impinging air jets, specific studies have shed light on the gas-substrate heat exchange during cold-gas dynamic spraying. Ryabinin, *et al.* [71] coupled the results of a finite difference code with experimental data to estimate the Nusselt number of an impinging hot air jet originating

from a cold spray unit. Figure 1-6 presents the results of their study for spatially-varying Nusselt number of an impinging cold spray air jet for stand-off distance of 10 mm. The temperature and pressure of the air jet were 100°C and 660 kPa, respectively, at the cold spray console.

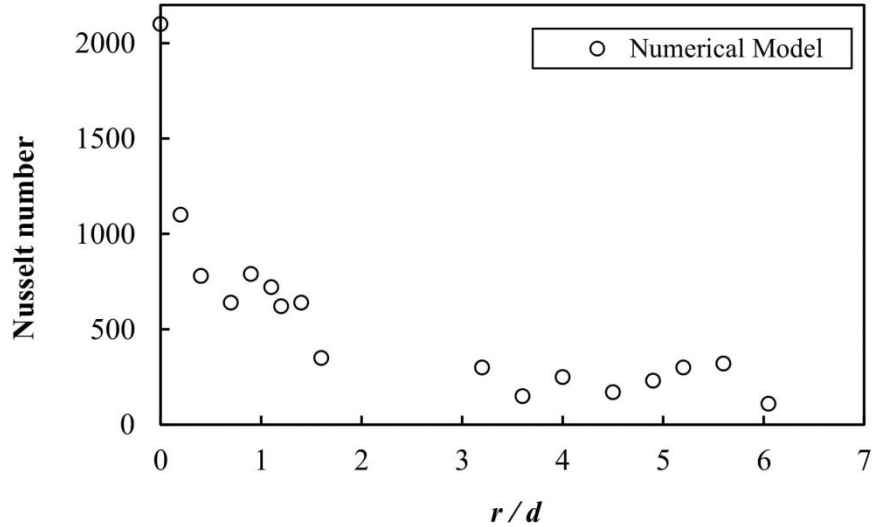


Figure 1-6: Variation of Nusselt number with non-dimensional radial distance from the stagnation point of the jet [71].

In a complementary work, McDonald, *et al.* [72] employed the Nusselt number obtained by Ryabinin, *et al.* [71] to investigate the effect of substrate thickness, substrate properties, and the motion of the cold spray nozzle on the temperature distribution of the substrate. It was suggested that the non-dimensional Peclét number played a major role in determination of the substrate temperature distribution during axial motion of the nozzle. Figure 1-7 shows the variation of the non-dimensional maximum surface temperature with the natural logarithm of the Peclét number. While these studies have focused on numerical and experimental investigation of heat transfer during jet impingement, the development of detailed analytical and mathematical models that are capable of predicting the Nusselt number and heat transfer coefficient *a priori* before experimentation is still lacking.

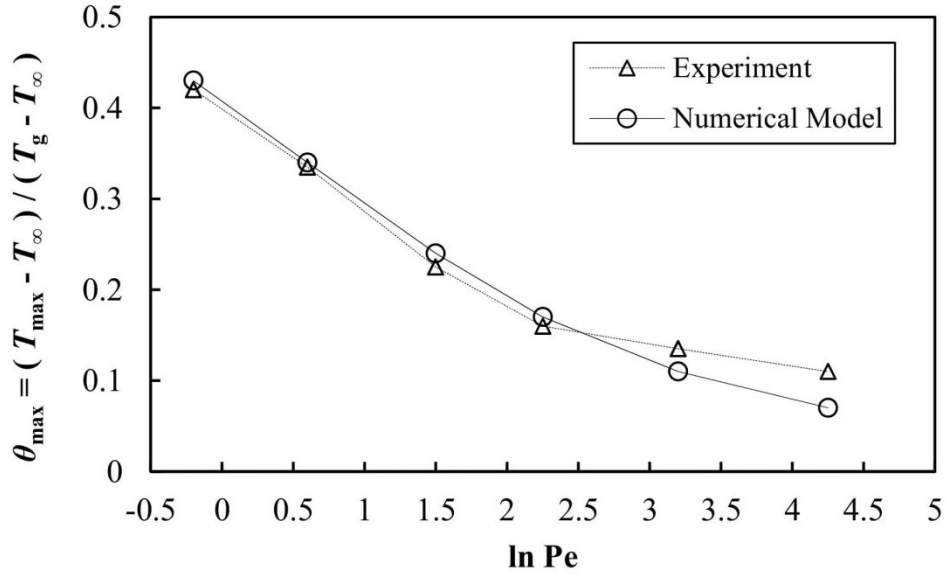


Figure 1-7: Non-dimensional maximum surface temperature of steel 1020 substrates with the natural logarithm of the Peclet number [72].

Cold spray process parameters, such as the temperature and the pressure of the propellant gas, can also affect the heat transfer rate from the gas jet to the substrate [7, 73 - 75]. For instance, an early experimental and analytical work by Striegl and Diller [73] showed that the entrainment of cold ambient air affected the temperature of the impinging air jet, which in turn, affected the local heat transfer rate and the heat transfer coefficient. Moreover, it has been shown that higher gas pressure causes an increase in gas density, resulting in increased acceleration of the particles [25]. On the other hand, an alternative to increasing the speed of the gas and the particles is to pre-heat the propellant gas [24, 25]. Therefore, the study of the effect of the gas temperature and pressure on the heat transfer coefficient and heat exchange between the under-expanded gas and the substrate is required.

1.5. Effect of Substrate Parameters on Heat Transfer Coefficient

In addition to the influence of the process parameters, the surface roughness of the substrate may also affect the substrate temperature distribution and the heat transfer rate between the substrate and the impinging cold spray air jet. In this regard, the effect of patterns on fabricated surfaces on the heat transfer coefficient of an impinging air jet on those types of surfaces has been studied [76 - 78]. Chakroun, *et al.* [76] patterned a surface with cubes of 1 mm length, which were distributed uniformly along the substrate to simulate a rough surface. It was shown that the local and average Nusselt number of the impinging air jet on the fabricated rough surface with Reynolds number ranging from 6,500 to 19,000 increased from 8.9% to 28% compared to that on the smooth surface. In a similar study, Beitelmal, *et al.* [77] employed a circular array of protrusions of 0.5 mm base diameter and 0.5 mm high. The results of their study indicated that the Nusselt number over the rough surface increased up to 6% for an impinging air jet with Reynolds number ranging from 9,600 to 38,500. In a recent numerical study, Cobbartean and Rahman [78] calculated the Nusselt number for an impinging air jet with Reynolds number of 500 to 1,000 over a rough surface consisting of indentation depths ranging from 0.125 to 0.5 mm. While these studies have placed emphasis on substrates with patterned surfaces, an investigation of the effect of the surface roughness generated by grit-blasting on the heat transfer coefficient of the impinging air jet, within the domain of application of cold spraying is still lacking.

The effect of the substrate thickness on the heat transfer coefficient and the surface temperature of the substrate was cursorily studied. In a numerical study by McDonald, *et al.* [72], the effect of substrate thickness on the maximum surface temperature of the substrate of

different materials was explored. It was shown that for all the materials that were studied, the maximum surface temperature decreased as the thickness of the substrate increased. A complementary study with emphasis on the effect of the substrate thickness on the gas-substrate heat transfer coefficient can serve to expand on the findings of previous investigations.

1.6. Transient Temperature Distribution during the Cold Spraying Process

As discussed in detail in Sections 1.3 and 1.4 of this Chapter, numerous studies have been conducted to investigate the heat transfer coefficient between the under-expanding air jet (hereafter the “heat source”) that was produced by a cold spray nozzle and the target substrate. The estimated heat transfer coefficient was utilized to predict the external heat flux, as well as the temperature distribution within the substrate. However, in these studies, the air jet that was generated was a stationary heat source in the mathematical modeling. Consequently, the model was capable of estimating the temperature distribution within the substrate that was exposed to a stationary heat source. In the actual cold spraying process, however, movement of the cold spray nozzle is a necessary condition for fabrication of a coating. Accordingly, it is expected that the temperature distribution within a substrate that is exposed to a travelling heat source would be different from the case in which the heat source is stationary. In this regard, in a numerical study by Chen, *et al.* [79], a three-dimensional model based on Finite Element Analysis (FEA) was developed to simulate the transient coating build-up process and the heat transfer between the impinging air-particle jet and the target substrate in cold spray. In their proposed model, the transient temperature distribution during the movement of the heat source was simulated. The heat transfer coefficient and the particle-gas temperature prior to impact on the substrate were

determined by simulation with the ANSYS-Fluent software. Despite the aforementioned numerical study, a detailed analytical investigation on the effect of the movement of the heat source on the surface temperature profile of the substrate is of interest. Moreover, in the aforementioned studies, the effect of the presence of the in-flight particles on the heat transfer coefficient, and in turn the external heat flux, was neglected, while in some cases, the presence of the particles may influence the flow pattern and the heat transfer coefficient of the air jet [80]. Therefore, the effect of the presence of the particles on the heat transfer coefficient of the exposed moving heat source requires further investigation.

A few analytical studies on the modeling of the heat conduction problem with moving heat sources have been performed to predict the temperature distribution in a surface or a rod within a wide range of applications [81 - 84]. Kim [81] used a Fourier series procedure in the mathematical modeling to determine the transient temperature field caused by a moving heat source. In a finite difference study, Song and Kovačević used a moving coordinate system to develop a three-dimensional heat transfer model with application to friction stir welding [82]. In another analytical-numerical study by Al-Huniti [83], the thermal behavior of a rod that was exposed to a moving point heat source was investigated. In the aforementioned study, Laplace transformation and the Riemann-sum approximation was utilized to predict the temperature distribution within the rod. Unlike in these studies that dealt with a point, plane, or surface heat source, the air jet that is generated by a cold spray nozzle typically produces a Gaussian-shaped heat flux on the substrate [58].

A detailed study was performed by Manca, *et al.* [85] to predict the temperature distribution within a finite length solid that was exposed to a moving circular Gaussian heat source. The circular Gaussian heat source in their study was known and given; however, the heat

source generated by a typical cold spray nozzle is mostly undefined and strongly dependent on process parameters such as the working gas pressure, temperature, and stand-off distance of the nozzle from the substrate surface [71, 72]. Therefore, determination of the temporally- and spatially-varying heat flux on the substrate is further required. The numerical-experimental study by McDonald, *et al.* [72] investigated the effect of the movement of the impinging air jet that was generated by a cold spray unit on the surface temperature of a flat substrate. The heat flux from the gas from the cold spray nozzle was determined numerically by using a finite difference method. However, a complementary analytical study that enables the prediction of the transient temperature profile in a substrate exposed to a moving heat source within the application of cold spraying is still lacking.

1.7. Summary

Cold-gas dynamic spraying is a coating fabrication process in which a supersonic gas flow is produced and used to propel un-molten metal or alloy powder particles to deposit, with high impact forces, upon a substrate to form a highly adherent coating. Due to the high velocity of the under-expanding gas jet upon the substrate, and the high temperature of the impinging jet, a significant amount of thermal energy is expected to be transferred from the gas jet to the substrate. The high velocity of the impinging gas on the flat substrate, furthermore, ensures that the predominant mode of heat transfer is convection. Therefore, determining the heat transfer coefficient will enable determination of the heat transfer rate from the impinging gas jet to the substrate, or previous layers of the deposited coating. The final quality of cold-sprayed coatings is noticeably influenced by gas-substrate heat exchange due to the dependence of the adhesion

strength of the particles on the substrate temperature, i.e., the adhesion strength of cold-sprayed particles can be increased by heating the substrate. Therefore, studying the effects of the cold spray parameters on the heat exchange and surface temperature of the substrate and the coating becomes important. On the other hand, process parameters, such as the temperature and the pressure of the propellant gas, and substrate parameters, such as the substrate roughness and thickness, can also affect the heat transfer rate from the gas jet to the substrate. Higher gas pressure causes an increase in gas density, resulting in increased acceleration of the particles. Moreover, an alternative to increasing the speed of the gas and the particles is to pre-heat the propellant gas. In this regard, the study of the effect of the gas temperature and pressure on the heat transfer coefficient and heat exchange between the under-expanded gas and the substrate is required.

In the actual cold spraying process, movement of the cold spray nozzle is a necessary condition for fabrication of a coating. Accordingly, it is expected that the temperature distribution within a substrate that is exposed to a travelling heat source would be different from the case in which the heat source is stationary. Moreover, the presence of the in-flight particles may influence the heat transfer rate between the air-particle jet and the substrate. This is likely due to the change in the flow pattern and turbulence intensity of the impinging air jet. Therefore, the effect of the presence of the particles on the heat transfer coefficient of the exposed moving heat source requires further investigation. With respect to the aforementioned points, a robust analytical study that enables the prediction of the transient temperature profile in a substrate exposed to a travelling cold spray air jet (moving heat source) within the application of cold spraying is still lacking.

1.8. Objectives

The main objectives of this doctoral research program were to:

- 1) Develop a robust mathematical model to determine the temperature distribution within a flat substrate that was exposed to impingement of a cold spray air jet;
- 2) Design an experiment to predict the spatially-varying adiabatic wall temperature of an under-expanding cold spray air jet;
- 3) Develop a semi-empirical analytical model to predict the spatially-varying heat transfer coefficient of an under-expanding cold spray air on a flat substrate;
- 4) Study the effect of the nozzle stand-off distance and the time that the nozzle remained stationary on the substrate on the heat transfer coefficient;
- 5) Study the effect of the cold spray process parameters on the heat transfer coefficient;
- 6) Investigate the effect of the substrate parameters on the heat transfer coefficient and the surface temperature profile;
- 7) Develop an analytical model to determine the temperature distribution within a substrate that was exposed to a moving heat source (travelling cold spray air jet); and
- 8) Study the effect of the velocity of the cold spray air jet on the maximum temperature of the substrate.

1.9. Thesis Organization

The present thesis document consists of six chapters with the following structure: Chapter 1 summarizes the background, definitions, and literature review for this doctoral research project. Chapter 2 focuses on the development of a robust heat conduction model for determination of the temperature distribution within flat substrates that was exposed to a

stationary, supersonic cold spray air jet. The developed model was employed to predict the spatially-varying heat transfer coefficient of an under-expanding cold spray air jet. The effect of the stand-off distance of the cold spray nozzle and the time that the nozzle remained stationary on the substrate was also investigated. The experimental setup that was used to impinge the cold spray supersonic air jet and further verification of the developed models has also been included in this Chapter. In Chapter 3 of this dissertation, the effect of the process parameters, namely the total gas and the total temperature of the air jet, and the substrate parameter, namely the thickness and the surface roughness, on the heat transfer coefficient and the surface temperature profile of the substrate was investigated. In Chapter 4, a modified mathematical model, based on the travelling wave solution, was developed to determine the temperature distribution with a substrate that was exposed to a travelling cold spray air jet. The effect of the velocity of the travelling air jet was also studied in this Chapter. Chapter 5 summarizes the overall conclusions from this thesis. Finally, Chapter 6 presents suggestions for future studies for extension and modification of the current research work.

CHAPTER 2

Analytical Determination of the Heat Transfer Coefficient of the Impinging Air Jet during Cold Spraying

A semi-empirical analytical model was developed to determine the heat transfer coefficient of an impinging air jet generated by a cold spraying nozzle. A low-pressure cold spraying unit was utilized to produce hot air jets that impinged upon a flat substrate surface. An infrared camera was used to measure the surface temperature of the substrate at different time intervals. A method involving Green's functions was employed to solve a transient two-dimensional heat conduction problem to obtain an expression for the temperature distribution within the substrate. By coupling the analytical results of temperature distribution and experimental surface temperature data, the radial variation of the non-dimensional heat transfer coefficient of the impinging air jets upon the substrate was estimated. The model was utilized to investigate the dependency of the heat transfer coefficient on the time that the cold spray nozzle remained stationary over the substrate surface. The effect of the stand-off distance of the nozzle on the radial variations of the heat transfer coefficient was also studied. The surface temperature profiles of the substrate that were obtained by the semi-empirical analytical model was verified by comparing with that from experimental results.

Some sections of the work presented in this chapter have been published in A. Mahdavi, A. McDonald, "Analytical Study of the Heat Transfer Coefficient of the Impinging Air Jet during Cold Spraying", *Int. J. Therm. Sci.*, 2018, 130, 289-297; and A. Mahdavi, A. McDonald, "Analytical Evaluation of Temperature Distribution within a Substrate under an Impinging Cold

Spray Hot Air Jet”, in: *International Thermal Spray Conference (ITSC 2016)*, May 10-12, 2016 (Shanghai, People’s Republic of China), ASM International, (2016), # 4706, 5 pages on compact disk.

Nomenclature

b	thickness of the substrate (m)	<i>Greek symbols</i>	
C	arbitrary coefficient	α	thermal diffusivity (m^2/s)
D	cold spray nozzle diameter	β	eigenvalues in axial coordinate
f	function in Green’s function equation ($^{\circ}\text{C}$)	Δ	uncertainty
F	function in Green’s function equation ($^{\circ}\text{C}$)	δ	thickness of the substrate (m)
Fo	Fourier number	ε	emissivity
G	Green’s function ($^{\circ}\text{C}$)	η	non-dimensional radius
h	heat transfer coefficient ($\text{W}/\text{m}^2\text{-K}$)	θ	non-dimensional temperature
J	Bessel function	λ	eigenvalues in radial coordinate
k	thermal conductivity ($\text{W}/\text{m-K}$)	σ	Stefan–Boltzmann constant ($\text{W}/\text{m}^2\text{-K}^4$)
n	number of measurements	τ	time dummy variable (s)
N	Norm of the differential equation	χ	precision coefficient
Nu	Nusselt number	ψ	non-dimensional stand-off distance
r	radial coordinate	<i>Subscripts</i>	
r'	radial dummy variable (m)	AW	adiabatic wall
SD	standard deviation	B	bias uncertainty
t	time (s)	E	repeated experimental uncertainty
T	temperature ($^{\circ}\text{C}$)	g	propellant gas
T_0	substrate initial temperature ($^{\circ}\text{C}$)	i	numerator in radial coordinate
U	arbitrary function	j	numerator in axial coordinate
V	arbitrary function	n	nozzle
z	axial coordinate	s	substrate
z'	axial dummy variable (m)	∞	ambient

2.1. Experimental Procedure

2.1.1. Low-Pressure Cold Spray System

A supersonic hot air jet was generated by utilizing a low-pressure cold-gas dynamic spraying unit (SST Series P, Centerline, Ltd., Windsor, ON, Canada). The temperature and the pressure of the air jet were, respectively, set at 300°C and 660 kPa (96 psig) at the cold spray unit console. The nozzle of the cold spray torch was a 140 mm-long converging-diverging de Laval nozzle, with throat and exit diameters of 2.54 mm and 6.3 mm, respectively. A robot (Motoman-HP20, Yaskawa Electric Corp., Waukegan, IL, USA) was employed to control the cold spray nozzle during the experiments. The cold spray nozzle was directed at the center of the front surface of the substrate and was held stationary at the desired stand-off distance (SOD), which was the distance between substrate and the nozzle. The stand-off distances in this study were chosen to be 15, 30, 50, and 100 mm to cover a wide range of the substrate-nozzle stand-off distances.

2.1.2. Substrate Preparation

In this study, Aluminum 6061-T6 was used as the substrate. This material is known to have a relatively high thermal conductivity to increase heat conduction through the substrate. Thus, this material should achieve steady-state thermal conditions quickly after impingement of the hot air jet onto the substrate. The geometry of the substrate was a disk with dimension of 200 mm in diameter and 1.5 mm in thickness. In order to prevent the back surface of the substrate from exchanging heat with the ambient air, a thermal insulator material, vitreous aluminosilicate

fiber (ISAFORM 2300° L.O., Insulation Specialties of America, Inc., Wanatah, IN, USA), was attached at the back surface of the substrate. The substrate was mounted on a substrate holder. A leveling device (9" Magnetic Torpedo Level, Logix, China) was employed to ensure that the impinging air jet was normal (perpendicular) to the substrate during the experimental procedure. Subsequently, it was expected that the under-expanding air flow over the substrate was symmetrical with respect to the stagnation point of the impinging air jet. Figure 2-1 shows the actual image and the schematic of the experimental assembly.

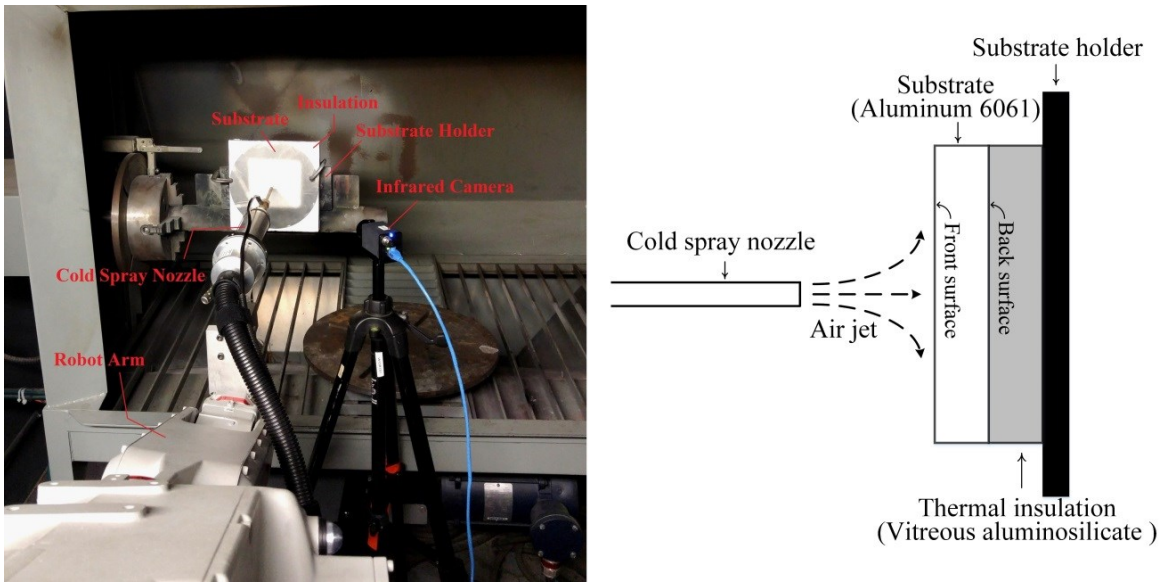


Figure 2-1: Image and schematic of the experimental assembly.

2.1.3. Temperature Measurements

The transient and steady-state temperatures of the front surface of the substrate were measured by using a calibrated infrared camera (FLIR A65, FLIR Systems, Inc., Nashua, NH, USA). The spatial resolution (IFOV) of the camera was 1.31 mrad. The infrared camera had a spectral range of 7.5 - 13 μm , and a time resolution of 12 ms. The image capture frequency of the camera was 9 Hz, and the measurement accuracy was $\pm 5^\circ\text{C}$ or 5% of the reading. Some

assumptions were made prior to the temperature measurement with the infrared camera. In order to enable more accurate measurements, the front surface of the substrate was painted black so as to make a black body. Accordingly, the emissivity of the substrate was set to a constant value of 0.96 on the infrared camera. The emissivity of the painted substrate was likely dependent on its temperature; however, since the infrared camera was only capable of receiving a single value for the object emissivity, the dependence of the emissivity on temperature was neglected. In addition, due to the short distances of the cold spray nozzle from the substrate, the infrared camera was not normal to the substrate (see Fig. 2-1). Therefore, the temperature measurements at some specific locations might be affected by the temperature of the in-flight air jet and the presence of the hot nozzle in the camera's field of view. To reduce the influence of the gas temperature on the substrate temperature readings from the infrared camera, the set points on the substrate that were behind the in-flight air jet on the infrared camera read-out panel were not considered. Each set of experiment, which was conducted to measure the surface temperature, was repeated three times to ensure the repeatability of the experimental results. The average of the experimentally-measured surface temperatures at each specific location for these three repetitions was considered. The standard deviations from the average of the experimentally-measured surface temperatures were evaluated as well.

2.2. Mathematical Model and Uncertainty Analysis

2.2.1. Mathematical Model

The under-expansion of the supersonic hot air jet generated by the low-pressure cold spray unit on the substrate allows for the release and eventual transfer of thermal energy from the

jet, predominantly by way of heat convection. In order to determine the temperature distribution within the substrate, values of the heat transfer coefficient will be required. A transient, three-dimensional heat conduction model could be developed to estimate the temperature distribution within the substrate, from which the heat transfer coefficient could be estimated. However, due to the axisymmetric nature of the impinging gas jet, the three-dimensional model can be reduced to a two-dimensional model [86]. Figure 2-2 shows a schematic of the geometry of the problem upon which the mathematical model was based. There was a heat flux from the impinging hot air jet on the exposed front surface of the substrate, while all other sides of the substrate were assumed to be insulated. This assumption was justified by the fact that the thickness of the substrate was small, resulting in a surface area of the sides that was much smaller than that of the front of the substrate. Therefore, the heat transfer rate from the sides was assumed to be negligible in comparison to the heat exchange with the front surface of the substrate.

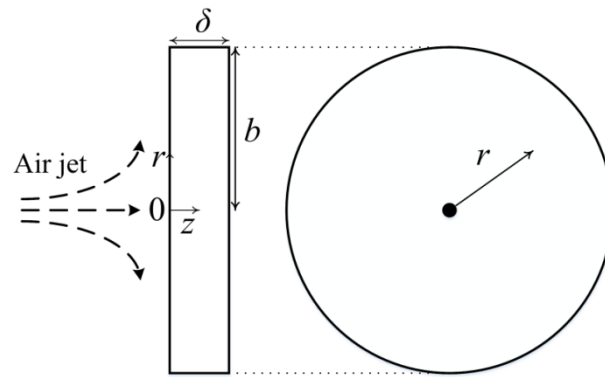


Figure 2-2: Schematic of the geometry for the mathematical model.

The governing equation of the transient two-dimensional heat conduction model is

$$\frac{1}{r} \frac{\partial}{\partial r} \left(r \frac{\partial T}{\partial r} \right) + \frac{\partial^2 T}{\partial z^2} = \frac{1}{\alpha_s} \frac{\partial T}{\partial t}. \quad (2-1)$$

The boundary conditions and initial condition are

$$T(r=0, z, t) = \text{finite}, \quad (2-2)$$

$$\frac{\partial T(r=b, z, t)}{\partial r} = 0, \quad (2-3)$$

$$-k_s \left[\frac{\partial T(r, z=0, t)}{\partial z} \right] = h(r) [T_{AW}(r) - T(r, z=0, t)] + \varepsilon \sigma [T^4(r, z=0, t) - T_\infty^4], \quad (2-4)$$

$$\frac{\partial T(r, z=\delta, t)}{\partial z} = 0, \quad (2-5)$$

$$T(r, z, t=0) = T_0. \quad (2-6)$$

A boundary condition of the third kind (Robin condition), including the effects of radiation from the substrate, was applied at the front surface of the substrate (at $z = 0$) to model the heat flux due to the under-expansion of the impinging jet. The second term on the right hand side of Eq. (2-4) represents the heat loss from the front surface by radiation to the ambient at temperature, T_∞ . It has been reported that if the relative temperature difference between the substrate and the ambient, $\frac{|T - T_\infty|}{T_\infty}$, is on the order of one or less, the radiation term in Eq. (2-4) can be linearized

and reformulated as [87]

$$\varepsilon \sigma [T^4(r, z=0, t) - T_\infty^4] \approx h_{\text{rad}} [T(r, z=0, t) - T_\infty], \quad (2-7)$$

where h_{rad} is the radiative heat transfer coefficient and is defined as [87]

$$h_{\text{rad}} = \varepsilon \sigma [T^3(r, z=0, t) + T(r, z=0, t)T_\infty^2 + T^2(r, z=0, t)T_\infty + T_\infty^3] \approx 4\varepsilon \sigma T_\infty^3. \quad (2-8)$$

In Eq. (2-8), ε is the emissivity of the substrate and it was assumed to be 0.96, and σ is the Stefan–Boltzmann constant ($\sigma = 5.67 \times 10^{-8} \text{ W/m}^2\text{-K}^4$). According to the experimental results in this study, the relative temperature difference between the substrate and the ambient was measured to be on the order of one. Therefore, the aforementioned assumption of linearization of the radiation term was valid and Eq. (2-4) can be expressed as

$$-k_s \left[\frac{\partial T(r, z=0, t)}{\partial z} \right] = h(r) [T_{AW}(r) - T(r, z=0, t)] + h_{\text{rad}} [T(r, z=0, t) - T_\infty]. \quad (2-9)$$

By applying a scale analysis on the radiation term in Eq. (2-9), it can be deduced that the radiation effects on the temperature distribution within the substrate was negligible. In other words, by incorporating the values of each term in Eq. (2-8), and considering $T_\infty = 21^\circ\text{C}$ (294 K), the radiative heat transfer coefficient will be on the order of one; while the convective heat transfer coefficient of an impinging air jet is expected to be on the order of 10^2 [71]. In light of the aforementioned scale analysis and in order to simplify the problem, the effects of radiation were not considered in the mathematical modeling. Therefore, Eq. (2-4) can be reformulated as

$$-k_s \left[\frac{\partial T(r, z=0, t)}{\partial z} \right] = h(r) [T_{AW}(r) - T(r, z=0, t)]. \quad (2-10)$$

It is well known that the convective heat transfer coefficient depends on the fluid motion on the surface [7]. Since the velocity of the air film over the substrate is expected to vary at different radial positions, the heat transfer coefficient, h , in Eq. (2-10) is considered to be a function of the radius. Green's functions were employed to solve the governing partial differential equation (Eq. (2-1)) along with the initial and boundary conditions. The general solution is expressed in terms of the two-dimensional Green's function as [87]

$$\begin{aligned}
T(r, z, t) = & \int_{r'=0}^b \int_{z'=0}^{\delta} G(r, z, t | r', z', \tau) F(r', z') r' dz' dr' \\
& - \alpha_s \int_{\tau=0}^t d\tau \int_{r'=0}^b G(r, z, t | r', z', \tau) \frac{1}{k_s} f(r', z', \tau)_{z'=0} r' dr',
\end{aligned} \tag{2-11}$$

where F and f represent the non-homogenous initial and boundary conditions of the governing equation, respectively. The Green's function shown in Eq. (2-11) can be obtained by solving Eq. (2-1) when all the non-homogenous boundary conditions are taken to be homogenous, which can be achieved by replacing the non-homogenous terms in the boundary conditions with zero. Using the separation of variables method, the expression for the Green's function is [87]

$$G(r, z, t | r', z', \tau) = \sum_{i=1}^{\infty} \sum_{j=1}^{\infty} \left(\frac{\exp[-\alpha_s (\lambda_i^2 + \beta_j^2) (t - \tau)]}{N(\lambda_i) N(\beta_j)} J_0(\lambda_i r) J_0(\lambda_i r') \right. \\
\left. \times [\tan(\beta_j \delta) \sin(\beta_j z) + \cos(\beta_j z)] [\tan(\beta_j \delta) \sin(\beta_j z') + \cos(\beta_j z')] \right), \tag{2-12}$$

where λ_i and $N(\lambda_i)$ are the eigenvalues and Norm of the differential equation in the radial coordinate ($0 \leq r \leq b$), respectively. The expressions of the eigenvalues and the Norm are given in Eqs. (2-13) and (2-14) as

$$\lambda_i J_1(\lambda_i b) = 0, \tag{2-13}$$

$$N(\lambda_i) = \int_{r=0}^b J_0^2(\lambda_i r) r dr. \tag{2-14}$$

In Eq. (2-12), β_j and $N(\beta_j)$ represent the eigenvalues and Norm of the differential equation in the axial coordinate ($0 \leq z \leq \delta$), respectively, and can be calculated from

$$\beta_j \tan(\beta_j \delta) - \frac{h(r)}{k_s} = 0, \quad (2-15)$$

$$N(\beta_j) = \int_{z=0}^{\delta} [\tan(\beta_j \delta) \sin(\beta_j z) + \cos(\beta_j z)]^2 dz. \quad (2-16)$$

Further details on the mathematical modeling are presented in Appendix A. Due to presence of the radially-dependent heat transfer coefficient in Eq. (2-15), the eigenvalues in axial coordinate are dependent on the radial distance from the stagnation point. Given this dependence, a shooting method was applied in order to calculate the eigenvalues for pointwise values of the heat transfer coefficient. Subsequently, by substituting the Green's function from Eq. (2-12) into Eq. (2-11), the final expression for the temperature distribution within the substrate is found to be

$$\begin{aligned} T(r, z, t) = & \sum_{i=1}^{\infty} \sum_{j=1}^{\infty} \left[T_0 \frac{\exp[-\alpha_s(\lambda_i^2 + \beta_j^2)t]}{N(\lambda_i)N(\beta_j)} J_0(\lambda_i r) [\tan(\beta_j \delta) \sin(\beta_j z) + \cos(\beta_j z)] \right. \\ & \times \int_{r'=0}^b \int_{z'=0}^{\delta} J_0(\lambda_i r') [\tan(\beta_j \delta) \sin(\beta_j z') + \cos(\beta_j z')] r' dz' dr' \\ & + \left(\frac{\alpha_s}{k_s} \right) \left[\frac{h(r)}{N(\lambda_i)N(\beta_j)} \right] J_0(\lambda_i r) [\tan(\beta_j \delta) \sin(\beta_j z) + \cos(\beta_j z)] \\ & \left. \times \frac{1}{\alpha_s(\lambda_i^2 + \beta_j^2)} \left[1 - \exp(-\alpha_s(\lambda_i^2 + \beta_j^2)t) \right] \int_{r'=0}^b J_0(\lambda_i r') T_{AW}(r') r' dr' \right]. \end{aligned} \quad (2-17)$$

Equation (2-17) represents the analytical solution to determine the temperature distribution within the substrate exposed to an impinging hot air jet of a cold spray unit. The heat transfer coefficient is unknown in Eq. (2-17). Thus, experimentally measured temperatures of the front surface of the substrate were used as input into Eq. (2-17) to facilitate determination of the heat transfer coefficient. A zero-dimensional code in MATLAB (MathWorks, Inc., Natick, MA, USA) was developed and an iterative process was conducted that involved Eqs. (2-15) and (2-

17) for the heat transfer coefficient until the analytically determined temperature of the front surface converged to the experimentally measured temperature to within less than 2%. The zero-dimensional MATLAB code is presented in Appendix B.

2.2.1 Propagation of Uncertainty in the Estimation of Heat transfer Coefficient

An uncertainty analysis was performed to determine the error propagation in the semi-empirical analytical heat transfer coefficient in Eq. (2-17). In this equation, the uncertainties of the eight variables, namely, $T(r, z, t)$, $T_{AW}(r)$, T_0 , α_s , k_s , b , δ , and β_j may affect the accuracy of the estimated heat transfer coefficient. The error associated with the thermo-physical properties of the substrate, α_s and k_s , were assumed to be zero, although they might have some errors in practice. These values were not measured and they were acquired from the literature. The dimensions of the substrate, b and δ , and the initial temperature of the substrate were taken to be constant; therefore, the associated errors were assumed to be zero. For both the temperature of the substrate front surface, $T(r, z, t)$, and the adiabatic wall temperature, T_{AW} , which were measured by using an infrared camera, the associated errors (ΔT) were the combination of (i) the bias uncertainty of the camera (ΔT_B), which was provided by the manufacturer as 5% of the reading and (ii) the uncertainty of the repeated experimental measurements (ΔT_E) [88]. The error associated with both the temperature of the substrate and the adiabatic wall temperature can be formulated as

$$\Delta T = \sqrt{\Delta T_B^2 + \Delta T_E^2} . \quad (2-18)$$

The uncertainty of the repeated experimental measurement (ΔT_E) can be obtained by taking into account the standard deviation (SD) for the average of the experimentally-measured surface temperatures as [88]

$$\Delta T_E = \chi \frac{SD}{\sqrt{n}}, \quad (2-19)$$

where n and χ are the number of measurements and the precision coefficient (or t -distribution value), respectively. The t -distribution is symmetric and bell-shaped, and is similar to the Gaussian (normal) distribution. However, the t -distribution has heavier tails, which corresponds to generating values that fall far from the mean value. It has been reported that a value of 2.92 for χ would give a confidence interval of 90% when the number of repetitions of experimental measurements is three [88, 89]. In other words, under the condition of the current study and according to the aforementioned parameters, if the same experimental procedure is used to measure the surface temperature, it is expected that the experimental data will be within the limits bounded by the standard deviation 90% of the time.

According to Eq. (2-15), the eigenvalues in the radial direction are dependent on the heat transfer coefficient. Thus, they would implicitly influence the accuracy of the calculation of the heat transfer coefficient in Eq. (2-17). In order to determine the error of the eigenvalues, an iterative process was performed. In this process, the initial value of the uncertainty of the eigenvalues was taken to be zero in Eq. (2-17), and subsequently, the uncertainty of the heat transfer coefficient was determined. The estimated uncertainty of the heat transfer coefficient was used to modify the error of the eigenvalues that are given by Eq. (2-15). The iterative

process was repeated until the analytically determined value of the uncertainty of the heat transfer coefficient converged to within less than 2% of the previous value.

The propagation of uncertainty in the eigenvalues in the radial direction was derived from Eq. (2-15) as [89]:

$$\frac{\Delta\beta_j}{\beta_j} = \frac{\Delta h}{h} \left(\frac{1}{k_s \sqrt{1 + \left(\frac{\delta \sec^2(\delta\beta_j)}{\tan(\delta\beta_j)} \right)^2}} \right). \quad (2-20)$$

The uncertainty of the heat transfer coefficient of the impinging air jet was determined at a pre-defined location, $(r = 0, z = 0)$, and a specific time, $(t = 1 \text{ s})$, as representative of the spatially and temporally varying heat transfer coefficient. This specific point was chosen since the stagnation point of the impinging air jet at $(r = 0, z = 0)$ is the most desired and complicated point of the jet impingement. The propagation of uncertainty in the determination of the heat transfer coefficient of the impinging air jet was derived as [89]:

$$\frac{\Delta h}{h} = \sqrt{\left(\frac{\Delta U}{U} \right)^2 + \left(\frac{\Delta V}{V} \right)^2}, \quad (2-21)$$

where U and V are defined as,

$$U = k_s [T(r = 0, z = 0, t = 1)], \quad (2-22)$$

$$V = \sum_{i=1}^{\infty} \sum_{j=1}^{\infty} \left(\left(T_0 \frac{\exp(-\alpha_s \lambda_i^2)}{N(\lambda_i)} \int_{r'=0}^b J_0(\lambda_i r') r' dr' \right) \frac{\exp(-\alpha_s \beta_j^2)}{N(\beta_j)} + \left(\frac{b^2 J_0(\lambda_i b)}{2N(\lambda_i)} \right) \left(\frac{1 - \exp(-\alpha_s (\lambda_i^2 + \beta_j^2))}{(\lambda_i^2 + \beta_j^2) N(\beta_j)} \right) T_{AW}(r=b) \right). \quad (2-23)$$

The uncertainty of U corresponds to the uncertainty of the temperature measurement of the infrared camera, and the uncertainty of V in Eq. (2-23) can be calculated from [89]:

$$\Delta V = \sqrt{\sum_{i=1}^{\infty} \sum_{j=1}^{\infty} \left((\Delta V_1)^2 + (\Delta V_2)^2 \right)}, \quad (2-24)$$

where

$$\Delta V_1 = \left(T_0 \frac{\exp(-\alpha_s \lambda_i^2)}{N(\lambda_i)} \int_{r'=0}^b J_0(\lambda_i r') r' dr' \right) \frac{\exp(-\alpha_s \beta_j^2)}{N(\beta_j)} \sqrt{4\alpha_s \beta_j^2 (\Delta \beta_j)^2 + \left(\frac{\Delta N(\beta_j)}{N(\beta_j)} \right)^2}, \quad (2-25)$$

$$\Delta V_2 = \left(\frac{b^2 J_0(\lambda_i b)}{2N(\lambda_i)} \right) \left(\frac{1 - \exp(-\alpha_s (\lambda_i^2 + \beta_j^2))}{(\lambda_i^2 + \beta_j^2) N(\beta_j)} \right) (T_{AW}(r=b)) \times \sqrt{\left(\frac{2\alpha_s \beta_j (\Delta \beta_j) \exp(-\alpha_s (\lambda_i^2 + \beta_j^2))}{1 - \exp(-\alpha_s (\lambda_i^2 + \beta_j^2))} \right)^2 + \left(\frac{2\beta_j (\Delta \beta_j)}{\lambda_i^2 + \beta_j^2} \right)^2 + \left(\frac{\Delta N(\beta_j)}{N(\beta_j)} \right)^2 + \left(\frac{\Delta T_{AW}}{T_{AW}} \right)^2}. \quad (2-26)$$

2.3. Results and Discussion

2.3.1. Determination of the Adiabatic Wall Temperature

The effect of viscous dissipation during the impingement and spreading of a compressible high-velocity air jet upon a substrate will affect the heat transfer coefficient of the air film [90].

Therefore, in order to take into account the effect of dissipation, the adiabatic wall temperature (T_{AW}) also needs to be estimated. Generally, determination of the adiabatic wall temperature requires complex mathematical modelling. The dependence of the adiabatic wall temperature on the thermo-physical properties of the fluid, the flow regime over the substrate, and the temperature distribution profile across the thermal boundary layer of the air film over the substrate increase the complexities of the modelling approach. In other words, incorporating the dissipative effects in the calculations requires knowledge of both the velocity and temperature distribution profiles within the air film boundary layers. Thus, the complexity will arise from non-linear terms in the governing equations of energy and momentum due to the physical coupling of the velocity distribution and temperature distribution profiles within the boundary layers over substrate [7].

In order to eliminate difficulties in the estimation of the adiabatic wall temperature, an experimental method was employed to measure this parameter. This method was based on the fact that the steady-state surface temperature of the substrate under the impinging jet represents the adiabatic wall temperature. The steady-state surface and adiabatic wall temperatures of the substrate were measured by using the infrared camera. Figure 2-3 shows the non-dimensional adiabatic wall temperature as a function of the non-dimensional radial distance from the stagnation point of the air jet on the substrate at different stand-off distances of 15, 25, 50, and 100 mm. As mentioned previously, for each specific location on the substrate, the experimental procedure was repeated three times, and the standard deviation was evaluated for the average of the experimentally-measured surface temperatures, as shown in Fig. 2-3. The standard deviations for all cases were found to be negligible. As observed from Fig. 2-3, the maximum deviation from the average value in the measurements was 4%. For the remaining figures in this chapter

that contained experimental measurements, the standard deviations were negligible as well, and thus, they do not appear in the figures. For the calculation of the error propagation in the analytically-estimated heat transfer coefficient, the standard deviation in Eq. (2-19) was taken to be 4%.

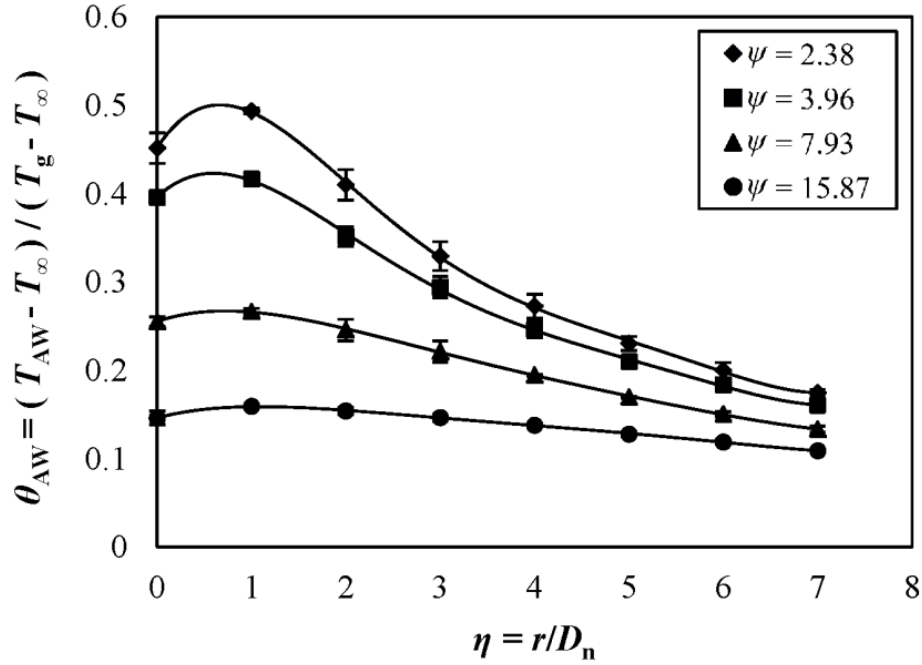


Figure 2-3: Curves of non-dimensional adiabatic wall temperature versus non-dimensional radius of the spreading air jet upon the substrate.

The radius from the stagnation point and the stand-off distance were non-dimensionalized with respect to the nozzle diameter as follows

$$\eta = \frac{r}{D_n}, \text{ and} \quad (2-27)$$

$$\psi = \frac{\text{SOD}}{D_n} \quad (2-28)$$

In order to extend the application of Fig. 2-3, the adiabatic wall temperature was also non-dimensionalized as

$$\theta_{AW} = \frac{T_{AW} - T_{\infty}}{T_g - T_{\infty}}. \quad (2-29)$$

In Eq. (2-29), the gas temperature (T_g) was taken to be 300°C and the ambient air temperature was measured as 21°C. According to Fig. 2-3, for all stand-off distances, the maximum adiabatic wall temperature occurred in the vicinity of the stagnation point of the jet at $\eta \approx 1$, but not at the stagnation point where the impact pressure and physical contact between the jet and the surface is expected to be high. Rahimi, *et al.* [59] have argued that as the jet spreads radially along the substrate due to the expansion of the compressible flow, the radial velocity of the spreading fluid increases and reaches a maximum value in the vicinity of the stagnation point. However, further radial growth of the wall film causes the flow to decelerate [59]. In light of this explanation, and by assuming the no-slip condition and direct contact of the wall jet with the substrate, the local velocity gradient within the boundary layer in the vicinity of the stagnation point becomes substantial. Since the heat generation term due to the viscous (frictional) dissipation effect in the energy conservation equation includes the square of the velocity gradient, the heating due to the frictional dissipation increases locally, resulting in higher adiabatic wall temperature in the vicinity of the stagnation point. Donaldson and Snedeker [58], however, have hypothesized that the maximum temperature in the vicinity of the stagnation point is due to the nature of the flow pattern of the under-expanded jet. At short distances from the nozzle exit, the supersonic jet undergoes a disk shock, resulting in the formation of a subsonic core while the surrounding jet is still supersonic. Impingement of this flow onto a substrate causes a significant pressure increase on the substrate around the stagnation point, while the pressure at the stagnation point is lower

than the surrounding pressure. Therefore, the flow will be directed radially toward the center of the substrate and form a circulating flow in this region [58]. The flow pattern of the impinging air jet over the substrate at small stand-off distances is illustrated in Fig. 2-4 [58]. According to the flow pattern shown in Fig. 2-4, the flow field at the central region on the substrate may behave as a solid body, directing the high temperature air at the center of the jet, not to the stagnation point, but over the periphery of the circulating flow toward a particular point in the vicinity of the stagnation point. As a result, the maximum temperature for small stand-off distances is observed to be approximately at $\eta = 1$.

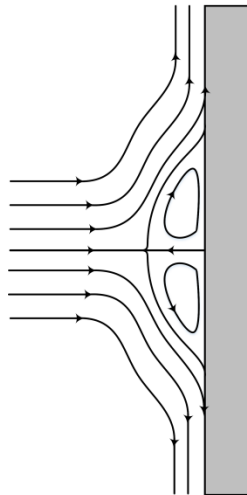


Figure 2-4: The flow pattern of the impinging air jet at small stand-off distances [58].

Figure 2-3 shows that at higher stand-off distances, variations in the adiabatic wall temperature as a function of radial distance from the stagnation point and the maximum adiabatic wall temperature decrease significantly. As Donaldson and Snedeker [58] observed, at higher distances from the nozzle exit, the velocity of the fluid in the jet core was still lower than the surrounding fluid in the jet; however, the velocity difference was insignificant compared to that for smaller distances from the nozzle exit. When the jet impinges onto the substrate, due to these

slight velocity differences within the air jet and as a result of the circulating flow, the pressure differences occurred around the stagnation point are expected to be much smaller than those observed for shorter stand-off distances. Therefore, the radial variation of the adiabatic wall temperature is expected to decrease with stand-off distances. Moreover, as the stand-off distance increases, a greater volume of cold ambient air was entrained and mixed into the hot air jet, resulting in a decrease of the temperature of the air jet. Thus, the maximum adiabatic wall temperature decreased at higher stand-off distances. This was also observed by Rahimi, *et al.* [59] and Ryabinin, *et al.* [71].

As the air film spread over the substrate, due to the deceleration of the spreading air film, the velocity gradient across the film becomes small, resulting in lower heat generation due to viscous dissipation. Therefore, the adiabatic wall temperature of the air film decreases for all stand-off distances, as shown in Fig. 2-3. In order to incorporate the adiabatic wall temperature into Eq. (2-10), the radially varying adiabatic wall temperature curves in Fig. 2-3 were fitted into a fifth order polynomial function to obtain an accurate correlation. The equation for the polynomial function is defined as

$$T_{AW}(\eta) = C_1\eta^5 + C_2\eta^4 + C_3\eta^3 + C_4\eta^2 + C_5\eta + C_6, \quad (2-30)$$

where the coefficients and the regression value (R^2) of Eq. (2-30) is presented in Table 2-1 for each non-dimensional stand-off distance. According to Table 2-1, the regression value (R^2) is almost equal to unity for all the non-dimensional stand-off distances, which suggests that there was good correlation of the curve-fitted polynomial with the experimental data. With knowledge of the adiabatic wall temperature, Eq. (2-17) can be utilized to determine the heat transfer coefficient of the impinging air jet on to the substrate.

Table 2-1: The coefficients and regression values of the fitted adiabatic wall temperature for different stand-off distances.

SOD	C_1	C_2	C_3	C_4	C_5	C_6	R^2
$\Psi = 2.38$	0.081	-1.723	13.55	-46.43	45.68	147.04	0.9997
$\Psi = 3.96$	0.053	-1.122	8.827	-30.3	27.7	131.47	0.9994
$\Psi = 7.93$	0.012	-0.26	2.257	-9.226	10.18	92.15	0.9997
$\Psi = 15.87$	0.008	-0.175	1.415	-5.475	7.741	61.75	0.9992

2.3.2. Determination of the Heat Transfer Coefficient

The shooting method was used to determine the spatially varying heat transfer coefficient in this study. To facilitate the determination of the heat transfer coefficient, the transient temperature of the substrate surface that was exposed to the cold spray air jet was measured with an infrared camera. The correlation equation for the adiabatic wall temperature of Eq. (2-30) and the experimental data for the transient surface temperature were substituted in Eq. (2-17) to determine the heat transfer coefficient. The heat transfer coefficient was estimated at three different non-dimensional times to study the dependence of the heat transfer coefficient on time. It is common to express the heat transfer coefficient as the non-dimensional Nusselt number, defined as

$$\text{Nu} = \frac{hD_n}{k_g} \quad (2-31)$$

The non-dimensional time was defined as the Fourier number (Fo), which is

$$Fo = \frac{\alpha_s t}{\delta^2}. \quad (2-32)$$

Figure 2-5 shows the radial variations of the non-dimensional Nusselt number for three different Fourier numbers at a fixed non-dimensional stand-off distance of $\psi = 2.38$. It should be noted that these Fourier numbers are representative of the system before steady state is achieved. It can be observed in Fig. 2-5 that the estimated profiles for Nusselt number nearly coalesce for all Fourier numbers, which suggests that the heat transfer coefficient of the under-expanded air jet upon the substrate was weakly dependent on time. It is expected that the time that the nozzle remained stationary over the substrate affected the temperature difference between the air film and the substrate, since the surface temperature approached that of the air film over time so as to achieve steady state. Unlike the natural convective heat transfer coefficient, the forced convective heat transfer coefficient is not heavily dependent on the temperature difference between the spreading air film and the substrate. Forced convective heat transfer coefficients are primarily dependent on the velocity of the fluid [7]. It should be noted that, as shown in Fig. 2-6, the fact that the heat transfer coefficient is almost independent of time does not suggest that the heat exchange rate between the air film and the substrate is also independent of time. The heat flux between the air film and the substrate was calculated by using Eq. (2-10) at the same Fourier numbers presented in Fig. 2-5. Figure 2-6 shows the temporal and radial variations of the heat flux on the substrate. Due to the high temperature difference between the spreading air film and the substrate at the early stages of spraying and jet impingement, the heat exchange rate was high. However, as time passed, the surface temperature of the substrate approached the temperature of the air film that flowed over the substrate, thus reducing the heat exchange rate.

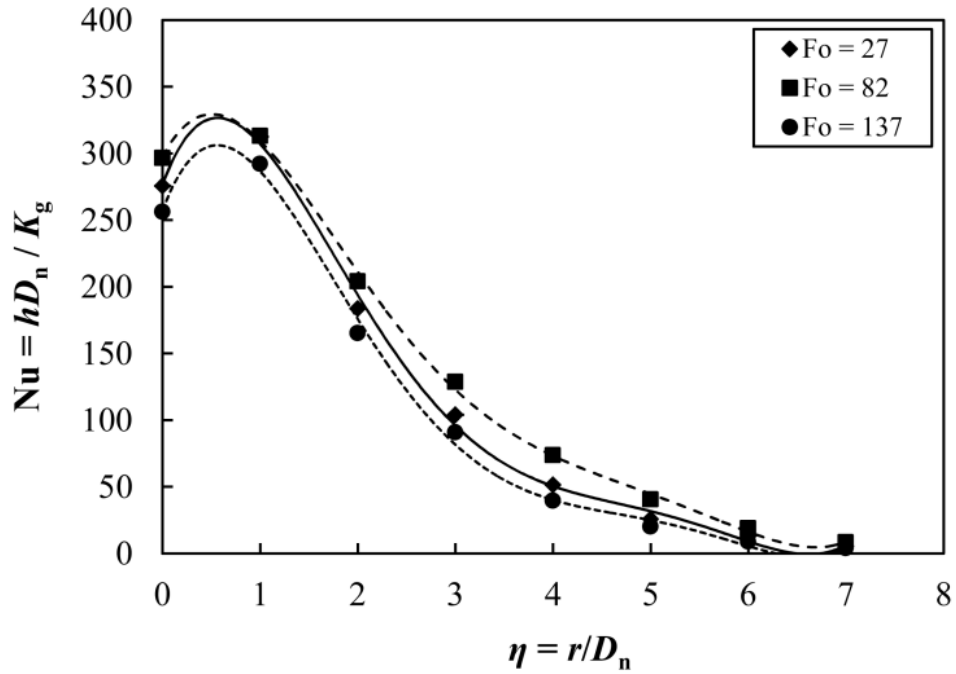


Figure 2-5: Curves of the Nusselt number of the impinging air jet as a function of non-dimensional radial distance from the stagnation point for different Fourier numbers.

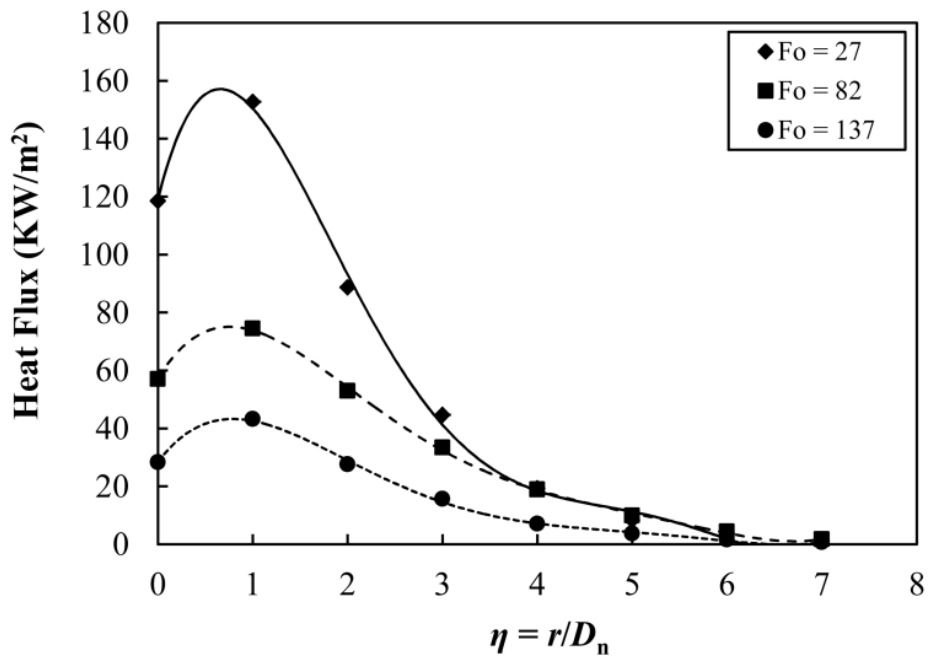


Figure 2-6: Curves of the heat flux between the air film and the substrate as a function of non-dimensional radial distance from the stagnation point for different Fourier numbers.

The maximum Nusselt number of the under-expanding air jet, like the adiabatic wall temperature profile of Fig. 2-3, occurs at approximately $\eta = 1$. It has been shown that the Nusselt number for laminar and turbulent compressible flows is directly proportional to the square root of the velocity of the fluid [90]. Therefore, it is expected that the Nusselt number will show a similar trend as the velocity variations along the wall jet. Accordingly, as shown in Fig. 2-5, after reaching a maximum value at $\eta \approx 1$, the Nusselt number decreases as the wall jet expands along the substrate. The existence of a maximum Nusselt number in the vicinity of the stagnation point may also be justified by considering the generation of turbulence due to the shear layer vortex between the air jet and the ambient air before reaching the substrate, which is transferred to the thermal boundary layer on the surface after impingement of the jet [91]. The exposed turbulence around the stagnation point can result in a local increase in heat transfer coefficient of the impinging air jet upon the substrate at short radial distances around the stagnation point. Fundamental theories by Reynolds [92] and Colburn [93] have shown that turbulent flows over flat plates produce higher skin friction coefficients, resulting in increased heat transfer coefficients. Further explanations will be provided in Chapter 3 of this thesis document.

An uncertainty analysis was conducted to predict the error propagation during estimation of the heat transfer coefficient of the impinging air jet. As mentioned, the estimated heat transfer coefficient at the stagnation point at ($r = 0, z = 0$) and at an arbitrary time ($t = 1$ s, or $Fo = 27$) was taken to be the representative of the spatially varying heat transfer coefficient. An arbitrary time was chosen since it has been shown in this study that the heat transfer coefficient was nearly independent of time. The results of the uncertainty analysis indicated that the semi-empirical analytical model for the heat transfer coefficient resulted in an error of 6.76%, which suggested that the uncertainty in the heat transfer coefficient values were mainly influenced by the error in

the temperature measurements of the infrared camera. The propagation of the error of the eigenvalues in the radial direction was found to be negligible, since according to Eq. (2-23), the small errors inherent in these terms were squared, which resulted in even smaller errors. The uncertainty in the dimensions of the substrate and the thermo-physical properties of the substrate were assumed to be zero in these calculations; however, they are likely expected to have negligible errors associated with them compared to the large uncertainties in the readings of the infrared camera.

2.3.3. Effect of the Nozzle Stand-off Distance on the Heat Transfer Coefficient

The semi-empirical analytical method of this study was further employed to study the effect of the nozzle stand-off distance on the heat transfer coefficient of the impinging air jet. Figure 2-7 presents the radial variations of the Nusselt number at different stand-off distances for $Fo = 27$. The data points were fitted with a fifth order polynomial curve to facilitate the comparison between results for each stand-off distances. As shown in Fig. 2-7, both the maximum Nusselt number and the radial variations of the Nusselt number decrease with the stand-off distance. Moreover, at higher radial distances from the stagnation point of the air jet, the estimated Nusselt number was observed to be greater for higher stand-off distances. These observations can be explained by illustration of Fig. 2-8, which was extracted from a study by Zuckerman and Lior [86]. As shown in Fig. 2-8, due to the entrainment of the surrounding ambient air into the air jet and viscous diffusion of momentum at the shear layer of the jet, the mass flow of the jet increases, resulting in spatially widening of the velocity profile of the jet and decreasing the magnitude of the maximum velocity within the air jet [86]. As the stand-off

distance increases, the magnitude of the maximum velocity within the air jet decreases; thus reducing the impact force of the jet onto the surface. Lower impact force results in a slower wall jet velocity along the substrate. Since the heat transfer coefficient of the wall jet directly relates to the flow velocity, the maximum Nusselt number decreases, as the stand-off distance increases. Moreover, due to the radially widening of the velocity profile in the air jet, a wider region of the substrate is affected by the direct impingement of the air jet, as the stand-off distance increases. Therefore, for higher stand-off distances, the wall jet velocity, and as a result the heat transfer coefficient, at higher radial distance from the stagnation point is expected to be greater than those for smaller stand-off distances. In addition, as the air jet widens, the generated turbulence by the shear layer vortices between the jet and the ambient air becomes larger. Subsequently, the turbulence effect will be pronounced at further radial distance from the stagnation point, thereby higher Nusselt number in this region.

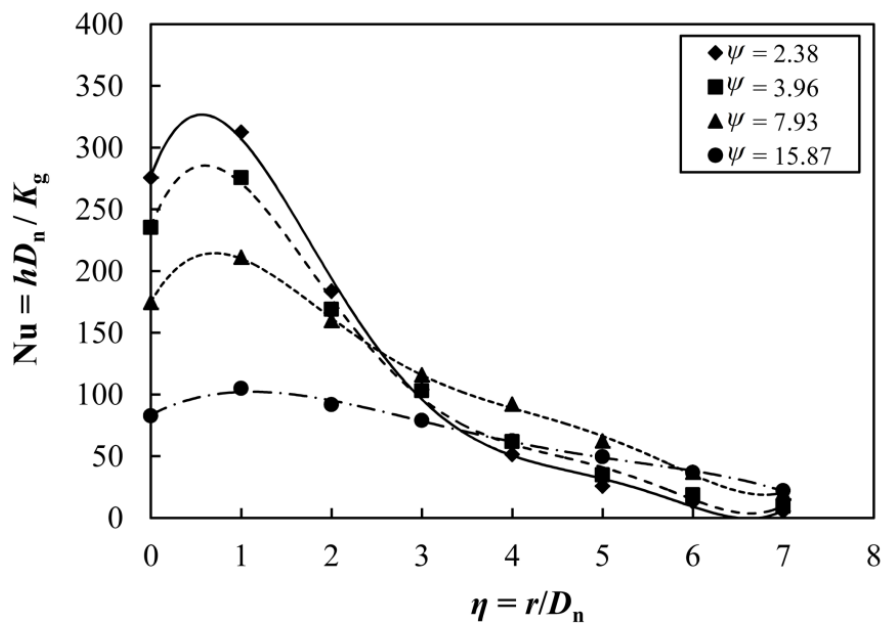


Figure 2-7: Curves of the Nusselt number of the impinging air jet as a function of non-dimensional radial distance from the stagnation point for different non-dimensional stand-off distances.

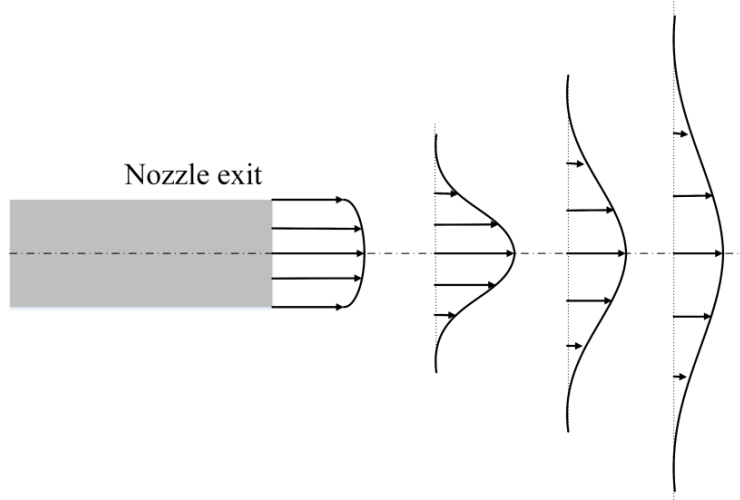


Figure 2-8: Schematic of the axial velocity distribution of the air jet [86].

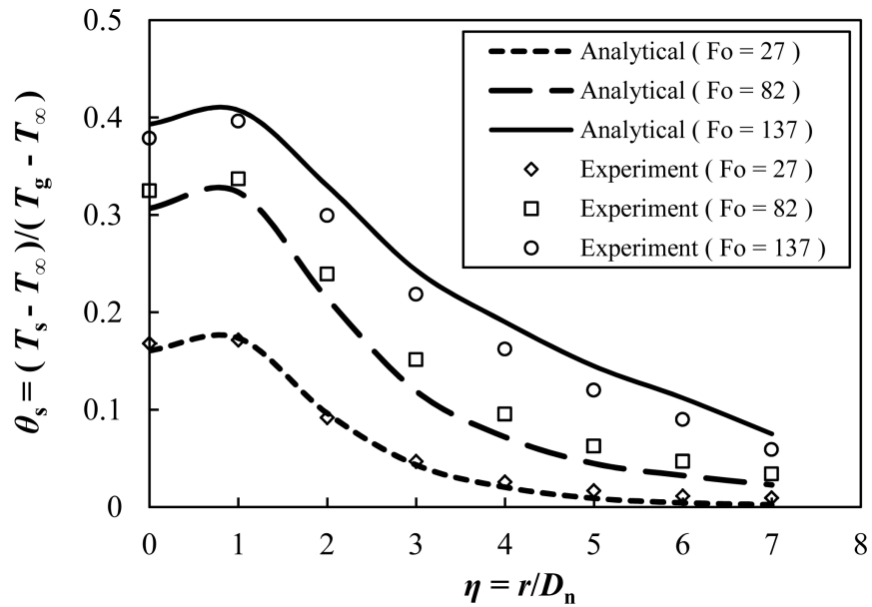
2.3.4. Verification of the Semi-Empirical Analytical Model

In order to validate the results of the heat transfer coefficient estimated from the proposed model, the heat transfer coefficient that was estimated at $Fo = 27$ was substituted into Eq. (2-17). The non-dimensional surface temperature distribution was calculated at Fourier numbers of 27, 82, and 137 and non-dimensional stand-off distances of 2.38, 3.96, 7.93, and 15.87. Similar to the adiabatic wall temperature, the surface temperature was non-dimensionalized as

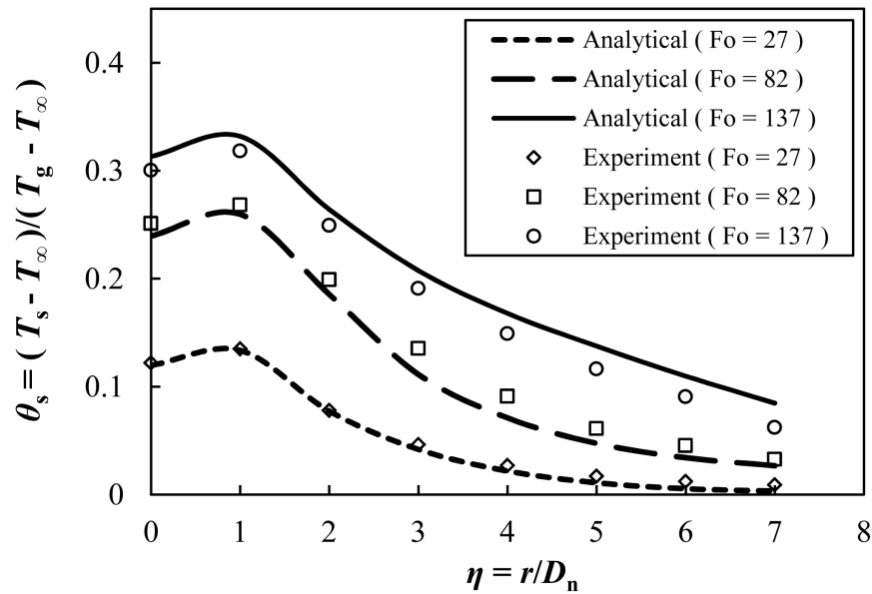
$$\theta_s = \frac{T_s - T_\infty}{T_g - T_\infty}. \quad (2-33)$$

The transient surface temperature of the substrate was measured experimentally. The results of the semi-empirical analytical model were then compared to the experimental results. Figure 2-9 shows a comparison of the predicted and experimentally measured non-dimensional surface temperatures for different stand-off distances. According to Fig. 2-9, the results from the semi-empirical analytical model were in good agreement with the experimental results. Even though

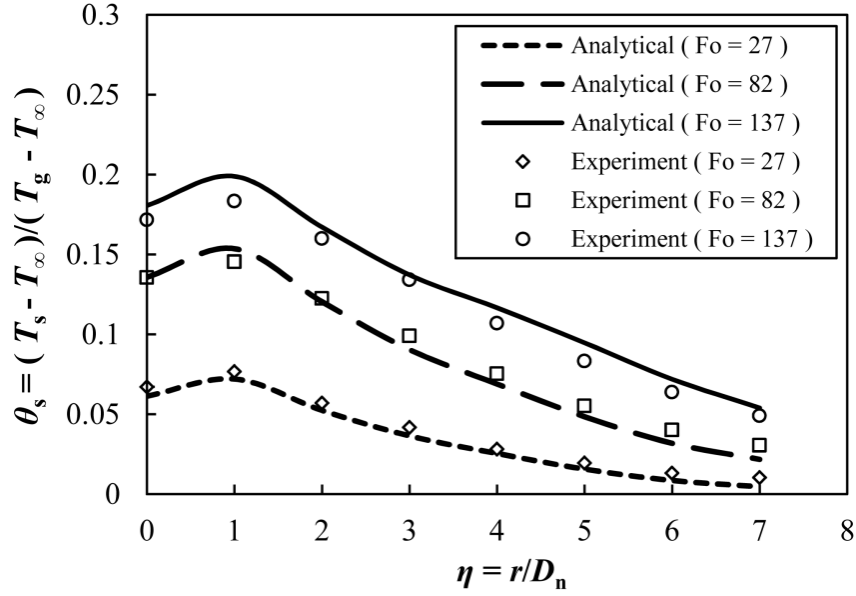
the heat transfer coefficient which was used in calculations was measured at $Fo = 27$, the results of the analytical model for higher Fourier numbers also coalesced closely with the experimental results, which confirmed that the heat transfer coefficient of an impinging air jet upon the substrate was independent of time.



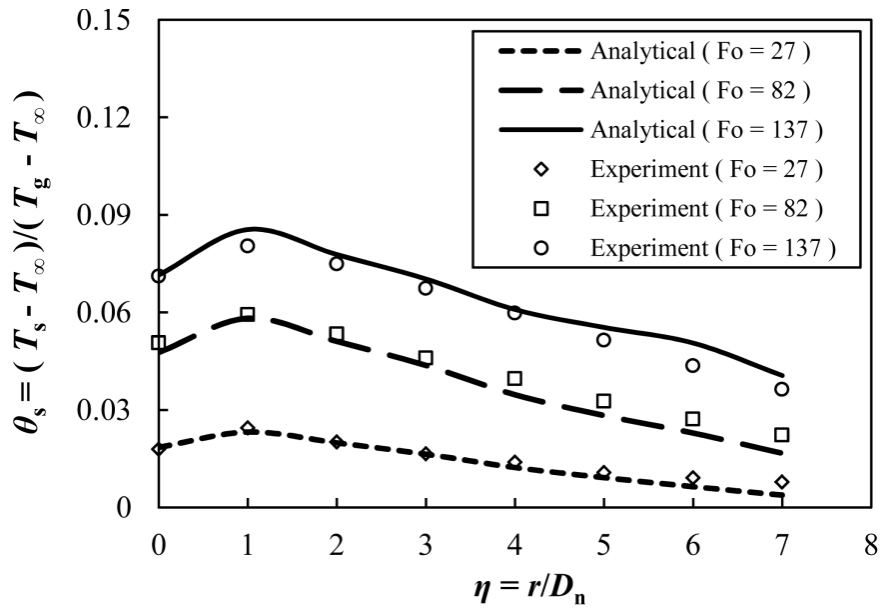
(a)



(b)



(c)



(d)

Figure 2-9: Non-dimensional surface temperature variation of the substrate at a) $\psi = 2.38$, b) $\psi = 3.96$, c) $\psi = 7.93$, and d) $\psi = 15.87$.

CHAPTER 3

Effect of Substrate and Process Parameters on the Gas-Substrate Heat Transfer Coefficient during Cold Spraying

The final quality of cold-sprayed coatings can be significantly affected by gas-substrate heat exchange, due to the dependence of the deposition efficiency of the particles on the substrate temperature distribution. In this chapter, the effect of the air temperature and pressure, as process parameters, and surface roughness and thickness, as substrate parameters, on the heat transfer coefficient of the impinging air jet was investigated. A low-pressure cold spraying unit was used to generate a compressed air jet that impinged on a flat substrate. The comprehensive mathematical model that was developed and coupled with experimental data to estimate the heat transfer coefficient and the surface temperature of the substrate was utilized. The effect of the air total temperature and pressure on the heat transfer coefficient was studied. The model and the experiments were further used to investigate the effect of the thickness and the roughness of the substrate on the heat transfer coefficient. The results of the current study were aimed to inform on the influence and effect of substrate and process parameters on the gas-substrate heat exchange and the surface temperature of the substrate on the final quality of cold-sprayed coatings.

Some sections of the work presented in this chapter have been published in A. Mahdavi, A. McDonald, “Effect of Substrate and Process Parameters on the Gas-Substrate Convective Heat Transfer Coefficient during Cold Spraying”, *J. Therm. Spray Technol.*, 2018, 27, 433-445; and A. Mahdavi, A. McDonald, “The Effect of Substrate Roughness on the Heat Transfer

Coefficient of an Impinging Cold Spray Air Jet”, in: *International Thermal Spray Conference (ITSC 2017)*, June 7-9, 2017 (Düsseldorf, Germany), ASM International, (2017), # 5171, 6 pages on compact disk.

Nomenclature

A	Surface area	\bar{V}	average velocity (m/s)
b	diameter of the substrate (m)	z	axial coordinate
c	speed of sound (m/s)	Z	compressibility factor
C_p	specific heat capacity (J/K)	z'	axial dummy variable (m)
C_f	skin friction coefficient		
D	cold spray nozzle diameter		<i>Non-dimensional parameters</i>
h	heat transfer coefficient (W/m ² -K)	Fo	Fourier number,
I	intensity of emitted radiation (W/sr-Hz)	Ma	Mach number,
J	Bessel function	Nu	Nusselt number,
k	thermal conductivity (W/m-K)	Re	Reynolds number,
N	Norm of the differential equation		
P	total pressure (Pa)		<i>Greek symbols</i>
\dot{Q}	Heat transfer rate	α	thermal diffusivity (m ² /s)
r	radial coordinate	β	eigenvalues in axial coordinate
R	surface roughness	δ	thickness of the substrate (m)
\bar{R}	gas constant (J/kg-K)	ε	emissivity
r'	radial dummy variable (m)	ζ	eigenvalues in radial coordinate
t	time (s)	η	non-dimensional radius
T	temperature / total temperature (°C)	θ	non-dimensional temperature
T_0	substrate initial temperature (°C)	λ	Wavelength (μm)
u'	Fluctuating component of velocity	μ	dynamic viscosity (kg/m-s)
\bar{u}	mean velocity	ρ	density (kg/m ³)
V	velocity (m/s)	τ	shear stress (N/m ²)

Subscripts

a	air	ku	kurtosis
ave	average	m	mean
AW	adiabatic wall	n	nozzle
b	black body	s	substrate / surface
e	real surface	sk	skewness
g	propellant gas	ss	steady-state
i	numerator in radial coordinate	w	wall
j	numerator in axial coordinate	∞	ambient

3.1. Experimental Procedure

3.1.1. Low-Pressure Cold Spray System

A low-pressure cold gas dynamic spraying unit (SST Series P, Centerline, Ltd., Windsor, ON, Canada) was utilized to produce a supersonic air jet. The details on the nozzle of the cold spray unit were described in Section 2.1.1 of Chapter 2 of this dissertation. In order to study the effect of the pressure and the temperature of the air jet, a range of the aforementioned parameters were used. The system parameters of the low-pressure cold spray unit that were used in this study are summarized in Table 3-1. The cold spray nozzle was directed at the center of the front surface of the substrate and was held stationary at the specified stand-off distance.

Table 3-1: Low-pressure cold spray system parameters.

Pressure range	660 – 830 kPa (96 – 120 psig)
Temperature range	100 – 300°C
Stand-off distance (SOD)	25 mm

3.1.2. Substrate Preparation

In this study, aluminium 6061-T6 was used as the substrate. Details on the material and its dimension were provided in Section 2.1.2 of Chapter 2. In order to investigate the effect of the thickness of the substrate, a range of the substrate thickness as 1.5, 2.5, or 6.5 mm was utilized. In order to prevent the back surface of the substrate from exchanging heat with the ambient air, the back surface was insulated, similar to the experimental procedure described in Section 2.1.2 of Chapter 2. In order to study the effect of the substrate roughness on the heat transfer coefficient and surface temperature of the substrate, the cold spray unit was used to grit-blast the 2.5 mm thick aluminium substrate by depositing garnet sand particles (Super Garnet, V.V. Mineral, Tamil Nadu, India). The morphology of the garnet sand particles was examined by using a scanning electron microscope (EVO MA 12, Zeiss, Cambridge, UK) that was set in the secondary electron mode. Figure 3-1 shows the morphology of the garnet sand particles. By using the image analysis software (ImagePro, Media Cybernetics, Bethesda, MD, USA), the average diameter of the garnet sand particles was measured to be $340 \pm 54 \mu\text{m}$ ($n = 5$), where n represents the number of particles. A confocal scanning microscope (Axio CSM 700, Carl Zeiss MicroImaging GmbH, Jena, Germany) was employed to study the topology and the roughness parameters of the grit-blasted substrate.

3.1.3. Temperature Measurements

The transient and steady-state temperatures of the front surface of the substrate were measured by using a calibrated infrared camera (FLIR A65, FLIR Systems, Inc., Nashua, NH, USA). Information on the infrared camera that was used in this study was presented in Section 2.1.3 of Chapter 2.

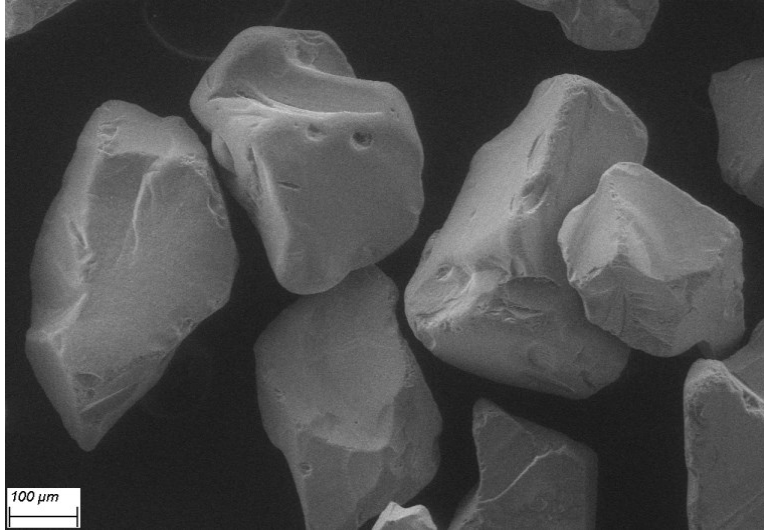


Figure 3-1: Morphology of the garnet sand particles.

In the case of smooth (polished) substrates, to ensure accurate measurements, the front surface of the substrate was painted black so as to approach conditions of a black body. Accordingly, the emissivity of the substrate was set to a constant value of 0.96 on the infrared camera. However, for the grit-blasted (roughened) substrate, it was not reasonable to paint the front surface, since the black paint would fill the asperities of the substrate and cause the rough surface to become smooth. Therefore, in order to measure the surface temperature of the roughened surface by using the infrared camera, the emissivity of the rough substrate was first evaluated. To this end, an experiment was conducted to measure the temperature-dependent emissivity of the rough aluminium substrate. A substrate holder was fabricated from copper, where two cartridge heaters (50 W Miniature High Temperature Cartridge Heater (D $\frac{1}{8}$ " \times $1\frac{1}{4}$ "), McMaster-Carr, Aurora, OH, USA) were embedded inside the copper holder. A temperature controller (CNI8A42, Omega Engineering Inc., Stamford, CT, USA) that was equipped with a J-type thermocouple was employed to adjust the temperature of the substrate holder to the desired set-point [8]. The assembly was used to heat the rough substrate. The surface temperature of the

substrate was measured by using an external J-type thermocouple. Simultaneously, the infrared camera was directed at the substrate. The emissivity that was indicated on the infrared camera was modified until the temperature measurement on the infrared camera read-out panel was in accord with the measurement of the thermocouple. Figure 3-2 shows a schematic of the experimental assembly that was used to measure the emissivity of the rough substrate.

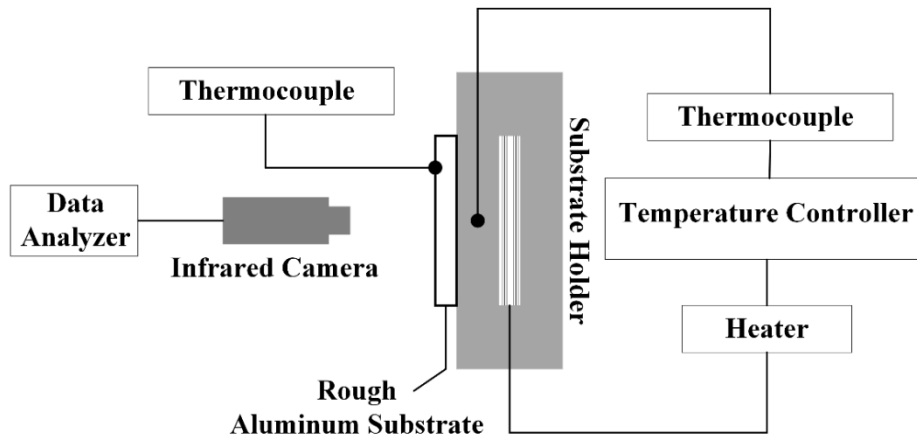


Figure 3-2: Schematic of the experimental assembly for measuring the emissivity of rough aluminium substrate [8].

3.2. Mathematical Model

Details about the mathematical modelling to estimate the heat transfer coefficient of the impinging air jet on a flat substrate were discussed in Section 2.2.1 of Chapter 2 of this dissertation. The results and discussion that will be presented in this Chapter are based on the semi-empirical analytical heat transfer coefficient and temperature distribution within the substrate exposed to an impinging hot air jet of a cold spray unit. A detailed description on the prediction of the heat transfer coefficient and the temperature distribution within the substrate are presented in Chapter 2.

3.3. Results and Discussion

3.3.1. *Effect of Process Parameters on the Heat Transfer Coefficient*

The radial variation of the heat transfer coefficient between the flat substrate and the impinging under-expanding supersonic air jet was estimated under various combinations of the air total pressure and total temperature of the gas jet. By definition, the total pressure represents the pressure of the air when it is adiabatically brought to rest, and it refers to the pressure of the air before it enters the converging-diverging nozzle. Similarly, the total temperature is defined as the air temperature before it enters the nozzle [94]. The thickness of the substrate was 1.5 mm. It was shown that the heat transfer coefficient of the under-expanding air jet is time-independent. In other words, the time that the nozzle remained stationary over the substrate would not affect the heat transfer coefficient of the impinging air jet. However, the temperature difference between the air film and the substrate can be affected by the duration of the impingement of the air jet over the substrate. The heat transfer coefficient is heavily dependent on the velocity of the under-expanding air jet, and since the velocity of the impinging jet is almost constant, the heat transfer coefficient would likely remain unchanged during the impingement of the air jet. Therefore, the heat transfer coefficient was estimated at an arbitrary time after the nozzle had been held stationary over the substrate. For most of the scenarios that were explored in this chapter, the heat transfer coefficient was estimated at $Fo = 81$. This value of Fo was calculated after 3 seconds of the nozzle remaining stationary over the substrate to ensure that the measurements of the surface temperature profile were obtained before reaching the steady-state condition in order to take into account the effect of time. The reason of measuring the surface temperature before reaching steady-state condition was to validate the capability of the model to

determine the surface temperature of the substrate at any desired time after impingement of the cold spray air jet. Similar to Chapter 2, the heat transfer coefficient was presented in the form of the non-dimensional Nusselt number.

The effect of the total pressure of the air jet on the Nusselt number of the impinging and spreading air jet was investigated. The total temperature of the air was set to 200°C on the cold spray unit console. Figure 3-3 shows the Nusselt number as a function of the non-dimensional radial distance from the stagnation point of the jet on the substrate at total pressures of the air of 660, 745, and 825 kPa. The radial distance from the stagnation point was non-dimensionalized with respect to the nozzle diameter as

$$\eta = \frac{r}{D_n} \quad (3-1)$$

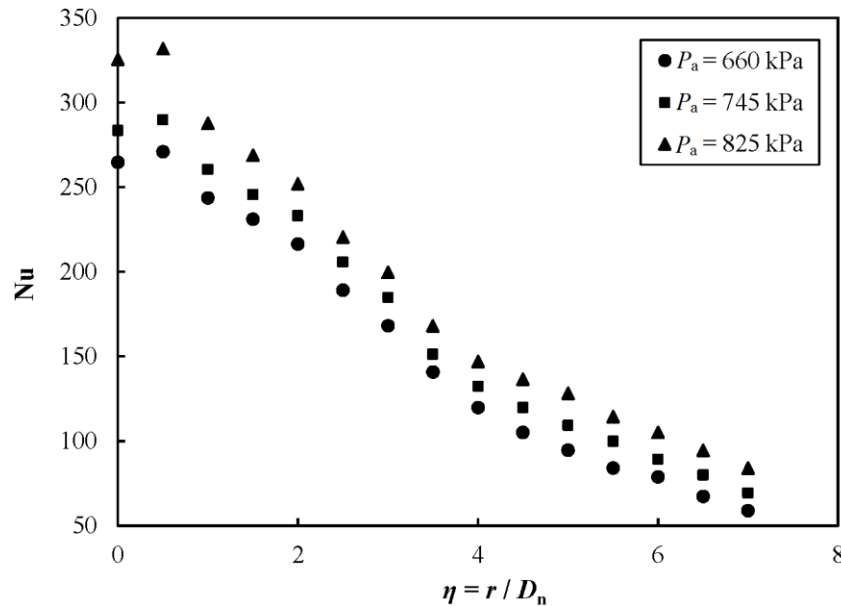


Figure 3-3: Radial variation of the Nusselt number of the under-expanding air jet over the substrate for different total pressures of the air jet

Figure 3-3 shows that the Nusselt number of the impinging air jet on the substrate increased as the total pressure of the air jet increased. This is likely related to the notable effect of the air pressure on the density of the air, which was the working fluid in this study. According to the equation of state of a real gas at constant temperature, the density of the air will increase with increasing air pressure. The equation of state of a real gas is [95]

$$P = Z\rho\bar{R}T, \quad (3-2)$$

where Z is the compressibility factor of the working gas. As a result of the increase in the density of the air, the momentum of the air jet increases. Given that the momentum of the gas will likely decrease as the jet impacts and spreads on the surface, the change in momentum will manifest itself as an increase in inertial force. Thus, the Reynolds number of the air jet will increase. By definition, the Reynolds number is the non-dimensional ratio of the inertial force and the viscous force within the fluid, and for an impinging jet it is expressed as

$$\text{Re} = \frac{\rho_a V_a D_n}{\mu_a}. \quad (3-3)$$

It has been reported that the Nusselt number for both laminar and turbulent compressible flow is directly proportional to approximately the square root of the Reynolds number of the fluid [90]. In light of the proportional relationship between the air pressure, air density, the Reynolds number, and the Nusselt number, it can be deduced that the increase in the gas pressure would increase the Nusselt number between the substrate and the air jet. Other air properties that affect the Nusselt number, such as thermal conductivity, dynamic viscosity, and Prandtl number are not noticeably dependent on the air pressures that are utilized during cold spraying [96].

The effect of the total temperature of the air on the Nusselt number of the impinging air jet was investigated. The total pressure of the air was set to 660 kPa on the cold spray unit console. Figure 3-4 presents the radial variation of the non-dimensional Nusselt number for three different air temperatures of 100, 200, and 300°C. The estimated profiles for the Nusselt number in Fig. 3-6 nearly coalesced for all air temperatures. Increasing the total temperature of the air decreased the density and increased the dynamic viscosity of the air [95], which directly corresponds to lower inertial force and higher viscous force of the impinging air jet. Therefore, it is expected that the Reynolds number of the impinging air jet, and as a result, the Nusselt number of the impinging air jet, decreased. But, along with the two aforementioned outcomes, increasing the total temperature of the air will increase the velocity of the air jet. In order to have supersonic air flow at the converging-diverging nozzle exit, the Mach number of the air at the location of the nozzle throat must be unity ($Ma = \frac{V_a}{c} = 1$) [94]. Since the speed of sound increases with an increase in the air temperature [95], the velocity of the air must increase in order that the Mach number at the nozzle throat remains constant at unity. The velocity of the air at the nozzle throat for a supersonic air jet is formulated as

$$V_a = \sqrt{\gamma \overline{RT}_a} . \quad (3-4)$$

It is expected that the increase in air velocity, as a result of the increase in the air temperature, would neutralize the effects of the reduction in inertial force, which was due to the decrease in the air density. Therefore, the Reynolds number of the air jet would not change significantly by increasing the total temperature of the air. Accordingly, the radial variation of the Nusselt number of the under-expanding air jets nearly coalesced as observed in Fig. 3-4.

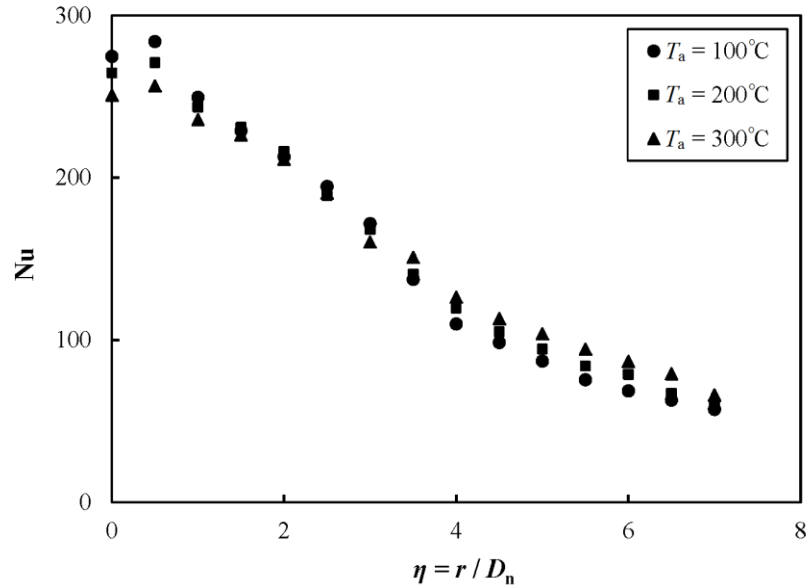


Figure 3-4: Nusselt number of the under-expanding air jet over the substrate versus non-dimensional radius for different total temperatures of air

Although the Nusselt number of the impinging air jet is independent of the total temperature of the air, this does not suggest that the heat transfer coefficient between the substrate and the impinging air jet is weakly dependent on the total temperature of the air. It is hypothesized that the dependence of the thermal conductivity of the air on its temperature would compensate for the changes in the heat transfer coefficient of the impinging air jet as a result of increasing the total temperature of the air. Therefore, the heat transfer coefficient at total temperatures of air of 100, 200, and 300°C for different radial distances from the stagnation point of the jet on the substrate was determined, as shown in Fig. 3-5. The results show that the heat transfer coefficient between the substrate and the impinging air jet increased slightly, as the total temperature of the air increased. This was due to the strong dependency of the heat transfer coefficient on the velocity of the air [90]. Taking into account Figs. 3-4 and 3-5, it can be inferred that studying the heat transfer coefficient may be more effective in investigating the heat

exchange between the substrate and the impinging air, especially when the thermo-physical properties of the working gas are highly dependent on process parameters such as temperature.

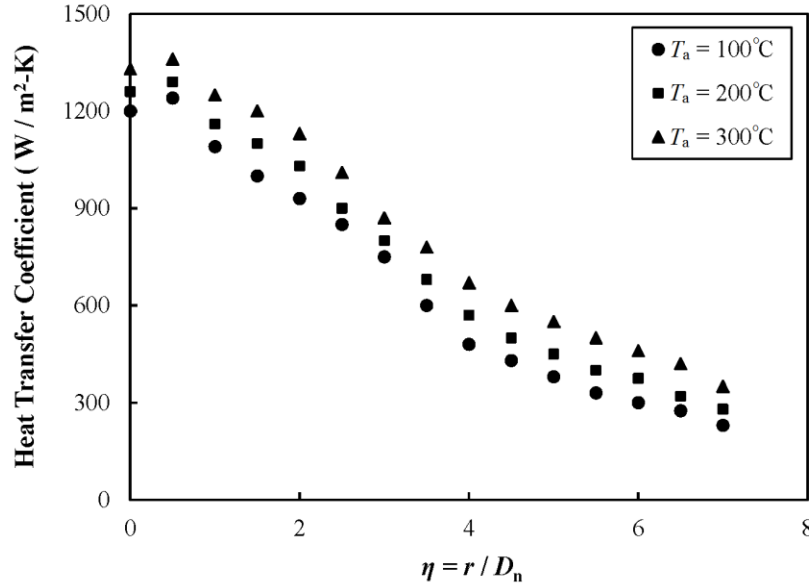


Figure 3-5: Heat transfer coefficient of the under-expanding air jet over the substrate versus the non-dimensional radius for different total temperatures of air.

3.3.2. Effect of Substrate Parameters on the Heat Transfer Coefficient

In order to improve the mechanical interlock between the substrate and the deposited coating during cold spraying, the substrate may be conventionally roughened by employing a surface preparation technique such as grit blasting or shot peening. These techniques are also used to decrease or remove the oxide layer that inherently grows on metal substrate surfaces to allow for further improvement of the adhesion of the coating on the substrate [97]. Increasing the roughness of the substrate may also affect the heat exchange between the substrate and the impinging air jet of the cold spray system, since it changes the surface topology from which the heat transfer occurs. Therefore, the effect of the surface roughness on the surface temperature

profile of the substrate and the heat transfer coefficient between the substrate and the impinging air jet was investigated. To that end, the cold spray unit was utilized to blast garnet sand particles onto the aluminium 6061-T6 substrate to roughen the surface. A confocal microscope was used to study and evaluate the topology and roughness parameters of the smooth and roughened substrates within a surface scan area of $1150 \times 1150 \mu\text{m}^2$ from the front surface of the substrate.

Figure 3-6 compares the surface topologies and the peaks and valleys of the asperities of the smooth and the roughened (grit-blasted) substrates. The contour bar on the left hand side of Fig. 3-6 shows the magnitude of the asperities on the smooth and rough substrates. The maximum values of the contour bars are different for the images. As shown in the figure, the magnitude of the peaks and valleys of the asperities on the rough (grit-blasted) surface is significantly higher than that on the smooth substrate. Three roughness parameters of the substrate, namely average roughness (R_{ave}), skewness (R_{sk}), and kurtosis (R_{ku}) [98] were investigated in order to provide a better understanding of the results shown in Fig. 3-6. By definition, the average roughness (R_{ave}) is the average of the distance of the asperities from a hypothetical mean plane. Skewness (R_{sk}) is defined to show the symmetry of the peaks and valleys of the asperities with regards to the hypothetical flat plane. Surfaces with positive R_{sk} have relatively high peaks, while surfaces with negative R_{sk} have deep valleys and fairly smoother plateaus [99]. Kurtosis (R_{ku}) represents the degree of pointedness of the asperities on the front surface. Surfaces with higher values of R_{ku} exhibit steep asperities; as the R_{ku} becomes smaller, the surface becomes smoother [99]. Table 3-2 shows the values of the aforementioned roughness parameters for both the smooth and rough aluminium substrates that were used in this study.

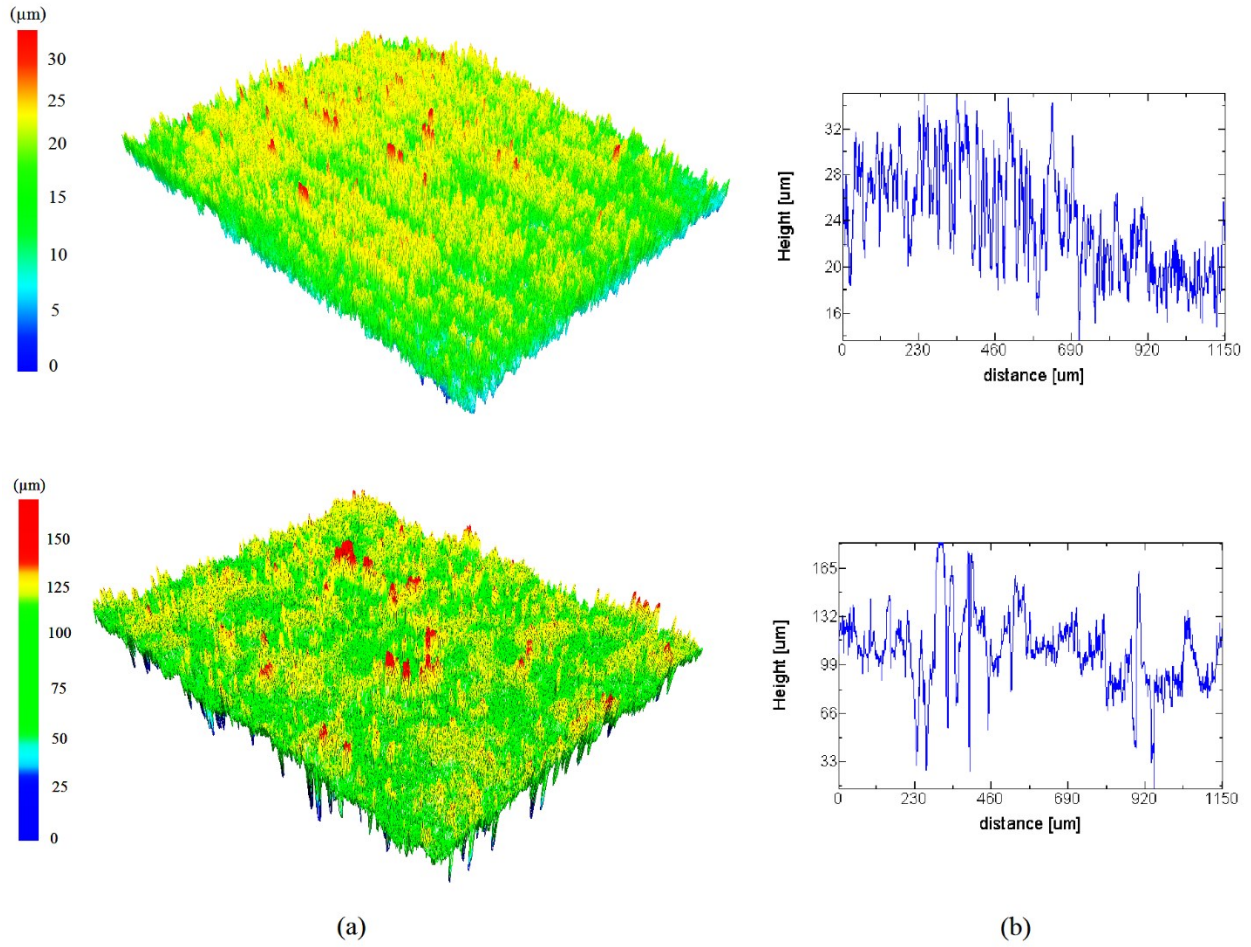


Figure 3-6: (a) 3-D representation of the surface topology and (b) cross-sectional profile of the front surface of the smooth (top) and rough (grit-blasted) (bottom) aluminium 6061-T6 substrates.

Table 3-2: Average roughness, skewness, and kurtosis of the smooth and the rough (grit-blasted) aluminium 6061-T6 substrates.

Aluminium 6061-T6 substrate	R_{ave} (μm)	R_{sk}	R_{ku}
Smooth	3.33	0.39	2.51
Rough (grit-blasted)	13.93	-0.59	5.28

According to the results presented in Fig. 3-6 and Table 3-2, grit-blasting significantly increased the average roughness of the substrate and created steep asperities on the surface of the substrate, as evidenced by the increase in R_{ku} . The negative value of skewness of the substrate after grit-blasting indicates that the grit-blasted surface consisted of deep valleys with smooth plateaus. There was also a greater number of asperities on the rough surface and their heights were larger than those on the smooth surface. This can be related to the physical structure of the garnet sand particles. As shown in Fig. 3-1, garnet sand consisted of particles with smooth and rounded edges. The rounded shape of the particles highly tends to generate surfaces with deep valleys, rather than pointed and sharp peaks after deposition on the substrate. With knowledge of the surface topology of the substrates, a qualitative comparison of the gas-substrate heat transfer coefficient between the smooth and rough substrate can be made.

It is likely that the increased roughness of the substrate would result in an increase in heat transfer coefficient between the impinging air jet and the substrate. Increasing the roughness of the substrate would likely result in higher magnitudes of the velocity fluctuations within the boundary layer of the impinging, spreading jet over the substrate because of tripping of the boundary layer flow that may occur. It was experimentally reported that roughness with heights of 15% to 25% of the boundary layer thickness increased both the longitudinal and vertical components of the velocity fluctuations [100]. As a result, the turbulence intensity of the flow, T_u , would increase, since it is defined as the ratio of the root-mean-square of the fluctuating velocity component and the mean velocity of the flow. The ratio is expressed as [100]:

$$T_u = \frac{\left(\overline{u'^2}\right)^{1/2}}{\bar{u}_m} . \quad (3-5)$$

Higher values of turbulence intensity and greater velocity fluctuation will produce higher shear stress in the turbulent flow over the substrate. Increased shear stress induced by the fluid on the substrate will be due to the increased velocity gradients, and momentum transfer by eddies within the turbulent boundary layer. A fundamental study by Reynolds [92] has shown that the heat transfer between the flow and the substrate is directly proportional to the fluid shear stress on the substrate. The aforementioned theory, known generally as the Reynolds analogy between shear stress and heat transfer, is expressed as [90]:

$$\frac{\bar{h}}{\rho \bar{u}_m C_p} = \frac{C_f}{2}, \quad (3-6)$$

where \bar{h} is the average heat transfer coefficient. In Eq. (3-6), C_f is the skin friction coefficient and it is defined as [90]:

$$C_f = \frac{\tau_w}{0.5 \rho \bar{u}_m^2}. \quad (3-7)$$

The Reynolds analogy is a simplified model that may be used as a first approximation of the heat transfer coefficient of and heat transfer from turbulent boundary layer flows over flat plates. The analogy is based on the assumption that the Prandtl number is unity. For air, the Prandtl number is approximately 0.71, which is close to unity. With the exception of the stagnation point where the air jet impacts the surface, it can reasonably be assumed that the jet that spreads radially over the surface does so as flow over a flat plate surface. Since increasing the roughness of the substrate would produce higher skin friction coefficient, resulting in an increase in heat transfer coefficient, this would in turn increase heat exchange between the air jet and the substrate. As a result of the increased heat exchange between the under-expanding air jet and the substrate,

higher surface temperatures of the roughened substrate are expected. In order to confirm the aforementioned hypothesis, the steady-state surface temperatures of both smooth and rough substrates were measured by using an infrared camera. Since the measurement of the infrared camera was dependent on the emissivity of the surface, the emissivity of the roughened aluminium substrate was first obtained experimentally.

Emissivity, ε , is the ratio of the intensity of emitted radiation from a surface to that emitted from a black body at a specific temperature. The radiation emitted from the real surface and the black body depends on both wavelength and the surface temperature [101]. The maximum wavelength emitted from the surface, directly depends on the surface temperature, according to Wien's displacement law that $\lambda_{\max}T = 2,898 \mu\text{m}\cdot\text{K}$ [7]. Therefore, the emissivity of the surface depends on the surface temperature. In order to measure the surface temperature of the grit-blasted substrate by using the infrared camera, the temperature-dependent emissivity of the substrate had to be evaluated first. Figure 3-7 shows the emissivity of the grit-blasted aluminium substrate as a function of the surface temperature.

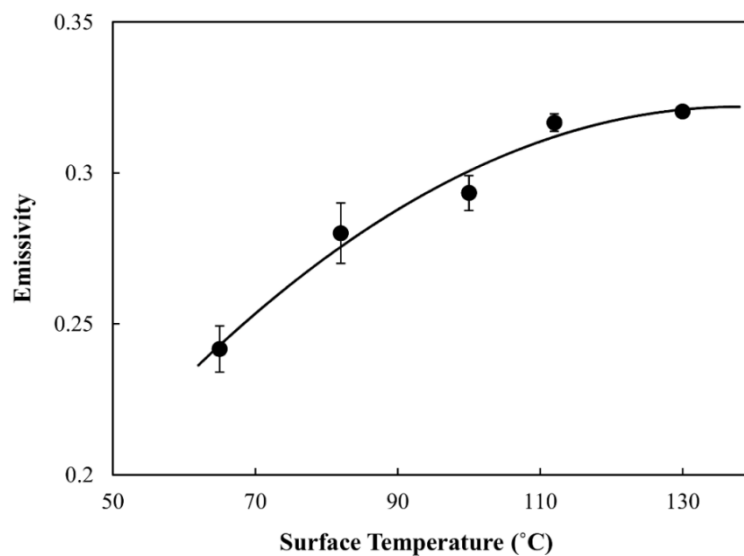


Figure 3-7: Emissivity of the grit-blasted Al 6061-T6 substrate at different surface temperatures.

The temperature range in Fig. 3-7 was selected to be in accordance with the range of surface temperatures that was collected for the smooth substrate. It was found that the emissivity of the roughened aluminium substrate at temperatures higher than 100°C approached 0.32, as shown in Fig. 3-7. Therefore, this estimated emissivity was used to estimate the steady-state surface temperature of the roughened substrate. The steady-state surface temperatures of both the smooth and rough substrates were measured by using the infrared camera. The cold spray unit was utilized to cause the impingement of the supersonic air jet at a total pressure of 660 kPa and a total temperature of 300°C on substrates with thickness of 2.5 mm. Figure 3-8 shows the comparison of the radial variation of the non-dimensional steady-state surface temperature of the rough substrate with that of the smooth substrate under the same cold spray process conditions. The steady-state surface temperature was non-dimensionalized as

$$\theta_{ss} = \frac{T_{ss} - T_{\infty}}{T_a - T_{\infty}} \quad (3-8)$$

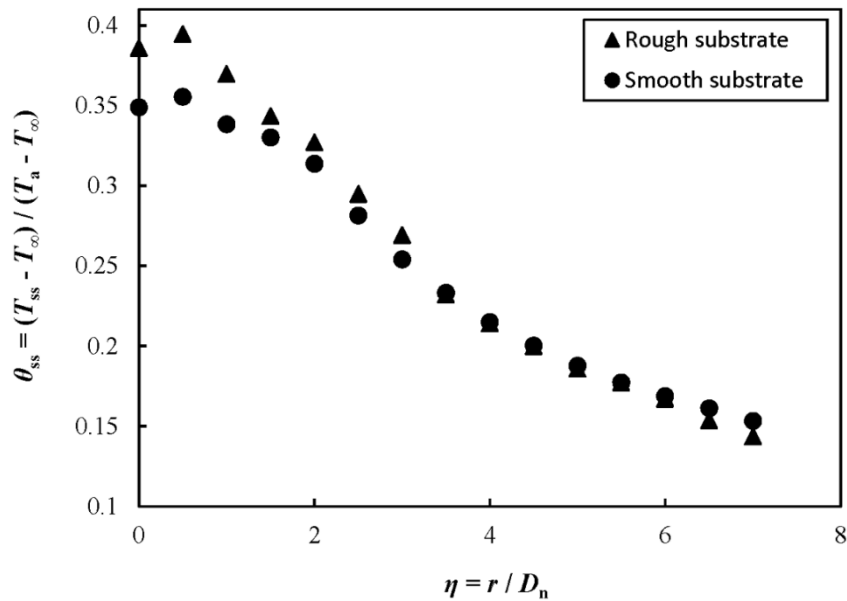


Figure 3-8: Comparison of the radial variation of the non-dimensional steady-state surface temperature of the rough and smooth substrates under cold spray air jet impingement.

As observed in Fig. 3-8, the steady-state surface temperature of the rough substrate was higher than that of the smooth substrate in the vicinity of the stagnation point of the impinging air jet. The measurements of the steady-state surface temperature of the rough substrate were obtained by assuming that the emissivity of the rough surface was close to 0.32. This assumption was made since the surface temperature, especially that at the vicinity of the stagnation point of the impinging air jet, was above 100°C. The result in Fig. 3-8 confirmed that the surface roughness would increase the surface temperature as a result of an increase in the heat transfer coefficient and heat transfer from the air jet to the substrate. In addition to the influence of the heat transfer coefficient on the increased surface temperature, the increased surface area of the rough substrate due to the asperities on the surface may have increased the heat transfer rate from the air to the surface, thus increasing the surface temperature. By comparing the cross-sectional profile of the smooth and rough substrates shown in Fig. 3-6, it is observed that there are more asperities on the rough surface and the height of those asperities are greater than those that are observed on the smooth surface. The asperities may act as fins, which extend and increase the surface area of the grit-blasted substrate, increasing the heat transfer rate. The increased heat transfer rate due to the increased surface area may be explained by way of Newton's Law of Cooling [7], which states that

$$\dot{Q} = hA_s \Delta T, \quad (3-9)$$

where A_s is the surface area through which the heat exchange occurs. The equation confirms that as the surface area increases, the heat transfer rate (\dot{Q}) from the air jet to the substrate increases. Also, according to Table 3-2, the high values of kurtosis produced steep asperities on the rough

surface, enhancing the performance of the extended surfaces or fins. The asperity fins, by increasing the heat transfer rate, produced higher surface temperatures on the rough substrate.

Observations from Fig. 3-8 also suggest that the steady-state surface temperature of the rough substrate did not differ from that of the smooth substrate at distances that were farther downstream from the stagnation point. It is likely that the surface temperature measurements at those regions might be significantly affected by the inevitable errors in the estimates of emissivity of the substrate. Since the temperature of the surface decreased as the distance from the stagnation point increased, the emissivity of the substrate likely decreased as well. Since the infrared camera used a fixed value of emissivity as an input, in this case it was set at 0.32, there was likely some error in the surface temperature measurements taken at points that were farther downstream from the stagnation point. Having taken into account the possible errors in the temperature measurement in those regions, it was also possible that due to the higher heat transfer rate between the under-expanding air jet and the rough substrate in the vicinity of the stagnation point, the air that reached the outer regions of the substrate became cooler, resulting in lower temperature rise in comparison to flow over the smooth substrate.

The surface temperature profile of the substrate under an impinging air jet may be affected by the thickness of the substrate. It is, however, expected that the heat transfer coefficient of the impinging air jet on the substrate will be independent of the thickness of the substrate since the heat transfer coefficient mainly depends on geometry of the surface that is in contact with the fluid, the fluid properties, the flow regime (that is, laminar or turbulent flow), and in some cases, the temperature difference between the fluid and the surface [7]. Therefore, the effect of the substrate thickness on the heat transfer coefficient of the impinging air jet and the surface temperature of the substrate was investigated. The cold spray unit was utilized to

cause the impingement of the compressed air jet on the substrate at a total temperature of 300°C and at a total pressure of 660 kPa. The heat transfer coefficient that was estimated for a substrate with thickness of 1.5 mm was substituted into Eq. (2-13) that was presented in Section 2.2.1 of Chapter 2. The non-dimensional surface temperature of the substrate was calculated at a Fourier number of 81 and for substrate thicknesses of 2.5 and 6.5 mm. Figure 3-9 shows a comparison of the estimated and experimentally-measured non-dimensional surface temperature for the different thicknesses. Although the heat transfer coefficient, which was used in the calculations, was measured at $\delta = 1.5$ mm, the results of the semi-empirical analytical model that pertain to the thicker substrates was in close agreement with the experimental results, confirming that the heat transfer coefficient of an impinging air jet upon the substrate was independent of the thickness of the substrate. It was also observed that the surface temperature of the substrate decreased as the radial distance from the stagnation point of the impinging air jet increased, and as the thickness of the substrate increased. A similar observation was reported by McDonald, *et al.* [72]. Due to the increase in the thickness of the substrate, the volume of the substrate increased; thus, a higher quantity of thermal energy was conducted thorough the substrate. Therefore, the surface temperature of the thicker substrate was lower than that of the substrate with lower thickness.

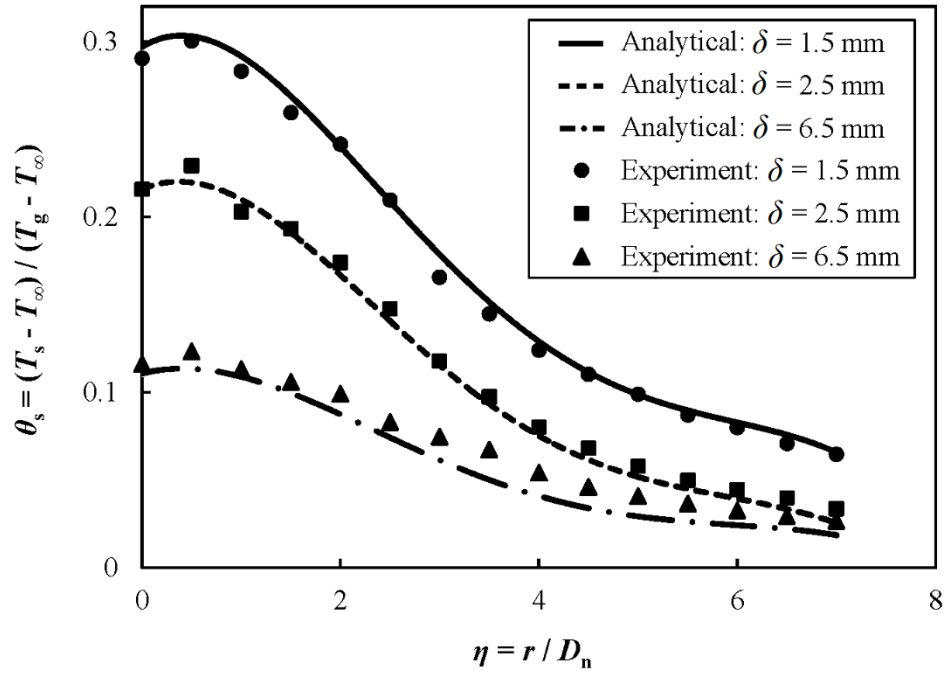


Figure 3-9: Comparison of predicted and experimentally-measured non-dimensional surface temperature variation of the substrate at different substrate thicknesses.

CHAPTER 4

Semi-empirical Analytical Determination of Transient Temperature Distribution within a Flat Substrate during a Cold Spray Deposition Process

A three-dimensional heat conduction model was developed to determine the transient temperature distribution within a flat substrate that was exposed to the impingement of a moving cold spray hot air jet during the deposition process. The travelling wave solution technique was utilized in order to take into account the effect of the movement of the heat source. A low-pressure cold spray unit was employed to generate the impingement of a compressed air jet on a flat substrate. By comparing the analytically-estimated and experimentally-measured surface temperature, the suitability of using average heat transfer coefficient in the mathematical modeling was assessed. The analytical model was further utilized to investigate the effect of the non-dimensional characteristic velocity of the travelling heat source on the surface temperature profile of the substrate.

Some sections of the work presented in this chapter have been or will be published in A. Mahdavi, A. McDonald, “Semi-empirical Analytical Determination of Transient Temperature Distribution within a Flat Substrate during a Cold Spray Deposition Process”, *Surf. Coat. Technol.*, under review (Manuscript number: SURFCOAT-D-18-00724); and A. Mahdavi, A. McDonald, “Determination of the Temperature Distribution of a Substrate Exposed to a Moving Cold or Thermal Spray Heat Source”, in: *International Thermal Spray Conference (ITSC 2018)*, May 7-10, 2018 (Orlando, FL, USA), ASM International, (2018), # 44653, 6 pages on compact

i	numerator in x-coordinate	n	nozzle
j	numerator in y-coordinate	s	substrate/surface
m	numerator in z-coordinate	∞	ambient

4.1. Experimental Procedure

Details on the low-pressure cold spraying, namely process parameters and information on the nozzle, that were employed to generate the impingement of a moving compressed air jet upon a flat substrate were discussed in Section 2.1.1 of Chapter 2 on this dissertation. The assumptions of the mathematical modeling, which will be discussed in detail later, required that the powder feeder be bypassed from the system in order to neglect the presence of the particles. The moving air jet was considered as the heat source in this Chapter. A programmed robot (Motoman- HP20, Yaskawa Electric Corp., Waukegan, IL, USA) was used to support, move, and direct the nozzle over the substrate. The robot was also utilized to keep the stand-off distance (SOD) of the nozzle – the distance between the exit of the nozzle and the surface of the substrate – at 15, 25, and 50 mm during the experiments. The robot was programmed to pass the nozzle over the substrate in the horizontal direction with velocities of 2.5, 5, and 10 mm/s.

Details on the substrate material, insulation material, and temperature measurements were presented in Sections 2.1.2 and 2.1.3 of Chapter 2. The geometry of the substrate was a rectangular plate with dimension of 200 mm \times 500 mm. The thickness of the substrate was 1.5 mm. The back surface of the substrate was insulated to prevent it from exchanging heat with ambient air. Figure 4-1 shows the schematic of the experimental assembly that was used in this study. The direction of the nozzle movement is shown. The drawing shown in Fig. 4-1 is not to scale.

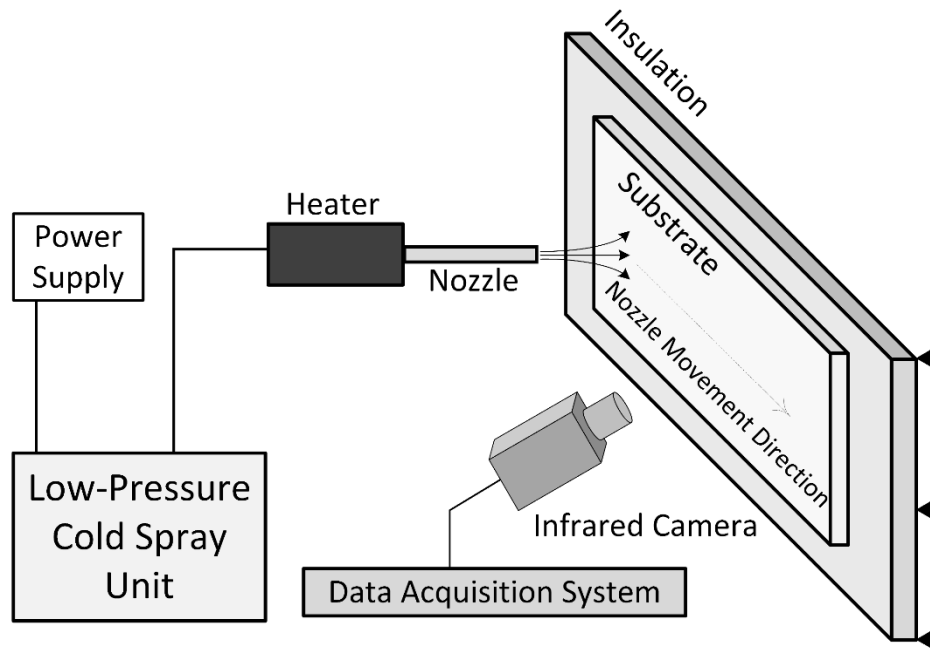


Figure 4-1: Schematic of the experimental assembly and nozzle movement direction.

4.2. Mathematical Model

In Sections 2.2 and 2.3 of Chapter 2, a detailed semi-empirical analytical model was developed that was capable of estimating the spatially-varying heat transfer coefficient between a flat substrate and an impinging air jet generated by a cold spray system. In that model, the movement of the heat source was not considered and a stationary heat source was taken into account. However, in the present model, the heat transfer coefficient of a stationary heat source that was estimated previously was used and implemented in a modified mathematical model. Subsequently, the modified model was used to predict the surface temperature profile of a flat substrate that was exposed to a moving heat source.

The schematic of the geometry of the mathematical model is shown in Fig. 4-2. According to the experimental assembly, an external heat flux from the impinging air jet on the front surface was assumed, while the back surface of the substrate was insulated. The surface area of the sides was much smaller than that of the front surface of the substrate; therefore, the heat exchange from the area bounded by the sides of the substrate was neglected as small compared to the amount of thermal energy that was transferred between the heat source and the front surface.

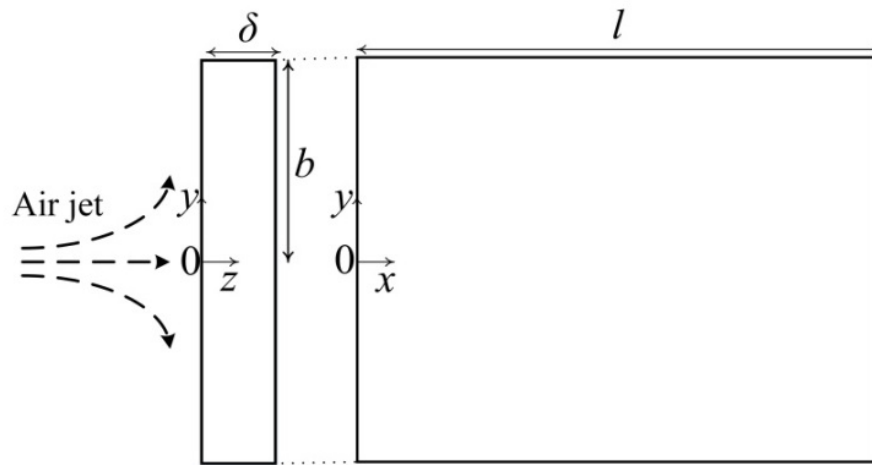


Figure 4-2: Schematic of the geometry for the mathematical model.

The governing equation for the transient three-dimensional heat conduction model is

$$\nabla^2 T(x, y, z, t) = \frac{1}{\alpha_s} \frac{\partial T(x, y, z, t)}{\partial t}. \quad (4-1)$$

The boundary conditions and initial condition are

$$-k_s \frac{\partial T(x=0, y, z, t)}{\partial x} = 0, \quad (4-2)$$

$$-k_s \frac{\partial T(x=l, y, z, t)}{\partial x} = 0, \quad (4-3)$$

$$-k_s \frac{\partial T(x, y=-b, z, t)}{\partial y} = 0, \quad (4-4)$$

$$-k_s \frac{\partial T(x, y=b, z, t)}{\partial y} = 0, \quad (4-5)$$

$$-k_s \frac{\partial T(x, y, z=0, t)}{\partial x} = h(x, y)[T_{AW}(x, y) - T(x, y, z=0, t)], \quad (4-6)$$

$$-k_s \frac{\partial T(x, y, z=\delta, t)}{\partial y} = 0, \text{ and} \quad (4-7)$$

$$T(x, y, z, t=0) = T_0. \quad (4-8)$$

The external heat flux on the front surface of the substrate is given by Eq. (4-6), where h is the spatially-varying heat transfer coefficient between the front surface and the stationary under-expanding air jet, and T_{AW} represents the adiabatic wall temperature of the impinging air jet over the substrate. The values of the spatially dependent heat transfer coefficient (h) and adiabatic wall temperature (T_{AW}) were reported in Sections 2.3.1, 2.3.2, and 2.3.3 of Chapter 2 of this dissertation. Since the effect of the movement of the heat source was not taken into account in the aforementioned set of equations, the temperature distribution that was determined by solving the governing equation (Eq. (4-1)) was in reference to a substrate that was exposed to a stationary heat source. In order to predict the temperature distribution within a substrate that was

exposed to a moving heat source, the travelling wave solution technique was applied to the proposed mathematical model [102]. According to this technique, the origin of the heat source was transformed such that the Cartesian coordinate system travelled along with the heat source with the same velocity [87]. To that end, a new variable (ξ) was introduced to combine the velocity of the moving heat source with the coordinate along which the heat source moved, in order to incorporate the movement of the heat source. In the current study, the heat source moved in the x -direction. Thus, the new variable was formulated as [87]

$$\xi = x - ut . \quad (4-9)$$

In the numerical and analytical studies on the evaluation of the temperature distribution within the medium affected by a travelling heat source with application to welding, grinding, and laser hardening, the moving heat source was considered as a point, line, or surface heat source [82]. Therefore, it was relevant to incorporate the heat source as an energy generation term in the governing equation of the problem. However, in the present study, the cold spray nozzle heat source produced a Gaussian-shaped heat flux profile that was applied as a boundary condition to the front surface of the substrate. Thus, the heat source was incorporated into a Robin boundary condition (boundary condition of the third kind or convection boundary condition), rather than as an energy generation term in the governing equation. Subsequently, to apply the travelling wave solution to the mathematical model of this problem, the transformation of the origin was applied only to the boundary condition that included the external heat source (see Eq. (4-6)). To that end, Eq. (4-6) was modified as

$$-k_s \frac{\partial T(x, y, z = 0, t)}{\partial x} = h(\xi, y) [T_{AW}(\xi, y) - T(x, y, z = 0, t)]. \quad (4-10)$$

Equation (4-10) represents the boundary condition for a travelling Gaussian heat flux over a substrate in which the velocity is the same as that of the cold spray nozzle (heat source). The boundary condition of Eq. (4-6) was replaced by the modified boundary condition of Eq. (4-10). Then, a Green's function approach was used to solve the governing equation of this problem (see Eq. (4-1)). A foundational mathematical description of the Green's function is out of the scope of the current study and can be found elsewhere [87]. The final expression for the temperature distribution within the substrate that was exposed to the moving heat source was found to be

$$\begin{aligned}
T(x, y, z, t) = & \sum_{i=1}^{\infty} \sum_{j=1}^{\infty} \sum_{m=1}^{\infty} \left[\frac{T_0 \exp(-\alpha_s (\lambda_i^2 + \beta_j^2 + \gamma_m^2) t)}{N(\lambda_i) N(\beta_j) N(\gamma_m)} \cos(\lambda_i x) \right. \\
& \times [\cos(\beta_j y) - \tan(\beta_j b) \sin(\beta_j y)] [\tan(\gamma_m \delta) \sin(\gamma_m z) - \cos(\gamma_m z)] \\
& \times \int_{x'=0}^l \int_{y'=-b}^b \int_{z'=0}^{\delta} (\cos(\lambda_i x') [\cos(\beta_j y') - \tan(\beta_j b) \sin(\beta_j y')] [\tan(\gamma_m \delta) \sin(\gamma_m z') - \cos(\gamma_m z')] dx' dy') \\
& + \left(\frac{\alpha_s}{k_s} \right) \frac{\cos(\lambda_i x) [\cos(\beta_j y) - \tan(\beta_j b) \sin(\beta_j y)] [\tan(\gamma_m \delta) \sin(\gamma_m z) - \cos(\gamma_m z)]}{N(\lambda_i) N(\beta_j) N(\gamma_m)} \\
& \times \int_{\tau=0}^t \int_{x'=-b}^l \int_{y'=-b}^b (\exp(-\alpha_s (\lambda_i^2 + \beta_j^2 + \gamma_m^2) (t - \tau)) \cos(\lambda_i x') [\cos(\beta_j y') - \tan(\beta_j b) \sin(\beta_j y')] \\
& \times h(x' - u\tau, y') T_{Aw}(x' - u\tau, y') dx' dy' d\tau \Big].
\end{aligned} \tag{4-11}$$

In Eq. (4-11), λ_i , β_j , and γ_m are the eigenvalues in the x -direction (bounded by $0 \leq x \leq l$), y -direction (bounded by $-b \leq y \leq b$), and z -direction (bounded by $0 \leq z \leq \delta$), respectively, and they can be obtained from

$$\lambda_i = \frac{[(i-1)\pi]}{l}, \quad (4-12)$$

$$\beta_j = \frac{[(j-1)\pi]}{b}, \text{ and} \quad (4-13)$$

$$\gamma_m \tan(\gamma_m \delta) - \frac{h(x-ut, y)}{k_s} = 0. \quad (4-14)$$

In Eq. (4-11), $N(\lambda_i)$, $N(\beta_j)$, and $N(\gamma_m)$ are the Norms of the differential equations in the x -direction, y -direction, and z -direction, respectively, and are expressed as

$$N(\lambda_i) = \int_{x=0}^l [\cos(\lambda_i x)]^2 dx, \quad (4-15)$$

$$N(\beta_j) = \int_{y=-b}^b [\cos(\beta_j y) - \tan(\beta_j b) \sin(\beta_j y)]^2 dy, \text{ and} \quad (4-16)$$

$$N(\gamma_m) = \int_{z=0}^{\delta} [\tan(\gamma_m \delta) \sin(\gamma_m z) - \cos(\gamma_m z)]^2 dz. \quad (4-17)$$

Equation (4-11) expresses the analytical evaluation of the transient temperature distribution within the flat substrate that was exposed to a moving heat source generated by a cold spray nozzle. Values of the spatially-varying heat transfer coefficient (h) and the adiabatic wall temperature (T_{AW}) were substituted into Eq. (4-11). In order to solve the explicit expression for the transient temperature distribution within the substrate, $T(x, y, z, t)$, a zero-dimensional code in MATLAB (MathWorks, Inc., Natick, MA, USA) was developed. The calculation of the terms in

the infinite series of Eq. (4-11) was terminated once the final solution converged to within 2% of the sum.

4.3. Results and Discussion

4.3.1. Effect of the Presence of the Particles on the Heat Transfer Coefficient

The spatially-varying heat transfer coefficient of the impinging air jet was required in order to solve for the final values of the transient temperature distribution within the substrate. To this end, the semi-empirical analytical model that was developed in Chapter 2 was used to predict the heat transfer coefficient of the cold spray impinging air jet. The effect of the presence of the powder particles in the air jet was not considered in the aforementioned model that was employed to determine the heat transfer coefficient of the air jet. However, the presence of metal or alloy powder particles in the propellant supersonic air jet is necessary for fabrication of the cold spray coatings. Therefore, a challenging issue may arise as to whether or not the presence of micron-sized particles considerably affects the heat transfer coefficient of the under-expanding air jet on the substrate. In numerical and analytical modeling of multi-phase flow, the assumption that there is no collision between the solid particles is generally accepted in order to simplify the modeling, especially when the gas-particle mixture is sufficiently dilute [103]. Under experimental and practical conditions of actual cold spraying, the aforementioned assumption is reasonable when the volume fraction of the particles in the air-particle jet is sufficiently low [24]. On the other hand, the particle-air interaction within the jet may affect the heat transfer coefficient of the impinging air jet. In this regard, the particle-air jet interaction is characterized by the non-dimensional Stokes number. The Stokes number is defined as the ratio of the

momentum response time of the particle (κ_p) to the characteristic time of the flow field (D_n/u_g). The momentum response time of the particle is defined as the time that a particle requires to respond to any changes in velocity and it is expressed as [103]

$$\kappa_p = \frac{\rho_p d_p^2}{18\mu_g}. \quad (4-18)$$

Accordingly, the Stokes number is expressed as

$$\text{Stk} = \kappa_p \frac{u_g}{D_n}. \quad (4-19)$$

According to Eq. (4-19), small Stokes number ($\text{Stk} < 1$) relates to particles whose momentum response times are less than the characteristic time of the flow field. Thus, for small Stokes number, the particles have adequate time to respond to variations in the velocity of the flow field. As a result, the velocity of the particles is approximately the same as that of the gas flow. Moreover, particles with small Stokes number will not affect the flow field significantly and will not induce turbulence in the flow [104]. On the other hand, for large Stokes number ($\text{Stk} \gg 1$), the particle velocity will be marginally affected by the gas flow velocity [103]. In other words, when the Stokes number of the particles is relatively large, the presence of the particle will have an effect on the velocity and the pattern of the flow field, since they are unable to travel with the flow field with the same velocity [103]. In a numerical study, Tang, et al. [105] studied the effect of the Stokes numbers of the particles on the flow pattern of a free stream jet. Figure 4.3 is extracted from Tang, *et al.* [105], and shows the effect of the Stokes number on the simulated developing vortex of particle dispersion that was produced by a bluff body.

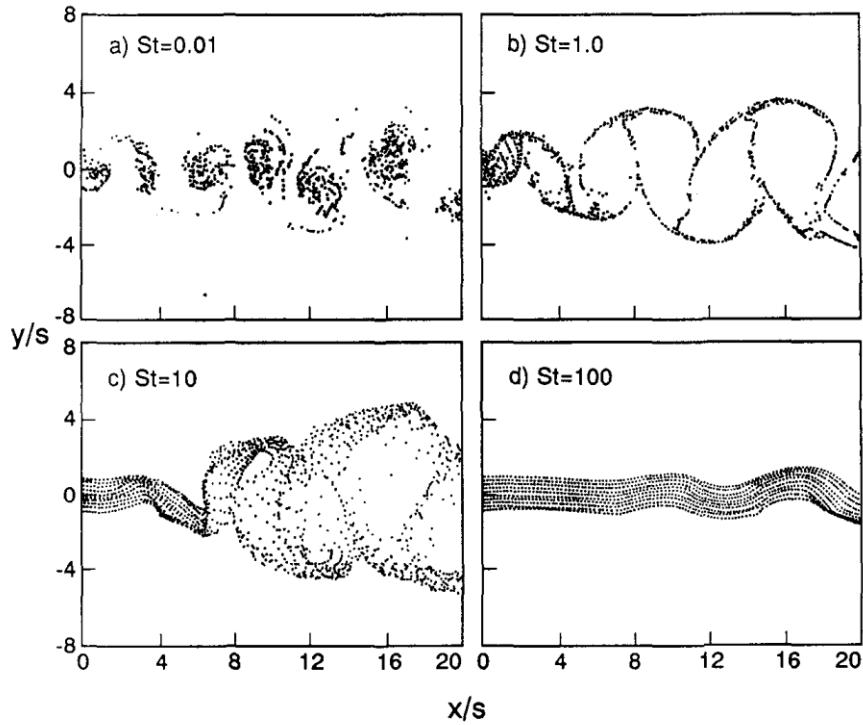


Figure 4.3: Results of the numerical simulation of the particle dispersion pattern over a range of Stokes numbers, extracted from Tang, *et al.* [105]. The vertical and horizontal coordinates were non-dimensionalized with respect to the width of the bluff body.

It is expected that for a dilute gas-particle jet mixture, which contains particles with small Stokes number, the particles will follow the air jet flow pattern during the impingement and under-expansion of the air jet over the substrate [80]. In other words, the velocity and flow pattern of the impinging and under-expanding air jet will likely be negligibly affected by the presence of the particles. Consequently, the analytically-estimated heat transfer coefficient that was determined for an under-expanding cold spray air jet without taking into account the particles will likely apply to the conditions of an actual cold spray air-particle jet mixture, since the heat transfer coefficient is primarily dependent on the velocity, turbulence, and flow pattern of the working fluid. Therefore, the current study focused on a dilute cold spray air-particle jet

mixture whose particles had a sufficiently small Stokes number. Kim, *et al.* [106] showed that the Stokes number of particles with average diameter of 1 μm under approximately the same cold spray system parameter conditions that were considered in this study would be small (on the order of $\text{Stk} \sim 0.1$). However, the powder particles in cold spraying are typically larger than 1 μm . Thus, their Stokes numbers will be on the order of $\text{Stk} \sim 1$, which in turn could produce some uncertainty in the suitability of using the assumption of small Stokes number in the mathematical model. In the current study, it was assumed that the sizes of the particles were in a range such that their Stokes numbers were on the order of unity or less. Thus, since the Stokes numbers were on the order of 1 or less, the analytically-estimated heat transfer coefficient values that were estimated in Chapter 2 of this dissertation were used in the current study to investigate the effect of the movement of the cold spray heat source on the substrate surface temperature profile.

Prior to predicting the surface temperature profile of a substrate that was exposed to a moving cold spray heat source by using the spatially-varying heat transfer coefficient ($h(r)$) values in the mathematical modeling, the effect of employing an average heat transfer coefficient, in lieu of the spatially-varying heat transfer coefficient values, to determine the surface temperature profile was studied. It was believed that the use of an average heat transfer coefficient would be less computationally onerous; however, it was expected that errors might propagate during the analytical determination of and into the surface temperature profile values.

In order to assess the suitability of using the average heat transfer coefficient in the model, the mathematical model was used to predict the surface temperature profile of a substrate that was exposed to a stationary cold spray heat source. To that end, the velocity of the heat source was taken to be zero in the mathematical model. The cold spray heat source was directed

at the center of the substrate (at $x = l/2, y = 0, z = 0$) and the surface temperature profile was measured by using the infrared camera at an arbitrary time, which in this case was 10 seconds after the impingement of the cold spray air jet on the substrate. The time was presented in the form of the non-dimensional Fourier number. The Fourier number was evaluated at 10 seconds after the impingement of the cold spray air jet on the substrate, and was found to be 137. In order to evaluate the average heat transfer coefficient of the impinging air jet, the spatially-varying heat transfer coefficient was integrated over a region on the substrate surface that was seven times that of the nozzle diameter ($7D_n$), which likely encompassed the region of the front surface of the substrate that was most affected by the impinging air jet. The physical region and limits of integration were chosen according to experimental observation. It was observed that the increase in the surface temperature of the substrate beyond the region that was bounded by $7D_n$ on the substrate was negligible. The average heat transfer coefficient (\bar{h}) was evaluated by

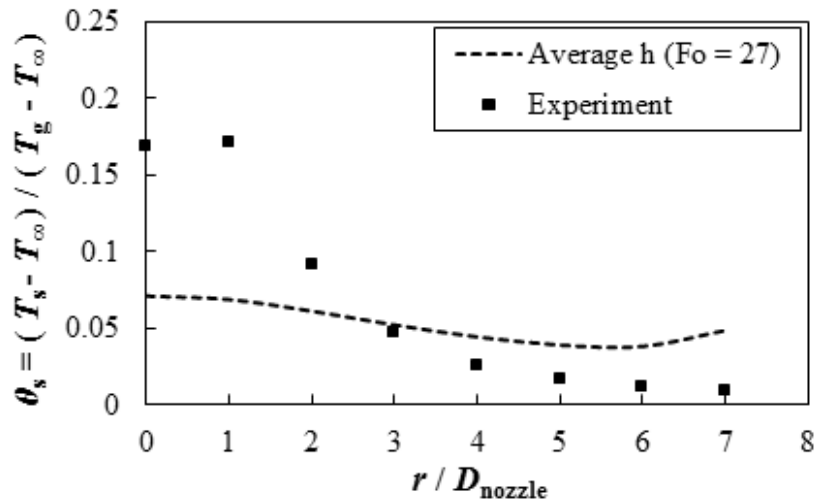
$$\bar{h} = \frac{1}{A_s} \int_{r=0}^{7D_n/2} h(r)(2\pi r dr), \quad (4-20)$$

where A_s is the surface area of a region of that is seven times that of the nozzle diameter on the substrate front surface and it was calculated as

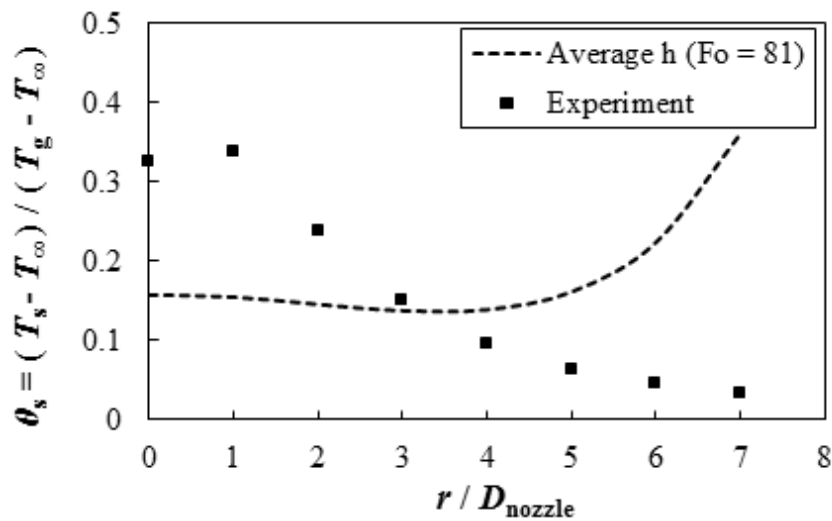
$$A_s = \frac{49\pi D_n^2}{4}. \quad (4-21)$$

Both the average heat transfer coefficient values that were obtained from Eq. (4-20) and the spatially-varying heat transfer coefficient values that were obtained in Section 2.3 of Chapter 2 were separately substituted in Eq. (4-11) to determine the transient surface temperature profile of a substrate that was exposed to a stationary impinging air jet. The non-dimensional surface

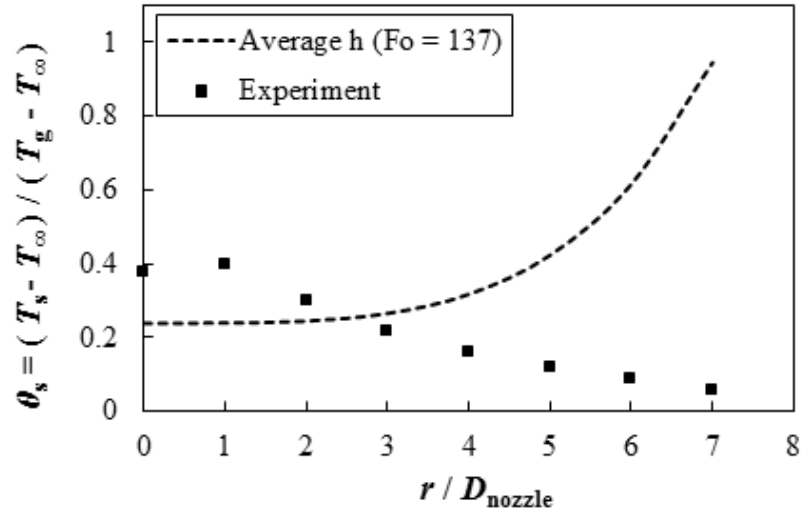
temperature profiles (for both average and spatially-varying heat transfer coefficients) were predicted at a Fourier numbers of 27, 81, and 137. Figure 4-4 shows comparisons of the experimentally-measured and analytically-estimated non-dimensional surface temperature profiles that were obtained when values for the average and the spatially-varying heat transfer coefficients as functions of the non-dimensional distance from the stagnation point were used.



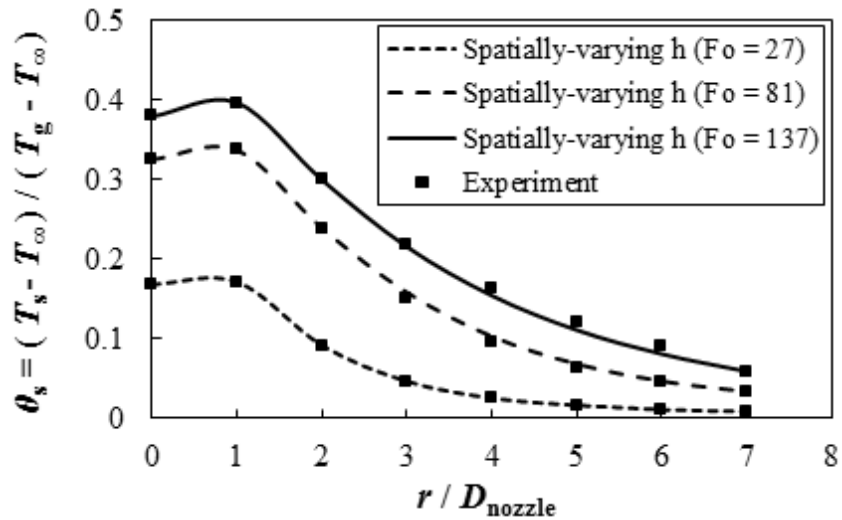
(a)



(b)



(c)



(d)

Figure 4-4: Comparison of the experimental and analytical non-dimensional temperature profile at different Fourier numbers for (a) – (c) average and (d) spatially-varying heat transfer coefficient.

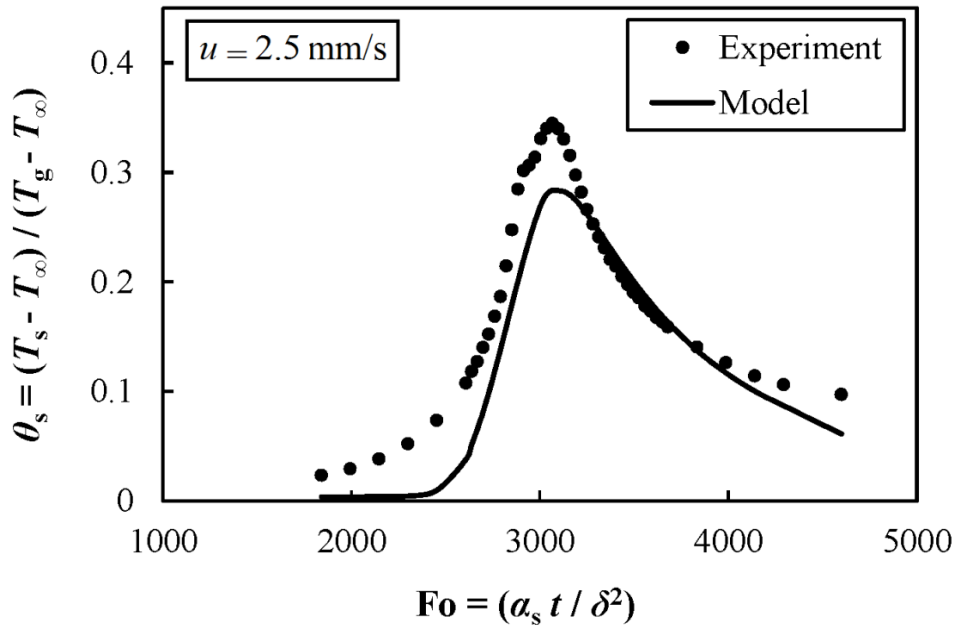
It was found that by using the average heat transfer coefficient in the mathematical modeling, there were substantial deviations between the predicted substrate surface temperatures

and those obtained from the experiments. However, the analytically-estimated surface temperature that was obtained by using the spatially-varying heat transfer coefficient was in good agreement with the experimental data. Due to the radial variation of the velocity of the under-expanding air flow along the substrate and the strong dependence of the heat transfer coefficient on the velocity of the air flow, the heat transfer coefficient was significantly dependent on the distance from the stagnation point of the jet. In addition, according to Newton's law of cooling, the estimated temperature is highly dependent on the variation of the heat transfer coefficient. Therefore, use of the average heat transfer coefficient would miss the effects of spatial variation of this parameter, which in turn would produce errors in predicting the local surface temperature profile of the substrate. Therefore, the spatially-varying heat transfer coefficient should be used in the heat conduction model in order to predict the transient surface temperature of the substrate that is exposed to a moving cold spray heat source.

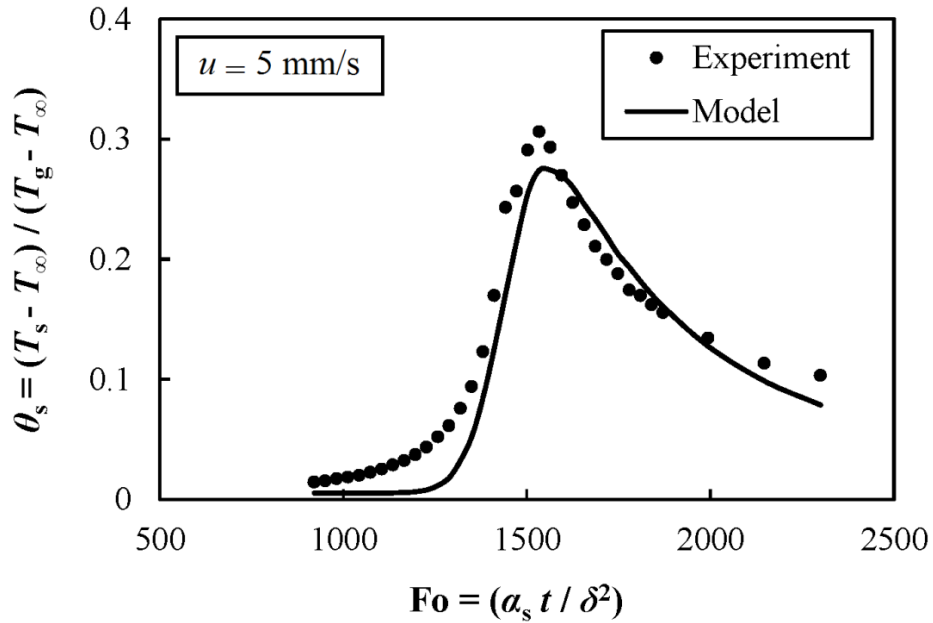
4.3.2. Surface Temperature Profile of the Substrate Exposed to a Moving Heat Source

The spatially-varying heat transfer coefficient was used in the analytical model to determine the temperature distribution within the substrate that was exposed to the moving heat source. In this regard, values of the spatially-varying heat transfer coefficient were substituted into Eq. (4-11) to predict the temporal variation of the temperature at an arbitrary point on the substrate. The aforementioned point on the substrate was the center of the front surface of the substrate (at $x = l/2, y = 0, z = 0$). Figure 4-5 shows a comparison of the temporal variation of the estimated and experimentally-measured non-dimensional temperature of the center of the front surface of the flat substrate that was exposed to a moving heat source with velocities of 2.5, 5,

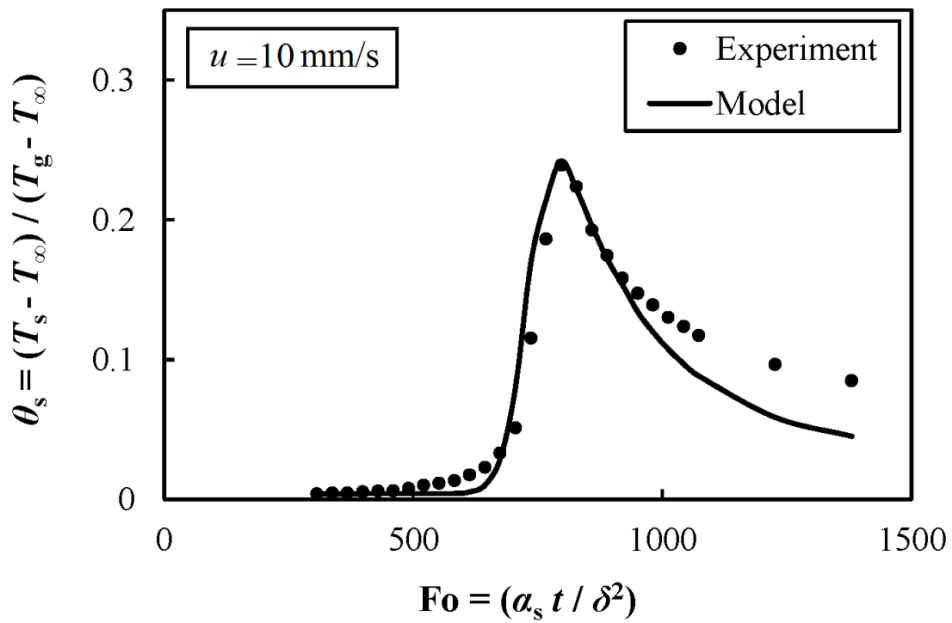
and 10 mm/s at different non-dimensional Fourier numbers. The maximum temperatures on all the curves shown in Fig. 4-5 corresponded to the moment when the heat source approached and passed the center of the front surface of the substrate. According to Fig. 4-5, the temporal variation of the temperature of the center of the substrate that was predicted by the analytical model was in good agreement with the experimental results. However, the analytical model slightly underestimated the maximum temperature of the center of the substrate at lower travelling velocities of the heat source. This could be likely due to the uncertainty in the semi-empirical analytical determination of the heat transfer coefficient values, which were mainly caused by the error in the temperature measurements of the infrared camera. Moreover, given that the dependence of the thermo-physical properties of the substrate material on temperature was not considered during the movement of the heat source over the substrate in the modeling, an additional error, originating from the thermo-physical properties, may have propagated through to the analytically-predicted temperature profile.



(a)



(b)



(c)

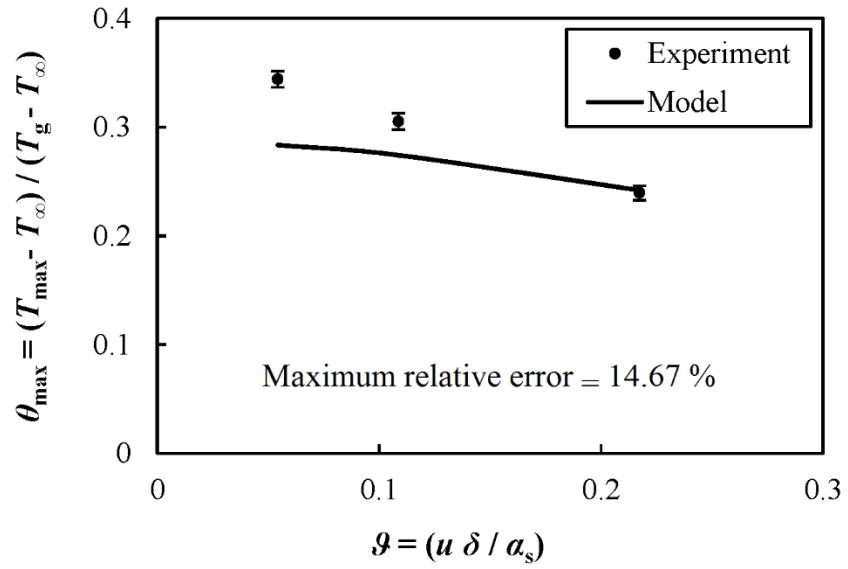
Figure 4-5: Comparison of the temporal variation of the predicted and experimentally-measured non-dimensional temperature at the center of the front surface of the flat substrate exposed to a heat source travelling with velocity of (a) 2.5 mm/s, (b) 5 mm/s, and (c) 10 mm/s at different Fourier numbers.

4.3.3. *Effect of Velocity of the Heat Source on Maximum Surface Temperature*

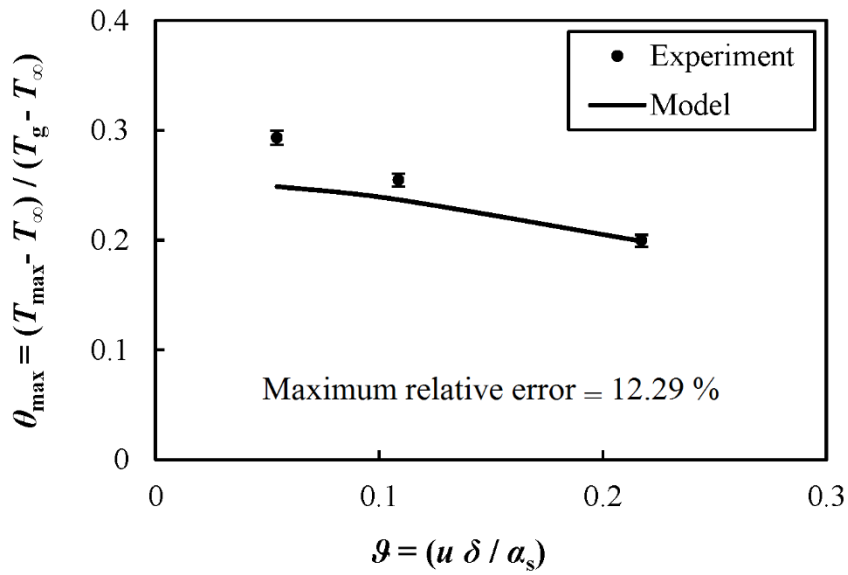
The results presented in Fig. 4-5 suggested that the maximum temperature of the substrate was higher when the heat source travelled at lower velocities. In order to investigate the influence of the velocity of the moving heat source on the maximum temperature of a range of substrate materials and thicknesses, a non-dimensional characteristic velocity (\mathcal{G}) was introduced as

$$\mathcal{G} = \frac{u}{\left(\frac{\alpha_s}{\delta}\right)}. \quad (4-22)$$

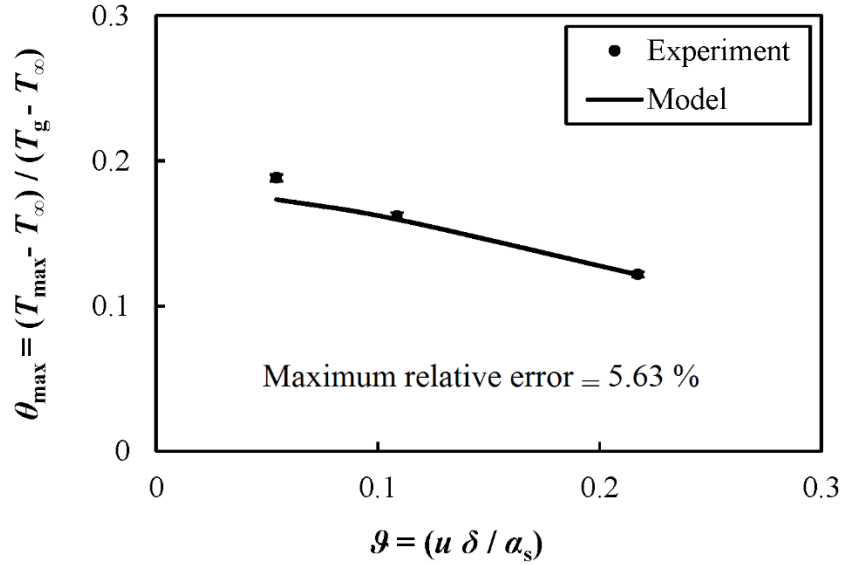
In Eq. (4-22), the denominator represents the characteristic velocity of energy due to heat conduction into the substrate. Therefore, the non-dimensional characteristic velocity (\mathcal{G}) can be defined as the ratio of the travelling velocity of the heat source to the characteristic velocity of heat conduction. The analytical model was further employed to estimate the maximum temperature of the front surface of the substrate that was exposed to the moving heat source with different non-dimensional characteristic velocities. Figure 4-6 shows comparisons of the analytically-estimated and experimentally-measured non-dimensional maximum temperature of the substrate at different non-dimensional characteristic velocities and at various non-dimensional stand-off distances of 2.38, 3.96, and 7.93.



(a)



(b)



(c)

Figure 4-6: Comparison of the predicted and experimentally-measured non-dimensional maximum temperature of the substrate as a function of the non-dimensional characteristic velocity of the moving heat source for different non-dimensional stand-off distance of (a) 2.38, (b) 3.96, and (c) 7.93.

As shown in Fig. 4-6, as the non-dimensional characteristic velocity decreased, the non-dimensional maximum temperature of the front surface of the substrate increased. In other words, at lower non-dimensional characteristic velocity, there was a larger input of energy due to the lower speed of the nozzle. Therefore, additional thermal energy from the heat source was conducted into the substrate material. With respect to the fact that the thickness of the substrate was constant for all cases, additional thermal energy resulted in higher surface temperatures. Similar observations were reported in a numerical-experimental study by McDonald, *et al.* [72]. In order to calculate the error of analytical determination of the non-dimensional maximum temperature of the front surface of the substrate that was exposed to a travelling heat source, the relative error (E) was defined as

$$E = \left| \frac{T_{\text{Model}} - T_{\text{Exp}}}{T_{\text{Exp}}} \right|, \quad (4-23)$$

where T_{Model} and T_{Exp} are the analytically-predicted and the experimentally-measured temperatures, respectively. The relative error of the analytically-predicted maximum surface temperature was calculated at each characteristic velocity for all stand-off distances indicated in Fig. 4-5, and was presented in the figure.

It was further observed that as the stand-off distance increased, the maximum surface temperature decreased. This result was due to a decrease in the heat transfer of the under-expanding air jet as a result of the increase in stand-off distance, as discussed in Section 2.3.3 of Chapter 2. In the case of the air jet that was generated by a cold spray nozzle, as the stand-off distance was increased, the magnitude of the velocity within the air jet decreased. This phenomenon was due to the entrainment of the surrounding ambient air into the air jet. As a result, the impact force of the jet onto the surface decreased since the momentum change was lower as a result of the lower air jet velocity upon impingement on the substrate surface. The lower impact force led to a reduced wall jet velocity along the substrate. Since the heat transfer coefficient of the under-expanding air jet over the flat substrate is positively correlated to the flow velocity, the maximum Nusselt number decreased, as the stand-off distance increased [90]. Newton's Law of Cooling suggests that lower heat exchange rates from the gas to the substrate will occur as the heat transfer coefficient decreases. Moreover, higher stand-off distances resulted in entrainment of more cold air from the surrounding ambient environment. The colder air cooled the air jet and reduced the forced convection heat transfer rate. Thus, lower surface temperature at higher stand-off distances occurred. Further details on the effect of the stand-off distance on the heat transfer rate are presented in another study [58].

CHAPTER 5

Conclusions

In this doctoral research project, the transient thermal evolution within the substrate during low-pressure cold spraying was investigated. Due to the strong dependence of the final quality of cold-sprayed coatings and the adhesion strength of the deposited coating on the temperature distribution within the substrates, knowledge of the gas-substrate heat exchange was required. With respect to the challenges and uncertainties regarding costly numerical modelling techniques such as Finite Element Analysis (FEA) or Computational Fluid Dynamics (CFD), which require precise discretization of the substrate, impinging air jet, and surrounding medium, and difficulty with conducting expensive experiments with cold or thermal spraying processes, a robust and comprehensive analytical modelling to predict the gas/substrate heat exchange and the temperature distribution within the target substrate is required. The proposed analytical model will be capable of predicting the temperature distribution within substrates with various materials and dimensions within the application of cold spraying. Moreover, the aforementioned model can be extended and modified to be applicable in other thermal spraying processes. Therefore, the primary purpose of the present research project was to develop a semi-empirical analytical model to estimate the heat transfer coefficient of an under-expanded air jet upon a flat substrate, and the temperature distribution within a substrate that was exposed to a moving impinging air jet during the cold spraying process.

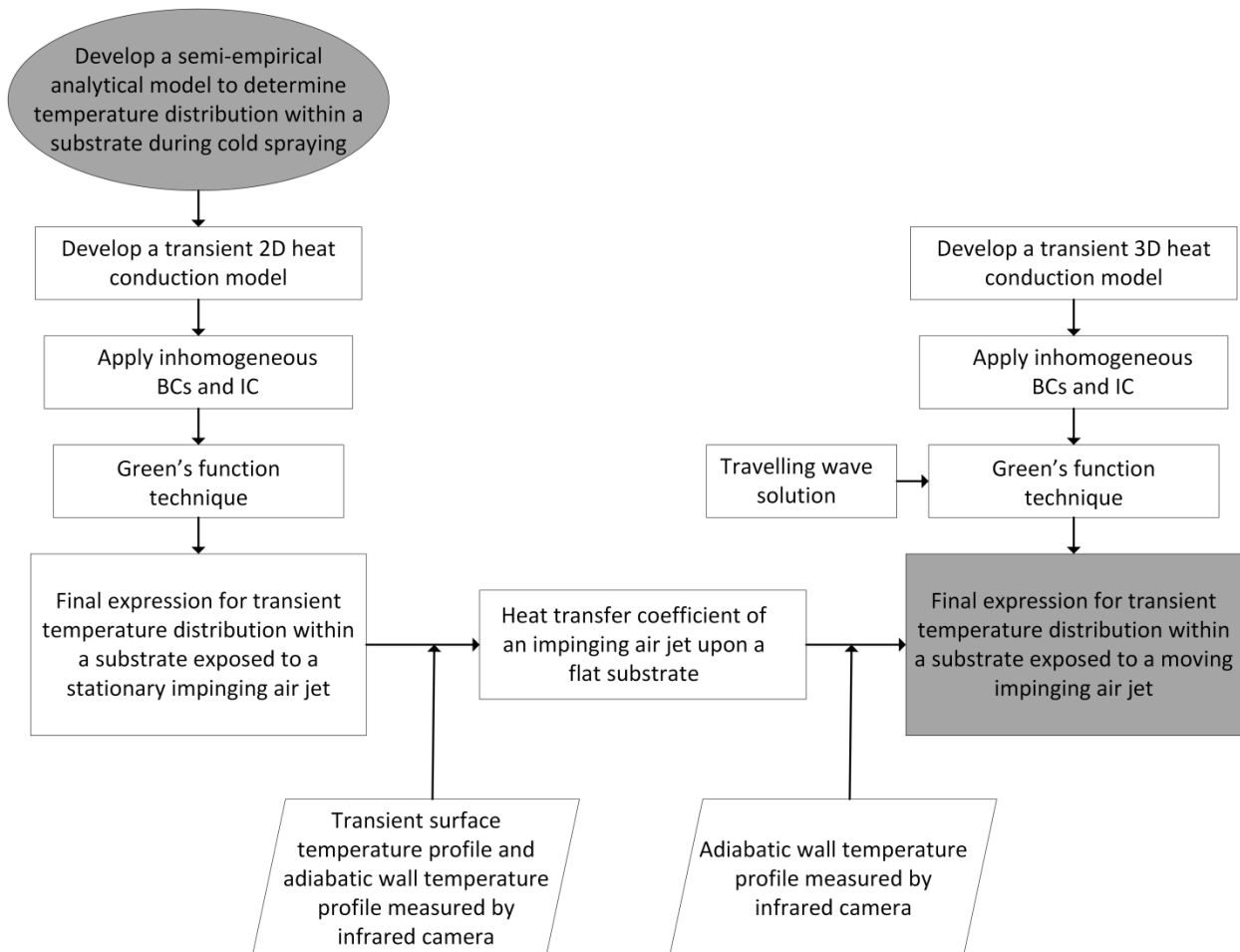


Figure 5-1: Flow chart of the sequential steps in semi-empirical analytical modelling of the current PhD research project.

A comprehensive method involving Green's functions was employed to solve a transient two-dimensional heat conduction problem to obtain an expression for the temperature distribution within the substrate. A low-pressure cold spraying unit was used to generate a compressed air jet that impinged on a flat substrate. By coupling the analytical results of temperature distribution and experimental surface temperature data, the radial variation of the adiabatic wall temperature and the non-dimensional heat transfer coefficient of the impinging air jets upon the substrate were estimated. The Nusselt number of the impinging air jet was

predicted at different non-dimensionalized times (Fourier number) and it was found that the Nusselt number is time independent. It was further found that the maximum values for the non-dimensional adiabatic wall temperature and the Nusselt number were present in the vicinity of the stagnation point of the air jet, which agreed with observations of other studies.

The model was applied to investigate the effect of the stand-off distance on the Nusselt number of the impinging air jet. It was found that by increasing the stand-off distance of the nozzle, the radial variations of the Nusselt number along the substrate decreased. The Nusselt number that was determined at the early moments of spraying ($Fo = 27$) was substituted into the semi-empirical analytical model to determine the surface temperature of the substrate at various Fourier number and stand-off distances. The results were compared to the experimental data and a good agreement between them was observed. The good agreement between the experimental results and the predictions of the model suggested that the estimated heat transfer coefficient of the cold spray gas jet can be used to estimate the surface temperature of the substrate at any time.

The effect of the air temperature and pressure, as process parameters, and surface roughness and thickness, as substrate parameters, on the heat transfer coefficient of the impinging air jet was investigated. It was found that increasing the total pressure of the air would increase the Nusselt number of the impinging air jet at all locations downstream of the stagnation point. It was further found that increasing the total temperature of the air jet did not affect the Nusselt number; however, it slightly increased the heat transfer coefficient of the impinging air jet on the substrate.

The effect of the roughness and thickness of the substrate, as the substrate parameters, on the surface temperature of the substrate and the heat transfer coefficient was studied. The heat

transfer coefficient of the impinging air jet on a roughened (grit-blasted) substrate increased, compared to that on a smooth substrate. It was further found that the heat transfer coefficient is independent of the thickness of the substrate. Moreover, it was shown that as the thickness of the substrate increased, the surface temperature decreased at all points downstream of the stagnation point. The heat transfer coefficient that was estimated for a substrate with thickness of 1.5 mm was substituted into the semi-empirical analytical model to determine the surface temperature of the substrate at different thicknesses. The results were compared to the experimental data and there was good agreement between the predicted and experimentally measured surface temperatures.

The semi-empirical analytically-estimated heat transfer coefficient and the heat conduction model that was developed were employed to assess the suitability of using average heat transfer coefficient in predicting the temperature distribution of a substrate surface during cold spraying. It was shown that under specific conditions, when the Stokes number of the particles is sufficiently small, the effect of the presence of the particles on the heat transfer coefficient of the impinging dilute air-particle jet can be neglected. It was further found that employing average heat transfer coefficient generated significant deviations between the predicted and experimental surface temperatures. It was concluded that the spatially-varying heat transfer coefficient should be used in the heat conduction model to predict the surface temperature of the substrate during the impingement of an actual cold spray air-particle jet with small Stokes number.

A three-dimensional heat conduction model was developed to determine the transient temperature distribution within a flat substrate that was exposed to the impingement of a moving cold spray hot air jet during the deposition process. The travelling wave solution technique was

utilized in order to take into account the effect of the movement of the heat source. A non-dimensional characteristic velocity was defined to study the effect the velocity of the moving heat source on the surface temperature of the substrate. The analytical model was further utilized to investigate the effect of the non-dimensional characteristic velocity of the travelling heat source on the surface temperature profile of the substrate. It was found that both the maximum temperature and the values of the temperature distribution of the substrate surface decreased as the non-dimensional characteristic velocity increased.

In conclusion, the significant contribution of the current PhD research project lies in predicting the transient temperature profile of a substrate that was exposed to a moving heat source generated by a cold spray nozzle *a priori* before experimentation, and which model may be extended for applications involving high-temperature heat source thermal spray torches. The results of this research project can be used in industry for preliminary evaluation of the expected temperature range in their applications, as well as commercial programs to predict the heat transfer rate between the cold spray impinging air jet and the target substrate. The proposed model can be modified and improved by incorporating the effect of the presence of the particles in order to develop a robust model which can predict the temperature distribution within the substrate/coating during the deposition by the cold spray system.

CHAPTER 6

Future Work and Extended Studies

This doctoral research program was mainly focused on advancement in the area of thermal and cold spraying by employing fundamental principles of heat transfer, fluid mechanics. This research project has made a noticeable contribution in development of empirical and analytical heat transfer models for the prediction of the heat transfer coefficient and the transient temperature distribution within a substrate during the impingement of a cold spray air jet. This research project, however, can be improved and expanded by complementary numerical and experimental studies. A few suggestions for future studies are presented as follows:

- 1) In the prediction of the heat transfer coefficient between the under-expanding air jet and the substrate during cold spraying, the effect of the presence of the in-flight particles was neglected. The assumption was likely valid when the sizes of the particles were in a range such that their Stokes numbers were on the order of unity or less ($d_p \leq 10 \mu\text{m}$). However, it is shown that the presence of the particles with greater diameter would likely affect the flow pattern and the turbulence intensity of the impinging air jet [105, 107]. Further numerical investigation is required to determine the error induced by the presence of the large particles in the impinging air jet in prediction of the heat transfer coefficient.
- 2) A complementary study may be conducted to develop a heat conduction model that is capable of determination of the temperature distribution within both the substrate

and the cold-sprayed deposited particle. In the present research project, the presence of the in-flight particles in the air jet was neglected; thus, the classical Fourier heat conduction model was employed to predict the temperature distribution within the substrate that was exposed to impinging cold spray heat source. However, the use of Fourier heat conduction for modelling the temperature distribution within the substrate during the impact of the solid particles generates large errors, since the collision of the particles occurs in a very short time (order of 10^{-9} s) [108, 109]. A solution for heat transfer modelling of the heat sources with extremely short duration or very high frequency that produces large temperature gradients, is to take into account the non-Fourier effects in the diffusion process and predicting the temperature distribution [110, 111]. The modified non-Fourier model, also known as the Cattaneo-Vernotte (C-V) heat conduction model or the hyperbolic heat conduction model, takes into account a new material property called phase lag of heat flux or thermal relaxation time in heat transfer modelling [112, 113]. A detailed experimental and analytical study based on non-Fourier heat conduction model for determination of the temperature distribution within the particle and the substrate during the particle impact is of interest.

- 3) The present analytical work can be expanded and enhanced by developing a fundamental heat transfer numerical model numerical based on Finite Element Analysis (FEA) to determine the transient temperature distribution in hard-faced metal coatings that are fabricated by cold gas dynamic spraying. Several numerical studies have been conducted to model the heat conduction within the deposited

particle (splat) and the substrate during the impact of a single particle [114 - 116]. While these studies have put emphasis on the dynamic and thermal behavior of a single particle impact, limited studies have been conducted on the simulation of the cold-sprayed coating build-up and the transient thermal evolution within the coatings during the deposition process [117]. In light of the significant effect of the substrate-coating temperature distribution on the microstructural characteristics of the fabricated coating, as well as the formation of the residual stresses during cold spraying [19], a detailed numerical study on predicting the thermal evolution in the deposited coating can provide insights into the final quality of the cold-sprayed coatings.

- 4) The presence of surface tensile stresses in the fabricated thermally-sprayed coating may cause the development and propagation of micron-size cracks, which eventually can accelerate fatigue failure [1]. A remarkable feature of the cold-sprayed coatings is that the developed residual stress in the coating is mostly compressive, which may contribute to the longevity of the fabricated coatings [19, 118]. On the other hand, it has been reported that the heat generation due to plastic deformation of the impacting particles on the substrate may anneal the material, thus eliminating compressive residual stress within the cold-sprayed coating [119, 120]. With respect to the indiscretion in the literature regarding the formation of the residual stress during impact of the particles with a wide range of temperatures and velocities, a comprehensive finite element analysis is required to relate the temperature distribution and stress distribution within the substrate and the cold-sprayed coatings.

References

- [1] P. Fauchais, J. Heberlin and M. Boulos, *Thermal Spray Fundamentals from Powder to Part*, New York, USA: Springer, 2014.
- [2] F. Hermanek, *Thermal Spray Terminology and Company Origins*, Materials Park: ASM International, 2011.
- [3] A. Vardele, C. Moreau, H. Ashrafizadeh, A. McDonald and 3. others, "The 2016 Thermal Spray Roadmap," *J. Therm. Spray Technol.*, vol. 28, no. 8, pp. 1376-1440, 2016.
- [4] B. Walser, "The Importance of Thermal Spray for Current and Future Application in Key Industries," *Spraytime*, vol. 10, no. 4, pp. 1-7, 2003.
- [5] M. Wewel, G. Langer and C. Wassermann, "The World of Thermal Spraying - Some Practical Applications," in *International Thermal Spray Conference*, Düsseldorf, Germany, 2002.
- [6] J. Davis, *Handbook of Thermal Spray Technology*, Materials Park: ASM International, 2004.
- [7] L. Jiji, *Het Convection*, Springer – Verlag, 2006.
- [8] H. Ashrafizadeh, P. Mertiny and A. McDonald, "Evaluation of the Effect of Temperature on Mechanical Properties and Wear Resistance of Polyurethane Elastomers," *Wear*, Vols. 368-369, pp. 26-38, 2016.
- [9] A. McDonald, M. Lamontagne, C. Moreau and S. Chandra, "Impact of Plasma-Sprayed Metal Particles on Hot and Cold Glass Surfaces," *Thin Solid Films*, vol. 514, no. 1-2, pp. 212-222, 2006.
- [10] M. Dewar, A. McDonald and A. Gerlich, "Interfacial Heating during Low-Pressure Cold-Gas Dynamic Spraying of Aluminum Coatings," *J. Mater. Sci.*, vol. 47, no. 1, pp. 184-198,

2012.

- [11] P. Fauchais and A. Vardelle, "Heat, Mass and Momentum Transfer in Coating Formation by Plasma Spraying," *Int. J. Therm. Sci.*, vol. 39, no. 9-11, pp. 852-870, 2000.
- [12] P. Fauchais and G. Montavon, "Thermal and Cold Spray: Recent Developments," *Key. Eng. Mat.*, vol. 384, pp. 1-59, 2008.
- [13] R. Smith and R. Knight, "Thermal Spraying I: Powder Consolidation – from Coating to Forming," *J. Minerals, Metals & Mater. Soc.*, vol. 47, no. 8, pp. 32-39, 1995.
- [14] G. Nelson, J. Nychka and A. McDonald, "Flame Spraying Deposition of Titanium Alloy-bio-active Glass Composite Coatings," *J. Therm. Spray Technol.*, vol. 20, pp. 1339-1351, 2011.
- [15] T. Stoltenhoff, H. Kreye and H. Richter, "An Analysis of the Cold Spray Process and Its Coatings," *J. Therm. Spray Technol.*, vol. 11, no. 4, pp. 542-550, 2002.
- [16] H. Kim, C. Lee and S. Hwang, "Fabrication of WC-Co Coatings by Cold Spray Deposition," *Surf. Coat. Technol.*, vol. 19, pp. 335-340, 2005.
- [17] Y. Lee, H. Ashrafizadeh, G. Fisher and A. McDonald, "Effect of Type of Reinforcing Particles on the Deposition Efficiency and Wear Resistance of Low-Pressure Cold-Sprayed Metal Matrix Composite Coatings," *Surf. Coat. Technol.*, vol. 324, pp. 190-200, 2017.
- [18] J. Karthikeyan, "The Advantages and Disadvantages of Cold Spray Coating Process," in *The Cold Spray Materials Deposition Process: Fundamentals and Application*, 1st ed. ed., V. Champagne, Ed., Cambridge – Woodhead, Elsevier, 2007.
- [19] J. Villafuerte, *Modern Cold Spray – Materials, Process, and Application*, J. Villafuerte, Ed., Springer International Publishing, 2015.
- [20] A. Papyrin, V. Kosarev, S. Klinkov, A. Alkhimov and V. Fomin, *Cold Spray Technology*, 1st ed. ed., Oxford: Elsevier, 2007.

- [21] V. Kosarev, S. Klinkov, A. Alkhimov and A. Papyrin, "On Some Aspects of Gas Dynamic of the Cold Spray Process," *J. Therm. Spray Technol.*, vol. 12, no. 2, pp. 265-281, 2003.
- [22] F. Gärtner, T. Stoltenhoff, T. Schmidt and H. Kreye, "The Cold Spray Process and Its Potential for Industrial Application," *J. Therm. Spray Technol.*, vol. 15, no. 2, pp. 223-232, 2006.
- [23] C. Li, H. Wang, Q. Zhang, G. Yang, W. Li and H. Liao, "Influence of Spray Materials and Their Surface Oxidation on the Critical Velocity in Cold Spraying," *J. Therm. Spray Technol.*, vol. 19, pp. 95-101, 2010.
- [24] T. Schmidt, H. Assadi, F. Gartner, H. Richter, T. Stoltenhoff, H. Kreye and T. Klassen, "From Particle Acceleration to Impact and Bonding in Cold Spraying," *J. Therm. Spray Technol.*, vol. 18, pp. 794-808, 2009.
- [25] E. Irissou, J.-G. Legoux, A. Ryabinin, B. Jodoin and C. Moreau, "Review on Cold Spray Process and Technology: Part I - Intellectual Property," *J. Therm. Spray Technol.*, vol. 17, pp. 495-516, 2008.
- [26] N. Chavan, B. Kiran, A. Jyothirmayi, P. Phani and G. Sundararajan, "The Corrosion Behavior of Cold Sprayed Zinc Coatings on Mild Steel Substrate," *J. Therm. Spray Technol.*, vol. 22, pp. 463-470, 2013.
- [27] H. Assadi, F. Gartner, T. Stoltenhoff and H. Kreye, "Bonding Mechanism in Cold Gas Spraying," *Acta Mater.*, vol. 51, no. 15, pp. 4379-4394, 2003.
- [28] V. Luzin, K. Spencer, M. Zhang, N. Matthews, J. Davis and M. Saleh, "Residual Stresses in Cold Spray Coatings," in *Cold-Spray Coatings: Recent Trends and Future perspectives*, P. Cavaliere, Ed., Cham, Springer, 2017, pp. 451-480.
- [29] B. Marbanrad, H. Jahed and E. Toyserkani, "On the Evolution of Substrate's Residual Stress during Cold Spray Process: A Parametric Study," *Mater. Design*, vol. 138, pp. 90-102, 2018.

- [30] R. Fernández, D. MacDonald, A. Nastić, A. T. B. Jodoin and M. Vijay, "Enhancement and Prediction of Adhesion Strength of Copper Cold Spray Coatings on Steel Substrates for Nuclear Fuel Repository," *J. Therm. Spray Technol.*, vol. 25, no. 8, pp. 1577-1587, 2016.
- [31] Y. Xie, R. R. M. Planche, H. Liao, X. Suo and P. Herve, "Effect of Substrate Preheating on Adhesive Strength of SS 316L Cold Spray Coatings," *J. Therm. Spray Technol.*, vol. 25, no. 1-2, pp. 123-130, 2016.
- [32] X. Luo, Y. Li, C. Li, G. Yang and C. Li, "Effect of Spray Conditions on Deposition Behavior and Microstructure of Cold Sprayed Ni Coatings Sprayed with a Porous Electrolytic Ni Powder," *Surf. Coat. Technol.*, vol. 289, pp. 85-93, 2016.
- [33] S. Yin, X. Suo, Y. Xie, W. Li, R. Lupoi and H. Liao, "Effect of Substrate Temperature on Interfacial Bonding for Cold Spray of Ni onto Cu," *J. Mater. Sci.*, vol. 50, no. 22, pp. 7448-7457, 2015.
- [34] R. Kromer, S. Costil, C. Verdy, S. Gojon and H. Liao, "Laser Surface Texturing to Enhance Adhesion Bond Strength of Spray Coatings – Cold Spraying, Wire-arc Spraying, and Atmospheric Plasma Spraying," *Surf. Coat. Technol.*, pp. Article in Press, <https://doi.org/10.1016/j.surfcoat.2017.05.007>, 2017.
- [35] T. Schmidt, F. Gaertner and H. Kreye, "New Developments in Cold Spray Based on Higher Gas and Particle Temperatures," *J. Therm. Spray Technol.*, vol. 15, no. 4, pp. 488-494, 2006.
- [36] A. Papyrin, "Cold Spray Technology," *Adv. Mater. Process.*, vol. 159, no. 9, pp. 49-51, 2001.
- [37] T. Schmidt, F. Gartner, H. Assadi and H. Kreye, "Development of a Generalized Parameter Window for Cold Spray Deposition," *Acta Mater.*, vol. 54, pp. 729-742, 2006.
- [38] J. Henao, A. Concustell, I. Cano, N. Cinsa, S. Dosta and J. Guilemany, "Influence of Cold Gas Spray Process Conditions on the Microstructure of Fe-based Amorphous Coatings," *J.*

- Alloy. Compd.*, vol. 622, pp. 995-999, 2015.
- [39] M. Rokni, S. Nutt, C. Widener, V. Champagne and R. Hrabe, "Review of Relationship Between Particle Deformation, Coating Microstructure, and Properties in High-Pressure Cold Spray," *J. Therm. Spray Technol.*, vol. 26, no. 6, pp. 1308-1355, 2017.
- [40] D. Gilmore, R. Dykhuizen, R. Neiser, M. Smith and T. Roemer, "Particle Velocity and Deposition Efficiency in the Cold Spray Process," *J. Therm. Spray Technol.*, vol. 8, no. 4, pp. 576-582, 1999.
- [41] M. Fukumotot, H. Wada, K. Tanabe, M. Yamada, E. Yamaguchi, A. Niwa, M. Sugimoto and M. Izawa, "Effect of Substrate Temperature on Deposition Behavior of Copper Particles on Substrate Surface in the Cold Spray Process," *J. Therm. Spray Technol.*, vol. 16, no. 5-6, pp. 643-650, 2007.
- [42] R. Lima, J. Karthikeyan, C. Kay, J. Lindemann and C. berndt, "Microstructural Characteristics of Cold-sprayed Nanostructured WC-Co Coatings," *Thin Solid Films*, vol. 416, no. 1-2, pp. 129-135, 2002.
- [43] N. Melendez and A. McDonald, "Development of WC-Based Metal Matrix Composites Coatings Using Low-Pressure Cold Gas Dynamic Spraying," *Surf. Coat. Technol.*, vol. 214, pp. 101-109, 2013.
- [44] K. Hodder, H. Izadi, A. McDonald and A. Gerlich, "Fabrication of Aluminum-Alumina Metal Matrix Composites via Cold Gas Dynamic Spraying at Low Pressure Followed by Friction Stir Processing," *Mater. Sci. Eng. A*, vol. 556, pp. 114-121, 2012.
- [45] H. Koivuluoto, J. Lagerbom, M. Kylmalahti and P. Vuoristo, "Microstructure and Mechanical Properties of Low-pressure Cold-sprayed (LPCS) Coatings," *J. Therm. Spray Technol.*, vol. 17, no. 5-6, pp. 721-727, 2008.
- [46] J.-G. Legoux, E. Irissou and C. Moreau, "Effect of Substrate Temperature on the Formation Mechanism of Cold-Sprayed Aluminum, Zinc and Tin Coatings," *J. Therm.*

- Spray Technol.*, vol. 16, no. 5-6, pp. 619-626, 2007.
- [47] S. Yin, M. Meyer, W. Li, H. Liao and R. Lupoi, "Gas Flow, Particle Acceleration, and Heat Transfer in Cold Spray: A review," *J. Therm. Spray Technol.*, vol. 25, no. 5, pp. 874-896, 2016.
- [48] R. Dykhuizen and M. Smith, "Gas Dynamic Principles of Cold Spray," *J. Therm. Spray Technol.*, vol. 7, no. 2, pp. 205-212, 1998.
- [49] T. Jen, L. Li, W. Cui, Q. Chen and X. Zhang, "Numerical Investigations on Cold Gas Dynamic Spray Process with Nano- and Microsize Particles," *Int. J. Heat Mas Transfer*, vol. 48, no. 21-22, pp. 4384-4396, 2005.
- [50] B. Samareh, O. Stier, V. Luthen and A. Dolatabadi, "Assessment of CFD Modeling via Flow Visualization in Cold Spray Process," *J. Therm. Spray Technol.*, vol. 18, pp. 934-943, 2009.
- [51] T. Han, Z. Zhao, B. Gillispie and J. Smith, "Effects of Spray Conditions on Coating Formation by the Kinetic Spray Process," *J. Therm. Spray Technol.*, vol. 14, pp. 373-383, 2005.
- [52] A. Sova, M. Doubenskaia, S. Grigoriev, A. Okunkova and I. Smurov, "Parameters of the Gas-Powder Supersonic Jet in Cold Spraying Using a Mask," *J. Therm. Spray Technol.*, vol. 22, pp. 551-556, 2013.
- [53] H. Katanoda, "Numerical Simulation of Temperature Uniformity within Solid Particles in Cold Spray," *J. Solid Mech. Mater. Eng.*, vol. 2, pp. 58-69, 2008.
- [54] W. Ranz and W. Marshall, "Evaporation from Drops: Part I," *Chem. Eng. Prog.*, vol. 48, pp. 141-146, 1952.
- [55] Y. Watanabe, C. Yoshida, K. Atsumi, M. Yamada and M. Fukumoto, "Influence of Substrate Temperature on Adhesion Strength of Cold-Sprayed Coatings," *J. Therm. Spray Technol.*, vol. 24, no. 1-2, pp. 86-91, 2015.

- [56] Z. Arabgol, M. V. Vidaller, H. Assadi, F. Gartner and T. Klassen, "Influence of Thermal Properties and Temperature of Substrate on the Quality of Cold-Sprayed Deposits," *Acta Mater.*, vol. 127, pp. 287-301, 2017.
- [57] S. Yin, X. Wang, W. Li and X. Guo, "Examination on Substrate Preheating Process in Cold Gas Dynamic Spraying," *J. Therm. Spray Technol.*, vol. 20, pp. 852-859, 2011.
- [58] C. Donaldson and R. Snedeker, "A Study of Free Jet Impingement. Part 1. Mean Properties of Free and Impinging Jets," *J. Fluid Mech.*, vol. 45, pp. 281-319, 1971.
- [59] M. Rahimi, I. Owen and J. Mistey, "Impingement Heat Transfer in an Under-Expanded Axisymmetric Air Jet," *Int. J. Heat Mass Transfer*, vol. 46, pp. 263-272, 2003.
- [60] V. Ramanujachari, S. Vijaykant, R. Roy and P. Ghanegaonkar, "Heat Transfer due to Supersonic Flow Impingement on a Vertical Plate," *Int. J. Heat Mass Transfer*, vol. 48, pp. 3707-3712, 2005.
- [61] M. Limaye, R. Vedula and S. Prabhu, "Local Heat Transfer Distribution on a Flat Plate Impinged by a Compressible Round Air Jet," *Int. J. Therm. Sci.*, vol. 49, pp. 2157-2168, 2010.
- [62] V. Katti and S. Prabhu, "Experimental Study and Theoretical Analysis of Local Heat Transfer Distribution between Smooth Flat Surface and Impinging Air Jet from a Circular Straight Pipe Nozzle," *Int. J. Heat Mass Transfer*, vol. 51, no. 17-18, pp. 4480-4495, 2008.
- [63] G. Huang, "Investigations of Heat-Transfer Coefficients for Air Flow through Round Jets Impinging Normal to a Heat-Transfer Surface," *J. Heat Transfer*, vol. 85, no. 3, pp. 237-243, 1963.
- [64] H. Martin, "Heat and Mass Transfer between Impinging Gas Jets and Solid Surfaces," *Adv. Heat Transfer*, vol. 13, pp. 1-60, 1977.
- [65] L. Huang and M. El-Genk, "Heat Transfer of an Impinging Jet on a Flat Surface," *Int. J. Heat Mass transfer*, vol. 37, no. 13, pp. 1915-1923, 1994.

- [66] V. Narayanan, J. Seyed-Yagoobi and R. Page, "An Experimental Study of Fluid Mechanics and Heat Transfer in an Impinging Slot Jet Flow," *Int. J. Heat Mass Transfer*, vol. 47, no. 8-9, pp. 1827-1845, 2004.
- [67] B. Sagot, G. Antonini, A. Christgen and F. Buran, "Jet Impingement Heat Transfer on a Flat Plate at a Constant Wall Temperature," *Int. J. Therm. Sci.*, vol. 47, pp. 1610-1619, 2008.
- [68] F. Afroz and M. Sharif, "Numerical Study of Heat Transfer from an Isothermally Heated Flat Surface due to Turbulent Twin Oblique Confined Slot-Jet Impingement," *Int. J. Therm. Sci.*, vol. 74, pp. 1-13, 2013.
- [69] D. Singh, B. Premachandran and S. Kohli, "Effect of Nozzle Shape on Jet Impingement Heat Transfer from a Circular Cylinder," *Int. J. Therm. Sci.*, vol. 96, pp. 45-69, 2015.
- [70] T. Zhou, D. Xu, J. Chen, C. Cao and T. Ye, "Numerical Analysis of Turbulent Round Jet Impingement Heat Transfer at High Temperature Difference," *Appl. Therm. Eng.*, vol. 100, pp. 55-61, 2016.
- [71] A. Ryabinin, E. Irissou, A. McDonald and J.-G. Legoux, "Simulation of Gas-Substrate Heat Exchange during Cold-Gas Dynamic Spraying," *Int. J. Therm. Sci.*, vol. 56, pp. 12-18, 2012.
- [72] A. McDonald, A. Ryabinin, E. Irissou and J.-G. Legoux, "Gas-Substrate Heat Exchange during Cold-Gas Dynamic Spraying," *J. Therm. Spray Technol.*, vol. 22, no. 2-3, pp. 391-397, 2012.
- [73] S. Striegl and T. Diller, "The Effect of Entrainment Temperature on Jet Impingement Heat Transfer," *J. Heat Transfer*, vol. 106, no. 1, pp. 27-33, 1984.
- [74] B. Hollworth and L. Gero, "Entrainment Effects on Impingement Heat Transfer: Part II—Local Heat Transfer Measurements," *J. Heat Transfer*, vol. 107, no. 4, pp. 910-915, 1985.
- [75] M. Goodro, J. Park, P. Ligrani, M. Fox and H. Moon, "Effect of Temperature Ratio on Jet

- Array Impingement Heat Transfer," *J. Heat Transfer*, vol. 131, no. 1, pp. 1-10, 2008.
- [76] W. Chakroun, A. Abdel-Rahman and S. Al-Fahed, "Heat Transfer Augmentation for Air Jet Impinged on a Rough Surface," *Appl. Therm. Eng.*, vol. 18, pp. 1225-1241, 1998.
- [77] A. Beitelmal and M. Saad, "Effects of Surface Roughness on the Average Heat Transfer of an Impinging Air Jet," *Int. Comm. Heat Mass Transfer*, vol. 27, pp. 1-12, 2000.
- [78] M. Cobbertean and M. Rahman, "Numerical Analysis of Steady State Heat Transfer for Jet Impingement on Patterned Surfaces," *Appl. therm. Eng.*, vol. 103, pp. 481-490, 2016.
- [79] C. Chen, Y. Xie, C. Verdy, R. Huang, H. Liao, Z. Ren and S. Deng, "Numerical Investigation of Transient Coating Build-up and Heat Transfer in Cold Spray," *Surf. Coat. technol.*, vol. 326, pp. 355-365, 2017.
- [80] B. Samareh and A. Dolatabadi, "A Three-Dimensional Analysis of the Cold Spray Process: the Effects of Substrate Location and Shape," *J. Therm. Spray technol.*, vol. 16, pp. 634-642, 2007.
- [81] C.-K. Kim, "An Analytical Solution to Heat Conduction with a Moving Heat Source," *J. Mech. Sci. Technol.*, vol. 25, no. 4, pp. 895-899, 2011.
- [82] M. Song and R. Kovacevic, "Thermal Modeling of Friction Stir Welding in a Moving Coordinate system and Its Validation," *Int. J. Mach. Tools Manuf.*, vol. 43, pp. 605-615, 2003.
- [83] N. Al-Huniti, "Dynamic Response to a Rod due to a Moving Heat Source under the Hyperbolic Heat Condition Model," *J. Sound Vib.*, vol. 242, no. 2, pp. 629-640, 2001.
- [84] X. Ai, Z. Xu and C. Zhao, "Experimental Study on Heat Transfer of Jet Impingement with a Moving Nozzle," *Appl. Therm. Eng.*, vol. 115, pp. 682-691, 2017.
- [85] O. Manca, B. Morrone and V. Naso, "Quasi-Steady-State Three-Dimensional Temperature Distribution Induced by a Moving Circular Gaussian Heat Source in a Finite Depth Solid,"

- Int. J. Heat Mass Transfer*, vol. 38, no. 7, pp. 1305-1315, 1995.
- [86] N. Zuckerman and N. Lior, "Jet Impingement Heat Transfer: Physics, and Numerical Modelling," *Adv. Heat Transfer*, vol. 39, pp. 565-631, 2006.
- [87] M. Ozisik, *Heat Conduction*, second ed., New York: John Wiley & Sons, Inc., 1993.
- [88] T. Beckwith, R. Marangoni and J. Lienhard, *Mechanical Measurements*, sixth ed., Upper Saddle River: Pearson Education, 2006.
- [89] J. Taylor, *An Introduction to Error Analysis: The Study of Uncertainties in Physical Measurements*, second ed., Herndon: University Science Books, 1996.
- [90] A. Shapiro, *The Dynamics and Thermodynamics of Compressible Fluid Flow*, vol. II, New York: The Ronald Press Company, 1954.
- [91] K. Jambunathan, E. Lai, M. Moss and B. Button, "A Review of Heat Transfer Data for Single Circular Jet Impingement," *Int. J. Heat Fluid Flow*, vol. 13, pp. 106-115, 1992.
- [92] O. Reynolds, "On the Extent and Action of the Heating Surface of Steam Boilers," *Proc. Lit. Phil. Soc.*, vol. 4, pp. 7-12, 1874.
- [93] A. Colburn, "A Method of Correlating Forced Convection Heat Transfer Data and a Comparison with Fluid Friction," *Int. J. Heat Mass Transfer*, vol. 7, no. 12, pp. 1359-1384, 1964.
- [94] Y. Cengel and J. Cimbala, *Fluid Mechanics: Fundamentals and Applications*, third ed., New York: McGraw-Hill, Inc., 2013.
- [95] Y. Cengel and M. Boles, *Thermodynamics: an Engineering Approach*, 8th ed., New York: McGraw-Hill, Inc., 2014.
- [96] U. Prisco, "Size-dependent Distribution of Particle Velocity and Temperature at Impact in the Cold-gas Dynamic-spray Process," *J. Mater. Process. Tech.*, vol. 216, pp. 302-314,

- 2015.
- [97] C. Ziemian, M. Sharma, B. Bouffard, T. Nissley and T. Eden, "Effect of Substrate Surface Roughening and Cold Spray Coating on the Fatigue Life of AA2024 Specimens," *Mater. Design*, vol. 54, pp. 212-221, 2014.
- [98] A. McDonald, M. Lamontagne, S. Chandra and C. Moreau, "Photographing Impact of Plasma-sprayed Particles on Metal Substrate," *J. Therm. Spray Technol.*, vol. 15, no. 4, pp. 708-716, 2006.
- [99] P. Chauvy, C. Madore and D. Landolt, "Variable Length Scale Analysis of Surface Topography: Characterization of Titanium Surfaces for Biomedical Applications," *Surf. Coat. Technol.*, vol. 110, pp. 48-56, 1998.
- [100] L. Lyles, L. Disrud and R. Krauss, "Turbulence Intensity as Influenced by Surface Roughness and Mean Velocity in a Wind-tunnel Boundary Layer," *T. ASAE*, pp. 285-289, 1971.
- [101] C. Wen and I. Mudawar, "Emissivity Characteristics of Roughened Aluminum Alloy Surfaces and Assessment of Multispectral Radiation Thermometry (MRT) Emissivity Models," *Int. J. Heat Mass Transfer*, vol. 47, pp. 3591-3605, 2004.
- [102] A. Volpert, V. Volpert and V. Volpert, *Traveling Wave Solutions of Parabolic Systems, Translation of Mathematical Monographs, Vol 140*, Rhode Island: American Mathematical Society, 1994.
- [103] C. Crowe, *Multiphase Flow Handbook*, New York: Taylor & Francis Group, 2006.
- [104] C. Rogers and J. Eaton, "The Effect of Small Particles on Fluid Turbulence in a Flat-plate, Turbulent Boundary Layer in Air," *Phys. Fluids A-Fluid*, vol. 3, no. 5, pp. 928-937, 1991.
- [105] L. Tang, F. Wen, Y. Yang, C. Crowe, J. Chung and T. Troutt, "Self-organizing Particle dispersion Mechanism in Free Shear Flows," *Phys. Fluids A*, vol. 4, pp. 2244-2251, 1992.

- [106] J. P. D. Kim, J. Lee, D. Kim, S. Tark, S. Ahn, J. Yun, J. Gwak, K. Yoon, S. Chandra and S. Yoon, "Cold Spray Deposition of Copper Electrodes on Silicon and Glass Substrates," *J. Therm. Spray Technol.*, vol. 22, no. 7, pp. 1092-1102, 2013.
- [107] C. Crowe, T. Troutt and J. Chung, "Numerical Models for Two-Phase Turbulent Flows," *Annu. Rev. Fluid. Mech.*, vol. 28, pp. 11-43, 1996.
- [108] R. Dykhuizen, M. Smith, D. Gilmore, R. Neiser, X. Jiang and S. Sampath, "Impact of High Velocity Cold Spray Particles," *J. Therm. Spray Technol.*, vol. 8, no. 4, pp. 559-564, 1999.
- [109] M. Grujicic, J. Saylor, D. Beasley, W. DeRosset and D. Helfritch, "Computational Analysis of the Interfacial Bonding between Feed-powder Particles and the Substrate in the Cold-gas Dynamic-spray Process," *Appl. Surf. Sci.*, vol. 219, pp. 211-237, 2003.
- [110] M. Babaei and Z. Chen, "Transient Hyperbolic Heat Conduction in a Functionally Graded Hollow Cylinder," *J. Thermophys. Heat Transfer*, vol. 24, no. 2, pp. 325-330, 2010.
- [111] B. Adel-Hamid, "Modelling Non-Fourier Heat Conduction with Periodic Thermal Oscillation Using the Finite Integral Transform," *Appl. Math. Model.*, vol. 23, no. 12, pp. 899-914, 1999.
- [112] C. Cattaneo, "A Form of Heat Conduction Equation which Eliminates the Paradox of Instantaneous Propagation," *Compt. Rend.*, vol. 247, pp. 431-433, 1958.
- [113] P. Vernotte, "Some Possible Complications in the Phenomena of Thermal Conduction," *Compt. Rend.*, vol. 252, pp. 2190-2191, 1961.
- [114] W. Li, C. Zhang, C. Li and H. Liao, "Modeling Aspects of High Velocity Impact of Particles in Cold Spraying by Explicit Finite Element Analysis," *J. Therm. Spray Technol.*, vol. 18, no. 5-6, pp. 921-933, 2009.
- [115] P. Profizi, A. Combescure and K. Ogawa, "SPH Modeling of Adhesion in Fast Dynamics: Application to the Cold Spray Process," *C. R. Mecanique*, vol. 344, pp. 211-224, 2016.

- [116] F. Wang, W. Li, M. Yu and H. Liao, "Prediction of Critical Velocity During Cold Spraying Based on a Coupled Thermomechanical Eulerian Model," *J. Therm. Spray Technol.*, vol. 23, pp. 60-67, 2014.
- [117] C. Chen, Y. Xie, C. Verdy, R. Huang, H. Liao, Z. Ren and S. Deng, "Numerical Investigation of Transient Coating Build-up and Heat Transfer in Cold Spray," *Surf. Coat. Technol.*, vol. 326, pp. 355-365, 2017.
- [118] K. Spencer, V. Luzin, N. Matthews and M.Zhang, "Residual Stresses in Cold Spray Al Coatings: The Effect of Alloying and of Process Parameters," *Surf. Coat. Technol.*, vol. 206, pp. 4249-4255, 2012.
- [119] R. Ghelichi, S. Bagherifard, D. MacDonald, I. Fernandez-Pariente, B. Jodoin and M.Guagliano, "Experimental and Numerical Study of Residual Stress Evolution in Cold Spray Coating," *Appl. Surf. sci.*, vol. 208, pp. 26-33, 2014.
- [120] M. Saleh, V. Luzin and K. Spencer, "Analysis of the Residual Stress and Bonding Mechanism in the Cold Spray Technique Using Experimental and Numerical Methods," *Surf. Coat. Technol.*, vol. 252, pp. 15-28, 2014.

Appendix A

The governing equation of the transient two-dimensional heat conduction model is

$$\frac{1}{r} \frac{\partial}{\partial r} \left(r \frac{\partial T}{\partial r} \right) + \frac{\partial^2 T}{\partial z^2} = \frac{1}{\alpha_s} \frac{\partial T}{\partial t}. \quad (\text{A-1})$$

The boundary conditions and initial condition are

$$T(r=0, z, t) = \text{finite}, \quad (\text{A-2})$$

$$\frac{\partial T(r=b, z, t)}{\partial r} = 0, \quad (\text{A-3})$$

$$-k_s \left[\frac{\partial T(r, z=0, t)}{\partial z} \right] = h(r) [T_{\text{AW}}(r) - T(r, z=0, t)], \quad (\text{A-4})$$

$$\frac{\partial T(r, z=\delta, t)}{\partial z} = 0, \text{ and} \quad (\text{A-5})$$

$$T(r, z, t=0) = T_0. \quad (\text{A-6})$$

The Green's function technique was used to solve the transient 2D heat conduction model with inhomogeneous boundary conditions and the given initial condition. In order to determine the desired Green's function, the governing equation was considered as

$$\frac{1}{r} \frac{\partial}{\partial r} \left(r \frac{\partial \Psi}{\partial r} \right) + \frac{\partial^2 \Psi}{\partial z^2} = \frac{1}{\alpha_s} \frac{\partial \Psi}{\partial t}, \quad (\text{A-7})$$

with homogeneous boundary conditions and the initial conditions as

$$\Psi(r=0, z, t) = \text{finite}, \quad (\text{A-8})$$

$$\frac{\partial \Psi(r=b, z, t)}{\partial r} = 0, \quad (\text{A-9})$$

$$-k_s \left[\frac{\partial \Psi(r, z=0, t)}{\partial z} \right] = h(r) [T_{\text{AW}}(r) - \Psi(r, z=0, t)], \quad (\text{A-10})$$

$$\frac{\partial \Psi(r, z=\delta, t)}{\partial z} = 0, \text{ and} \quad (\text{A-11})$$

$$\Psi(r, z, t=0) = T_0. \quad (\text{A-12})$$

The separation of variable method was used to solve the homogeneous problem. Accordingly, the separation of function $\Psi(r, z, t)$ into space- and time-dependent functions was applied as

$$\Psi(r, z, t) = R(r)Z(z)\Gamma(t). \quad (\text{A-13})$$

Substitution of Eq. (A-13) into Eq. (A-7) gives

$$\frac{1}{R(r)} \frac{1}{r} \frac{d}{dr} \left(r \frac{dR(r)}{dr} \right) + \frac{1}{Z(z)} \frac{d^2 Z(z)}{dz^2} = \frac{1}{\tau(t)} \frac{1}{\alpha_s} \frac{d\Gamma(t)}{dt}. \quad (\text{A-14})$$

In Eq. (A-14), the left-hand side is a function of the space variables, merely, while the right-hand side is a function of time. Therefore, Eq. (A-14) holds if both sides are equal to the same constant. In addition, the first and the second terms in the left-hand side are only a function of r (radial coordinate) and z (axial coordinate), respectively. Further details about the separation of variables method can be found elsewhere [87]. The space-variable function $R(r)$ satisfies the differential equation

$$\frac{d^2 R(r)}{dr^2} + r \frac{dR(r)}{dr} + \lambda_1^2 r^2 R(r) = 0. \quad (\text{A-15})$$

Equation (A-15) is called Bessel's differential equation. In Eq. (A-15), λ_1 represents the eigenvalues in radial direction. The solution of Eq. (A-15) is

$$R(r) = A_1 J_0(\lambda_1 r) + B_1 Y_0(\lambda_1 r). \quad (\text{A-16})$$

The boundary conditions in radial direction are obtained by introducing the separated function (A-13) into the boundary conditions (A-8) and (A-9) as

$$R(r=0) = \text{finite}, \text{ then } B_1 = 0, \text{ and } R(r) = A_1 J_0(\lambda_1 r). \quad (\text{A-17})$$

$$\frac{dR(r=b)}{dr} = 0, \text{ then } \lambda_1 J_1(\lambda_1 b) = 0. \quad (\text{A-18})$$

The space-variable function $Z(z)$ satisfies the differential equation

$$\frac{d^2 Z(z)}{dz^2} - \beta_j^2 Z(z) = 0. \quad (\text{A-19})$$

In Eq. (A-19), β_j represents the eigenvalues in axial direction. The solution of Eq. (A-19) is

$$Z(z) = C_j \sin(\beta_j z) + D_j \cos(\beta_j z). \quad (\text{A-20})$$

Similarly, the boundary conditions in axial direction are obtained by introducing the separated function (A-13) into the boundary conditions (A-10) and (A-11) as

$$\frac{dZ(z=\delta)}{dz} = 0, \text{ then } C_j = \tan(\beta_j \delta) D_j, \text{ and } Z(z) = D_j [\tan(\beta_j \delta) \sin(\beta_j z) + \cos(\beta_j z)]. \quad (\text{A-21})$$

$$-k_s \frac{dZ(z=0)}{dz} + h(r)Z(z=0) = 0, \text{ then } \beta_j \tan(\beta_j \delta) - \frac{h(r)}{k_s} = 0. \quad (\text{A-22})$$

Finally, the function $\Gamma(t)$ satisfies the differential equation as

$$\Gamma(t) = \exp[-\alpha_s (\lambda_i^2 + \beta_j^2) t]. \quad (\text{A-23})$$

The final solution for the function $\Psi(r, z, t)$ is expressed by a linear superposition of the separated elementary solutions as

$$\Psi(r, z, t) = \sum_{i=1}^{\infty} \sum_{j=1}^{\infty} E_{ij} J_0(\lambda_i r) \left[\tan(\beta_j \delta) \sin(\beta_j z) + \cos(\beta_j z) \right] \exp[-\alpha_s (\lambda_i + \beta_j) t]. \quad (\text{A-24})$$

The application of the initial condition (Eq. (A-12)) gives

$$T_0 = \sum_{i=1}^{\infty} \sum_{j=1}^{\infty} E_{ij} J_0(\lambda_i r) \left[\tan(\beta_j \delta) \sin(\beta_j z) + \cos(\beta_j z) \right]. \quad (\text{A-25})$$

The unknown coefficient E_{ij} can be evaluated by taking into account the use of the orthogonality properties of the eigenfunctions in Eq. (A-25). Further explanations on the orthogonality properties can be found in textbooks [87]. The coefficient E_{ij} will be determined as

$$E_{ij} = \frac{\int_{r'=0}^b \int_{z'=0}^{\delta} T_0 J_0(\lambda_i r') \left[\tan(\beta_j \delta) \sin(\beta_j z') + \cos(\beta_j z') \right] r' dz' dr'}{\int_{r=0}^b \int_{z=0}^{\delta} J_0^2(\lambda_i r') \left[\tan(\beta_j \delta) \sin(\beta_j z') + \cos(\beta_j z') \right]^2 r dz dr}, \quad (\text{A-26})$$

where

$$N(\lambda_i) N(\beta_j) = \int_{r=0}^b \int_{z=0}^{\delta} J_0^2(\lambda_i r') \left[\tan(\beta_j \delta) \sin(\beta_j z') + \cos(\beta_j z') \right]^2 r dz dr. \quad (\text{A-27})$$

In Eq. (A-27), $N(\lambda_i)$ and $N(\beta_j)$ represent the Norms of the differential equation in the radial coordinate ($0 \leq r \leq b$) and axial coordinate ($0 \leq z \leq \delta$), respectively. By substituting Eq. (A-26) into Eq. (A-24), the function $\Psi(r, z, t)$ can be expressed

$$\Psi(r, z, t) = \int_{r'=0}^b \int_{z'=0}^{\delta} \sum_{i=1}^{\infty} \sum_{j=1}^{\infty} \left(\frac{T_0 \exp[-\alpha_s (\lambda_i^2 + \beta_j^2) t]}{N(\lambda_i) N(\beta_j)} J_0(\lambda_i r) J_0(\lambda_i r') \right) \times \left[\tan(\beta_j \delta) \sin(\beta_j z) + \cos(\beta_j z) \right] \times \left[\tan(\beta_j \delta) \sin(\beta_j z') + \cos(\beta_j z') \right] r' dz' dr'. \quad (\text{A-28})$$

The Green's function for $\tau = 0$ can be expressed as

$$G(r, z, t | r', z', \tau)_{\tau=0} = \sum_{i=1}^{\infty} \sum_{j=1}^{\infty} \left(\frac{T_0 \exp[-\alpha_s (\lambda_i^2 + \beta_j^2) t]}{N(\lambda_i) N(\beta_j)} J_0(\lambda_i r) J_0(\lambda_i r') \right) \times \left[\tan(\beta_j \delta) \sin(\beta_j z) + \cos(\beta_j z) \right] \times \left[\tan(\beta_j \delta) \sin(\beta_j z') + \cos(\beta_j z') \right]. \quad (\text{A-29})$$

Green's function $G(r, z, t | r', z', \tau)$ can be determined by replacing t by $(t - \tau)$ in Eq. (A-29) as

$$G(r, z, t | r', z', \tau) = \sum_{i=1}^{\infty} \sum_{j=1}^{\infty} \left(\frac{T_0 \exp[-\alpha_s (\lambda_i^2 + \beta_j^2) (t - \tau)]}{N(\lambda_i) N(\beta_j)} J_0(\lambda_i r) J_0(\lambda_i r') \right) \times \left[\tan(\beta_j \delta) \sin(\beta_j z) + \cos(\beta_j z) \right] \times \left[\tan(\beta_j \delta) \sin(\beta_j z') + \cos(\beta_j z') \right]. \quad (\text{A-30})$$

The general solution in terms of the two-dimensional Green's function for the boundary condition of third kind can be expressed as

$$\begin{aligned}
T(r, z, t) = & \int_{r'=0}^b \int_{z'=0}^{\delta} G(r, z, t | r', z', \tau) F(r', z') r' dz' dr' \\
& - \alpha_s \int_{\tau=0}^t d\tau \int_{r'=0}^b G(r, z, t | r', z', \tau) \frac{1}{k_s} f(r', z', \tau)_{z'=0} r' dr',
\end{aligned} \tag{A-31}$$

Finally, by substituting the Green's functions from Eqs. (A-29) and (A-30) into Eq. (A-31), the final expression for the temperature distribution within the substrate is found to be

$$\begin{aligned}
T(r, z, t) = & \sum_{i=1}^{\infty} \sum_{j=1}^{\infty} \left[T_0 \frac{\exp[-\alpha_s(\lambda_i^2 + \beta_j^2)t]}{N(\lambda_i)N(\beta_j)} J_0(\lambda_i r) [\tan(\beta_j \delta) \sin(\beta_j z) + \cos(\beta_j z)] \right. \\
& \times \int_{r'=0}^b \int_{z'=0}^{\delta} J_0(\lambda_i r') [\tan(\beta_j \delta) \sin(\beta_j z') + \cos(\beta_j z')] r' dz' dr' \\
& + \left(\frac{\alpha_s}{k_s} \right) \left[\frac{h(r)}{N(\lambda_i)N(\beta_j)} \right] J_0(\lambda_i r) [\tan(\beta_j \delta) \sin(\beta_j z) + \cos(\beta_j z)] \\
& \left. \times \frac{1}{\alpha_s(\lambda_i^2 + \beta_j^2)} [1 - \exp(-\alpha_s(\lambda_i^2 + \beta_j^2)t)] \int_{r'=0}^b J_0(\lambda_i r') T_{AW}(r') r' dr' \right].
\end{aligned} \tag{A-32}$$

Appendix B

The zero-dimensional MATLAB code to solve Eq. (2-17) is presented here.

```
%%%%% Determination of the Heat Transfer Coefficient of Under-expanding Cold Spray Air Jet %%%%%%

close all;
clear all;
clc

%%%% Initial information %%%

delta=1.5875e-3;           % Thickness of substrate (m)
K=167;                    % Thermal conductivity of substrate material (Al 6061) (W/m-K)
alpha=6.9e-5;             % Thermal Diffusivity of substrate material (m2/s)
Tinf=21;                  % Ambient Temperature (°C)
Ti=21;                    % Initial Temperature of substrate (°C)
Tg=300;                   % Air jet temperature at the Cold Spray Unit (°C)
Dn=0.0063;                % Nozzle diameter (m)
R0=10e-2;                 % Radius of substrate (m)

h=1870;                   % Initial guess for heat transfer coefficient (W/m2-K)
r=0*Dn;                   % Radius of interest (m)
z=0.0;                    % Depth of interest (m)
t=1;                       % Time of interest (s)

%%%% Eigenvalues in radial direction %%%
%%%%

Fun=@(lambda) lambda*besselj(1,lambda.*R0);
tol=1.e-6;
Nmax=100;

l=1;
c=0;

for i=1:2000;
    x1=c;
    x2=c+l;

    [root_out,flag_out]=mrf_bisection(Fun,x1,x2,tol,Nmax);
    final2(i,1)=root_out;

    c=c+l;
end

global egv_r

j=1;
for i=1:2000;
    if final2(i,1)==-1
```

```

else
    egv_r(j,1)=final2(i,1);
    j=j+1;
end
end
%%%

%%% Eigenvalues in axial direction %%%
%%%

Fun=@(beta) beta.*tan(beta.*delta)-h/K;
tol=1.e-6;
Nmax=100;

l=0.1;
c=0;

for i=1:200000;
    x1=c;
    x2=c+l;

    [root_out,flag_out]=mrf_bisection(Fun,x1,x2,tol,Nmax);
    final2(i,1)=root_out;

    c=c+l;
end

global egv_z

j=1;
for i=1:200000;
    if final2(i,1)=-1
    else
        egv_z(j,1)=final2(i,1);
        j=j+1;
    end
end
%%%

%%% Solving the final expression for temperature distribution within the substrate %%%

syms rr zz tt

%%% Adiabatic wall temperature %%%

Taw=0.0813*(rr./Dn).^5-1.7235*(rr./Dn).^4+13.5557*(rr./Dn).^3-46.4293*(rr./Dn).^2+45.6804*(rr./Dn).^1+
    147.0407;

%%%

sum=0.0;
cte=0.0;

for i=1:50;

```

```

j=1;

f1=rr.*(besselj(0,egv_r(i,1).*rr).^2).*((tan(egv_z(j,1).*delta).*sin(egv_z(j,1).*zz)+cos(egv_z(j,1).*zz)).^2);
Norm=double(int(int(f1,rr,0,R0),zz,0,delta)); % (Norm_lambda * Norm_beta)

f2=rr.*besselj(0,egv_r(i,1).*rr).*(tan(egv_z(j,1).*delta).*sin(egv_z(j,1).*zz) + cos(egv_z(j,1).*zz));
int1=double(int(int(f2,rr,0,R0),zz,0,delta));

f3=rr.*besselj(0,egv_r(i,1).*rr).*Taw;
int2=double(int(f3,rr,0,R0));

f4=exp(-alpha*(egv_r(i,1).^2 + egv_z(j,1).^2)*(t-tt));
int3=double(int(f4,tt,0,t));

%%% For uncertainty analysis %%%

ff3=rr.*besselj(0,egv_r(i,1).*rr);
intuncer=double(int(ff3,rr,0,R0));

cte=cte+(alpha/K).*(intuncer/Norm).*besselj(0,egv_r(i,1).*r).*(tan(egv_z(j,1).*delta).*sin(egv_z(j,1).*z)
+cos(egv_z(j,1).*z)).*int3

%%%

sum=sum+(Ti/Norm).*int1.*besselj(0,egv_r(i,1).*r).*(tan(egv_z(j,1).*delta).*sin(egv_z(j,1).*z)+
cos(egv_z(j,1).*z))*exp(-alpha*(egv_r(i,1).^2+egv_z(j,1).^2).*t)+
(alpha*h/K).*(int2/Norm).*besselj(0,egv_r(i,1).*r).*(tan(egv_z(j,1).*delta).*sin(egv_z(j,1).*z)+
cos(egv_z(j,1).*z)).*int3

end

T = (sum -Tinf)/(Tg-Tinf)
Nu=h*0.0063/0.0343

```